

Alma Mater Studiorum – Università di Bologna

DOTTORATO DI RICERCA IN

CHIMICA

Ciclo XXVI

Settore Concorsuale di afferenza: 03/C2 CHIMICA INDUSTRIALE

Settore Scientifico disciplinare: CHIM/04 CHIMICA INDUSTRIALE

**Electrospun Polymeric Scaffolds with Enhanced Biomimetic Properties for
Tissue Engineering Applications**

Presentata da: Andrea Fiorani

**Coordinatore Dottorato
Prof. Aldo Roda**

**Relatore
Prof.ssa Mariastella Scandola**

**Correlatore
Dr. Maria Letizia Focarete**

Esame finale anno 2014

Abstract

The present PhD Thesis is focused on the fabrication of fibrous polymeric scaffolds to be used in the field of tissue engineering and on the improvement of scaffold biomimetic properties. For scaffold fabrication electrospinning technique was employed, which allows to fabricate materials in the form of non-woven meshes (scaffold) made of micro or nanofibers. In order to enhance scaffold biomimetic properties two different approaches were followed: (1) the use of natural biopolymers, that increase the bioactivity and affinity of cells for the scaffold, and (2) the modification of the fiber surface chemistry, by either physical or chemical methods.

Scaffolds used in tissue engineering are usually made of synthetic polymers. In this Thesis, gelatin was chosen as the basic material, for its bioactive properties and excellent cellular affinity, however it lacks in mechanical properties. To overcome this problem, PLLA was employed as second material because it can confer mechanical stability to the scaffold. A co-electrospinning method was developed to fabricate a scaffold containing both gelatin and PLLA fibers and the parameters of the process were optimized. Scaffolds were fabricated with different ratio of gelatin to PLLA. Such scaffolds were characterized in terms of mechanical properties and a correlation was found with the composition of the scaffolds. Cell culture studies were performed to assess scaffold biomimetic properties. It was shown that the gelatin effectively improves cell growth and viability compared with the scaffold of pure PLLA. Worth noting is that co-electrospun scaffolds of gelatin and PLLA were more effective towards cell culture than a plain gelatin scaffold.

Scaffolds made of pure collagen fibers were also fabricated by electrospinning. Collagen is the major constituent of extracellular matrix proteins and greatly influences cell behavior. In this case, the collagen scaffold provides to cells both the structural support and the high biomimeticism. The properties of electrospun collagen fibers were studied from the point of view of the collagen structure (i.e. triple helix modifications), which is the main feature of collagen providing binding sites and signals for cells. Mechanical properties were studied before and after the crosslinking procedure. Crosslinking stabilizes fibers and it is mandatory for collagen scaffolds before cell culture studies. The crosslinking method was developed and optimized, by using a crosslinking reactant (1,4-Butanediol diglycidyl ether) used for the first time on electrospun collagen fibers, with very good results in terms of fibers stabilization. Cell culture on electrospun collagen scaffolds, with mesenchymal stem cells, showed good adhesion and morphology of cells.

With the aim to improve the scaffold-cell interactions the fibers surface chemistry was modified by plasma treatment at atmospheric pressure, in collaboration with the plasma research group of

Engineering Department (DIN). PLLA is a hydrophobic polymer and the objective of this study was to modify its surface properties towards a higher hydrophilicity. The modifications of thermal, mechanical, and surface properties (hydrophilicity) induced by plasma were studied. Plasma did not affect thermal and mechanical properties of electrospun PLLA, while it greatly influenced the surface chemistry of fibers. The major result was the introduction of carboxyl groups at the surface of the fibers that increase the hydrophilicity of the scaffold. This functionalization of fibers with carboxyl groups enhanced the fibroblast cell viability and spreading with to untreated PLLA scaffolds.

In alternative to the physical plasma treatment, surface modifications were also conducted by chemical reactions at the fiber surface of electrospun scaffolds made of a polysphorolipid (synthesized by the group of Prof. Gross, Rensselaer Polytechnic Institute, Troy, NY). The polymer repeating unit is formed by the sophorose group (a disaccharide) and the oleic acid. The aim of this “proof-of-concept” study was to introduce a biomolecule at the fiber surface. By developing a series of chemical reactions, monitored by X-ray photoelectron spettroscopy (XPS), an oligopeptide was covalently grafted on the surface of electrospun fibers. The first reaction is the oxidation of the 1,2 diols functionality of the sophorose moiety, to aldehydes. In a second step, a reductive amination with cysteamine was performed. The free thiol group of cysteamine was successively reacted with the oligopeptide, that carries a double bond. The reaction of thiol and the double bond is a “click” reaction performed under UV irradiation, that leads to grafting one oligopeptide every three repeating unit of polysphorolipid. This result demonstrates the feasibility of this type of fiber surface functionalization that can be performed to introduce interesting biomolecules with specific functionalities.

Contents

1. Introduction.....	5
1.1. Tissue Engineering.....	5
1.2. The Extracellular Matrix.....	7
1.3. Scaffolds for Tissue Engineering.....	10
1.3.1 Scaffold Fabrication.....	12
1.3.2 Electrospinning.....	16
1.3.3 Electrospun fibres functionalization.....	18
1.4. Synthetic and Natural Polymers.....	20
1.4.1 Synthetic Polymers.....	20
1.4.2 Natural Polymers.....	22
2. Materials and Methods	26
2.1 Materials	26
2.2. Scaffold Fabrication by Electrospinning	27
2.2.1 Co-electrospinning	28
2.3. Scaffold Functionalization	29
2.3.1 Non-thermal atmospheric plasma treatment	29
2.3.2 Chemical functionalization	30
2.4. Characterization Methods	31
3. Results and Discussion.....	34
3.1. Part A: Co-electrospun gelatin-poly(L-lactic acid) scaffolds: Modulation of mechanical properties and chondrocyte response as a function of composition	34
3.2. Part B: Comparative performance of collagen nanofibers electrospun from different solvents and stabilized by different crosslinkers	46
3.3. Part C: Carboxyl Surface Functionalization of Poly(L-lactic acid) Electrospun Nanofibers through Atmospheric Non-Thermal Plasma Affects Fibroblast Morphology.....	56
3.4. Part D: Fibrous mats of a sophorolipid polymer: fabrication by electrospinning and functionalization with biomolecules	68

4. Conclusions.....	87
5. References.....	89
List of Publications.....	105
Scientific congress and schools	105
Acknowledgments	106

1 Introduction

The aim of this Thesis was to design electrospun polymeric scaffolds, made of synthetic and/or natural macromolecules, with enhanced biomimetic properties to be used in the tissue engineering field. This is an interdisciplinary area and it attempts to provide solutions to develop biological substitutes that restore, maintain or improve tissue functions [1].

The success of an implantable scaffold is mainly determined by the response that it elicits to the biological environment, and this is favoured by the ability of the scaffolds to mimic the characteristic of the natural extracellular matrix (ECM), in terms of physical-mechanical, chemical, biochemical, topographical and morphological properties. The design of highly biomimetic scaffolds is therefore a challenging topic and it is nowadays a research subject of great interest among biomaterial scientists.

1.1 Tissue Engineering

Loss or injury of tissues or organs have dramatic effects on life quality. Strategies to replace tissues or to restore the functionalities of organs are therefore of capital importance in surgical medicine. During the last decades artificial generation of tissues, organs, or even more complex living organisms became feasible and this approach has been introduced in clinical medicine, parallel to the classical transplanting surgery of tissues or organs. Nowadays, new and functional biological tissues are fabricated by using cells mainly coupled with a scaffold, the latter being a natural, artificial or hybrid supporting matrix to guide tissue growth. In this context a new discipline called Tissue Engineering (TE) has emerged.

The new TE field has been outlined only since the mid-80's [2] and the first definition, reported in 1993 by Langer and Vacanti in the well-known Science paper [1], resumes the concepts of this discipline: "*Tissue engineering is an interdisciplinary field that applies the principles of engineering and life sciences toward the development of biological substitutes that restore, maintain, or improve tissue function*". This description pointed out the multidisciplinary approach occurring in TE: different scientists, such as chemists, physicists, biologists, engineers, physicians and surgeons need to closely cooperate, working together towards a common challenging effort.

The typical procedure of a TE approach starts from an *in vitro* cell culture onto a porous support (scaffold) made of a synthetic or natural bioresorbable material. The obtained cell-scaffold construct is then implanted *in vivo* and it is bioresorbed, while being replaced by the new natural extracellular matrix produced by cells.

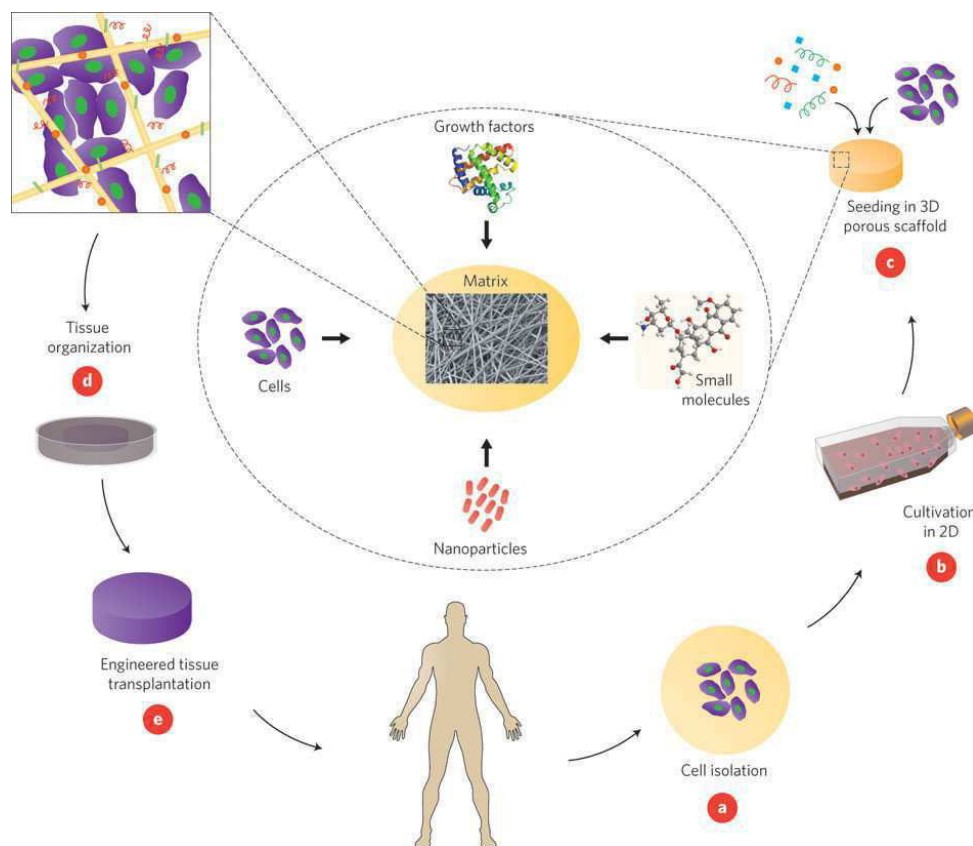


Figure 1.1 Representation of the tissue engineering concept. Reprinted from [3], Copyright (2011), with permission from Nature Publishing Group: Nature Nanotechnology

One of the major challenges of this science is to mimic nature as better as possible, to provide the best replacement or substitute for human care. This is a key target since it means better restoring or regenerative properties with lower immunogenic concern. Many cell types are used, they can be fully differentiated or stem cells, used in the field of regenerative medicine, they can migrate into the scaffold after its implantation from surrounding environment or they can be associated within the scaffold before implantation. TE and Regenerative Medicine (RM) deal with the transformation of these fundamental ideas to practical approaches.

TE uses synthetic or natural biodegradable scaffolding material, seeded with cells if necessary, to restore a damaged tissue or organ. RM, on the other hand, refers to multiple biomedical approaches to create living, functional tissues with the aim of repairing or replacing tissue/organ's functions that are lost due to age or diseases. Typically, the RM approaches involve the use of stem cells. It is therefore obvious that there isn't a clear distinction between TE and RM, the use of the two concepts remains often uncertain and scientists use the terms TE and RM interchangeably. TE should be considered a tool to perform RM, even if other methods can be used for RM [4]. A

difference that can be outlined between TE and RM is a more biological approach of the latter, leading to new potential applications of cell therapies and patient treatments [5].

Tissue engineering doesn't mean only restoring, maintaining, or improving tissue function, but it also deals with the developing of *in vitro* models for the study of basic biology and for drug discovery. Furthermore, stem cells culture and *in vitro* expansion onto scaffolds, can greatly reduce the need of tissue donors.

Some examples of engineered tissues concern skin substitutes, cartilage, corneal cell sheets, encapsulated pancreatic islets (i.e. Islets of Langerhans [6]), bone, bladder and blood vessels. Such tissues and organs replacement are already available and many studies are ongoing on that.

It is worth noting that strict requirements are needed for these materials in case of their commercialization and their use in clinic. The approving procedure is established by guidelines issued by national or international (World Health Organization: WHO) regulatory agencies. The most relevant agency is the Food and Drugs Administration of the United States [7] (U.S. FDA) that sets the standards to which many other agencies refer. The European Medicines Agency [8] (EMA) is the corresponding counterpart of FDA for the European Union, and the Agenzia Italiana del Farmaco [9] (AIFA) is the one for Italy.

Lots of products are already used in clinical application, but many others are in a proof-of-concept stage or they are waiting for approval. Furthermore, regulatory agencies, that must assess new therapies for safety and efficacy, have to be prepared to deal with sophisticated products. Indeed, FDA is always regarded as a model and a reference agency for its historical experience in novel products.

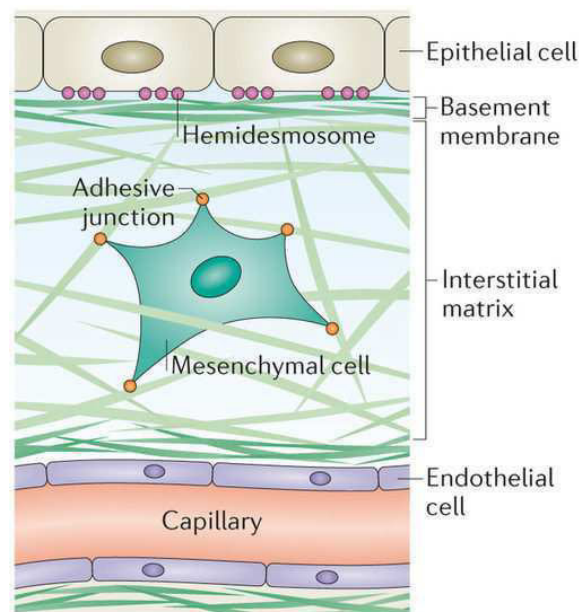
In conclusion, in an era of lacking of organs for transplantation and of growing need for replacements, TE gives hope to patients who urgently require tissue and organ substitutes.

1.2 The Extra Cellular Matrix

When performing tissue and organ replacement it is very important that scaffold for implantation or cell seeding mimics as much as possible the natural cellular environment. This may help to improve tissue regeneration/reconstruction and also to avoid scaffold rejection. Cells live in a complex matrix, the extracellular matrix (ECM), an environment made of different proteins which provide stimuli and signals for cell growth, division, differentiation, migration, and death [10] (Figure 1.2).

These signals include growth factors, differentiation factors, cytokines, and ion gradients [11]. Mechanical forces, electrical stimuli, and immobilized proteins, also regulate cell functions. In addition, a pivotal role of this matrix is its ability to provide structural support for cells. Due to this

complex combination of signals and structural properties fabrication of scaffolds that mimic the ECM represents a challenging endeavour.



Nature Reviews | Molecular Cell Biology

Figure 1.2 Schematic representation of ECM. Reprinted from [12], Copyright (2013), with permission from Nature Publishing Group: Nature Reviews Molecular Cell Biology

The ECM is composed of different biomacromolecules: collagen, glycoproteins, fibronectin, laminin, hyaluronic acid, proteoglycans, glycosaminoglycans, chondroitin sulfate proteoglycans and elastins. Furthermore it hosts growth factors, cytokines, and matrix-degrading enzymes and their inhibitors. The composition, distribution and organization of these molecules is dynamic and varies among different tissues. For example, the local concentration and biological activity of growth factors or cytokines can be modulated by the ECM, which serves as a reservoir to bind such molecules and protects them from degradation, to present them more efficiently to their receptors, or to affect their synthesis [13].

In the following paragraphs, a short description of the main proteins found in ECM is reported.

Collagen represents a wide family of different biomacromolecules counting at least 27 types, among collagens and proteins with collagen-like domains. They constitute one-third of all body protein [14]. Collagens make aggregates in combination with non-collagenous molecules to form macrostructures including fibrils, basement membranes, filaments, canals, and sheets.

Fibronectin is a glycoprotein, it can be found as soluble form in plasma and in insoluble form in loose connective tissues and basement membranes. Fibronectin is involved in cell migration, wound

healing, cell proliferation, blood coagulation and cell cytoskeleton maintenance. Fibronectin is the prototype for developing the RGD-peptides (L-arginine, glycine, and L-aspartic acid, Arg-Gly-Asp), widely used for artificial biomaterial functionalization to improve biomimetic properties [15].

Laminin is a common component of ECM found in basement membranes, it is used by many cell types for migration and it has a clear role in tissue morphogenesis. It is a favourite ECM substrate for neural cells [16].

Hyaluronic acid or hyaluronan is the only non-sulfated glycosaminoglycan and it is found in connective, epithelial, and neural tissues. A very important components of the extracellular matrix, hyaluronan contributes significantly to cell proliferation and migration.

Proteoglycans (PG) and Glycosaminoglycans (GAGs) are polysaccharides where the repeating unit is an amino sugar (N-acetylglucose amine or N-acetylgalactose amine) along with a uronic sugar (glucuronic acid or iduronic acid) or galactose [17]. Glycosaminoglycans interactions with fibroblast growth factor (FGF) have been implicated in cellular proliferation and wound repair [18]. Chondroitin sulfate proteoglycans (CSPGs) are proteoglycans (highly glycosylated proteins) consisting of a protein core and a chondroitin sulfate side chain. Chondroitin sulfate is a sulfated glycosaminoglycan. They are structural components of a large variety of human tissues, including cartilage. They are involved in cell adhesion, growth, receptor binding, cell migration [19]. They also interact with laminin, fibronectin, tenascin, and collagen.

Elastin is a protein of the connective tissue and it allows many tissues to recover their shape after extension. This protein is rich in hydrophobic amino acids such as glycine and proline, which form mobile hydrophobic regions bounded by crosslinks between lysine residues. Elastin is derived by cross-linking of soluble tropoelastin (water-soluble protein). Elastin is very important and common in tissue that require high elastic properties such as aorta, lungs, ligaments, skin, bladder, and cartilage [20].

One of the most relevant characteristic of ECM is its self-assembly property [21]. Protein and carbohydrate are secreted and ECM will self-associate in a highly ordered and predictable fashion that is specific of the tissue and the cell type producing the ECM. The interactions leading to self-assembly are based upon secondary and tertiary structures, which include charge properties, ion and metal bridges, hydrophobic domains, redox interactions, and covalent bonding. Self-assembly is prevalently conducted in the extracellular environment, but there is some evidence of assembly initiated during biosynthesis, thus in intracellular vesicles. Here, a “pre-assembled” matrix is created that induces faster rapid assembly when secreted into the extracellular compartment [22].

The structure of ECM and its complexity is fundamental because multiple biological processes require interactions between cells and in particular between the integrins (i.e. the transmembrane

cell receptors that mediate the attachment between a cell and its surroundings) and their external environment. Biomolecules derived from ECM can be used to coat and functionalize artificial scaffolds in order to modify their surfaces, thus improving cell growth and differentiation, selecting cell phenotype and directing their behavior.

1.3 Scaffolds for Tissue Engineering

Scaffolds play a key role in tissue engineering and their properties, often associated with the method of fabrication, are of fundamental importance in view of a successful tissue formation and regeneration. Tissue regeneration can be achieved by means of three basic approaches: (i) cell transplantation, (ii) scaffold-guided regeneration and (iii) cell-loaded scaffold implantation. The first one doesn't involve use of scaffold, but it is commonly used in regenerative medicine: healthy cells are transplanted by biopsy from a donor tissue, cells are expanded *in vitro* and then injected directly into the damaged tissue. With respect to this strategy, the use of scaffolds allows a more efficient and better targeted delivery of cells to the tissue to be regenerated.

Scaffold-guided regeneration makes use of a biodegradable scaffold directly implanted into the defect in order to promote tissue growth. For example this approach is used in case of peripheral nerve damage where a tubular scaffold connects the two nerve ends to guide regeneration. Another example involves bone defects, where a scaffold with the shape of the defect is usually implanted.

Cell-loaded scaffold implantation regards the seeding of cells, isolated from the patient, on a biodegradable scaffold. Then the cell-loaded scaffold is implanted into the defect in order to develop new functional tissue. Prior to implantation, the cells are usually cultured *in vitro*, in an environment that mimics the *in vivo* behaviour (through bioreactors, addition of growth factors and other nutrients [23], etc.).

Typical materials for tissue engineering scaffolds are synthetic polymers (polyesters, polyanhydrides, poly(ethylene glycol), polycarbonate, polyphosphazene, bioresorbable polyurethane, etc.), natural biopolymers (collagen, gelatin, fibrin, carbohydrates, etc.) and inorganic materials (hydroxyapatite, HA, tricalcium phosphate, TCP).

An ideal scaffold should be bi-dimensional (2D) or tri-dimensional (3D), highly porous, with interconnected pores and a large surface area. A porous structure is needed to supply adequate amount of nutrients and to allow disposal of metabolic waste by flow transportation, to achieve tissue regeneration through tissue in-growth. Furthermore, highly porous scaffolds allow cells to infiltrate and to obtain minimal diffusion constraints during cell culture. Due to high surface area-to-volume ratio, scaffold-cell interactions are maximised and vascularization is greatly favoured. It

has been reported that a porosity higher than 90% is preferable for tissue engineering applications [24]. However, it should be taken into account that the right porosity and pore size for tissue regeneration always depends on the type of tissue to be regenerated [25]. Indeed, scaffolds have been used with porosities varying from 55% to 74% for bone defect replacement, due to the achievement of better mechanical properties at lower porosities [26], and for bone regeneration pore sizes spanning over a very wide range (from 50 to 710 μm) have been suggested [24,27]. In the case of fibro-cartilaginous tissues the pore size requirement is in the range: 200 to 300 μm [28], whereas pores for vascularization are in the order of 5 μm [22].

The essential requirement of a scaffold is its biocompatibility. Biocompatibility means that the scaffold must not promote inflammatory response nor exhibit immunogenicity or cytotoxicity [29]. For example, poly(lactic acid) (PLA) is hydrolysed to lactic acid, a common by-product of muscle contractions in animals, which is further metabolized to carbon dioxide and water [30].

For TE applications, scaffolds have to be bioresorbable with a defined and adjustable degradation and resorption rate in order to match tissue growth rate, both *in vitro* or *in vivo*. Degradation rate also determines biocompatibility of implanted scaffold. Fast degradation could leave the new growing tissue without mechanical support prior to complete regeneration, moreover the surrounding tissue might not eliminate the by-products as fast as they are produced, leading to inflammation or toxicity [30,31]. Slow degradation, on the other hand, can hinder the growth of new tissue. To overcome this issue, biodegradation of synthetic polymeric scaffolds is usually tailored to match the requirement of mechanical support, by-products elimination and growth of new tissue. During scaffold degradation, cells are secreting their natural matrix and when the scaffold breaks down and disappears the new tissue will supply mechanical support by itself. Finally, biodegradability is a desirable factor because it avoids the problem of surgical removal.

The chemistry of scaffold's surface is a key aspect to take into account in scaffold design. In fact, since the scaffold must allow cell attachment, proliferation and differentiation, materials used for scaffold fabrication are critical because the nature of polymer surface can influence the ability of proteins and cells to attach to scaffold surface, then affecting proliferation and differentiation. For example, it is difficult to efficiently seed cells into scaffolds made of polymers with even relatively low hydrophobicity such as PLA and polyglycolic acid (PGA) [32]. For this reason different methods are commonly used to increase the hydrophilicity of polymeric scaffolds and to improve cell adhesion such as, among others: the use of hydrophilic polyvinyl alcohol (PVOH), pre-wetting with ethanol, hydrolysis with NaOH, oxidation with a perchloric acid mixture solution, oxygen or ammonia plasma discharge treatment, or adding cell adhesive proteins [33].

Not only surface chemistry but also bulk properties, such as mechanical properties, influence cell behaviour. Scaffolds have to match mechanical properties of the tissues at the implantation site in order to help regeneration by providing structural support during the early stages of tissue growth. If this match is missing, for example if the compressive strength of a scaffold is too low, the scaffold might be deformed or broken under mechanical stress and the tissue would grow deformed or it wouldn't grow at all. For the same reason, if the compressive strength is too high, cells might not develop in the proper way. Also the elastic modulus of the scaffolds is very important. Differences of elastic moduli between scaffold and tissue lead to different strain at the same stress and to scaffold delamination from the surrounding tissue. Furthermore, it was reported that undifferentiated cells cultivated on scaffolds with different elastic moduli could give distinct differentiation paths [34].

Finally, the need to produce scaffolds in a quite large amount to achieve off-the-shelf products should be taken into account. It is of fundamental importance that biomaterials for tissue engineering are cost-effective and with constant properties, because surgeons and patients need large supply of scaffolds with known properties and performances to meet the growing demand and to speed up research progress. Patient's needs cannot wait researchers that make scaffolds one by one at their research laboratory. "Accepting the challenge of imitating nature must include the development of cost-effective manufacturing processes" [35].

1.3.1 Scaffolds Fabrication

Since the mid-80s, many techniques have been developed to fabricate polymer scaffolds of complex architectures for the different tissue engineering applications [36].

Scaffolds for tissue engineering are usually fabricated with biocompatible polymers, proteins or inorganic materials. First of all, their properties depend by the material used, but scaffold fabrication techniques are equally important to determine their characteristics. Porosity, degradation rate, mechanical strength, surface chemistry and the possibility to host bioactive molecules (proteins, ECM-like peptides and DNA) are all influenced by fabrication methods. The incorporated bioactive molecules shouldn't be inactivated by fabrication techniques in order to perform their function by promoting cell adhesion, migration, proliferation and differentiation [37]. Moreover, a careful selection of polymers, additives and fabrication techniques allow to tailor scaffold characteristics for a precise application. Mechanical properties of scaffolds are a direct consequence and a combination of polymer bulk properties, scaffold geometry, incorporation of strength enhancing additives and the scaffold fabrication technique. The fabrication process should not affect biocompatibility and biodegradability because patient safety is the major concern for any

tissue engineering application. Crystallinity of polymers, for example, is affected by processing method. Polymers with higher crystallinity exhibit increased tensile strength at the expense of slower degradation rates, while lower crystallinity diminishes the strength of the scaffold and reduces the scaffold's lifetime. Every method has its own advantages and disadvantages, therefore the appropriate technique must be selected for every specific tissue.

This thesis is focused on polymers for tissue engineering applications therefore, both this chapter and the following one will only discuss polymers, both synthetic and natural, and the established processing methods for scaffold fabrication. These include Solvent Casting/Particulate Leaching, Gas Foaming, Gas Foaming/Particulate Leaching, Freeze-Drying, Rapid Prototyping of Solid Free Forms, Extrusion, Injection Molding, Melt Molding, Melt Spinning, Phase Separation, Fibre Bonding, Peptide Self-Assembly and In Situ Polymerization. Electrospinning, the technique applied in this Thesis for scaffold fabrication, will be deeply and separately described in chapter 1.3.2.

Solvent Casting/Particulate Leaching (SC/PL): This technique allows to manufacture scaffolds with controlled pore size, porosity, surface-area to-volume ratio and crystallinity.

A bioresorbable polymer, mostly poly(lactic acid) (PLA) or poly(lactic acid-co-glycolic acid) (PLGA), is dissolved in a proper organic solvent (usually chloroform, CLF, or dichloromethane, DCM). A water-soluble porogen, for example NaCl, is sieved to a desired size range and it is added to the polymeric solution, which is cast into a mould of desired shape and then dried. The salt is leached in water leaving a porous polymeric scaffold with an interconnected network [38]. Porosity can be controlled up to 93% with pore size up to 500 μm and crystallinity (i.e. toughness) can be adjusted by annealing prior to porogen leaching. For soft-tissue applications a tough scaffold has been obtained by using PLGA and poly(ethylene glycol) (PEG) blends [39]. Other biocompatible porogens can be used such as sugars [40] or lipids [41]. In order to improve hydrophilicity of scaffold, therefore cells attachment, pre-wetting with ethanol or coating with poly(vinyl alcohol) (PVA) has been used [42]. Two major issues about SC/PL concern residual organic solvents that may affect cell viability [29] and the removal of bioactive molecules previously added, during salt leaching.

Gas Foaming (GF): This technique avoids the employment of organic solvents by using a supercritical gas, usually CO_2 , to mould the polymeric material [43]. Polymer disks are saturated with CO_2 under high pressure, then a pressure drop leads to nucleation and pore formation due to thermodynamic instability in the polymer/gas phase. This phenomenon is controlled by setting the pressure value and its reduction rate. Scaffolds have porosities up to 97% with pore size ranging from 100 to 500 μm . The process avoids high temperatures, thus allowing the incorporation of

bioactive molecule. The major drawback of this technique is the low interconnectivity of pores. Gas foaming technique with incorporation of particles followed by leaching demonstrates the creation of an interconnected network among pores, i.e. *Gas Foaming/Particulate Leaching (GF/PL)* [44], to overcome drawbacks of the SC/PL (i.e. organic solvents) and GF (i.e. poor interconnectivity).

Emulsion Freeze-Drying (EFD) and Freeze-Drying (FD): The emulsion freeze-drying (EFD) is a rapid method for fabrication of scaffolds with tuneable porosity and pore diameter, with an interconnected porous structure. A polymeric solution in organic solvent (example, PLGA in DCM) is mixed with double distilled water (ddw) and emulsified until homogeneity is achieved. The polymer solution is the continuous phase, while water is the dispersed phase. The emulsion is poured into a metal mould and rapidly frozen with liquid nitrogen. Now, DCM and water are sublimated under reduced pressure to obtain the scaffold [45]. The porosity is up to 90% and pore size around 13-35 μm and these parameters are adjustable by varying solvents, polymer, and their ratio. Scaffolds thicker than 1 cm can be fabricated by EFD.

Freeze-drying (FD) doesn't involve emulsification. Synthetic polymers are dissolved in organic solvents, frozen and then freeze-dried [46]. Such method is also used for collagen scaffolds fabrication by dispersing it in water and freeze-drying the suspension [47]. Ice crystals generate the pores and their size is determined by freezing rate, temperature, ionic concentrations, and pH.

Rapid prototyping of solid free forms (RP-SFF): RP-SFF are a family of scaffold production techniques developed in late 1980s through early 1990s. These techniques need computer aided design (CAD) programs to model a specific three-dimensional structure, therefore scaffolds are created by a Rapid Prototyping (RP) technique. RP techniques include *three-dimensional printing*, *laser sintering*, *stereolithography* and *fused-deposition modelling (FDM)*. The main advantages of RP-SFF are accurate control over porosity, pore size, pore shape and interconnectivity.

Three-dimensional printing utilizes a inkjet printer guided by CAD program. A thin layer of polymer powder is deposited on a piston surface. The inkjet dispenses a solvent for the polymer, by following the pattern of the scaffold, to bind together polymer particles. After a short bonding time, the piston is lowered by a single layer thickness and another layer of polymer powder and binding liquid is applied. The process is repeated until the 3D model created by the CAD software has been completed [48]. *Laser sintering* is similar to three-dimensional printing, but a high-powered laser is used instead of solvents to sinter the polymer particles. Particles fuse together because laser heats the polymer above its melt temperature [49]. *Stereolithography* uses light to polymerize or cross-link a photosensitive material. A fine layer of polymer solution and photo-crosslinking initiating agent (or a photocurable resin) are placed on a moveable platform. The photo-initiator reacts under UV light to form chemical bonds between polymer chains, while the platform is moved under CAD

software guide. To obtain 3D structures, consecutive layers of polymer solution are added and the process repeated [50]. *Fused-deposition modelling (FDM)* is a combination among extrusion and melt moulding (see below) with free-form scaffold fabrication. The polymer is heated and extruded through a nozzle fixed into a computer-controlled head, moving in the x-y plane. Each layer is deposited on a platform moving in the z axis. After a layer is cooled, platform is lowered and process is repeated until the 3D structure is completed [51].

Extrusion: Extrusion is a continuous fabrication method used to process polymers [52]. The pellets of polymer are melted, while a rotating screw homogenizes and pushes the melt through a die. Choosing the type of die allows to obtain various shapes such as tubing, pipe, film, sheet or wire. Extrusion produces non-porous morphology and for this reason different extrusion methods were developed to obtain porous scaffolds. They are similar to Particulate Leaching because the polymer is co-extruded with salts (NaCl [53]) or with a water soluble polymer (Poly(ethylene oxide) PEO [54]) and then the scaffold is immersed in water to leach away the soluble fraction.

Injection Moulding: Injection moulding is a process to form scaffolds by injecting and forcing polymers into a mould of the desired shape [55]. To get the desired shape, polymers are cooled, if thermoplastics or cured if they are thermosetting. Injection moulding doesn't allow the formation of porous structures therefore a wide range of processes were developed by using foaming or blowing agents [56].

Melt Molding: In this technique a polymer and porogen particles are combined in a mould and heated. For amorphous polymers above the glass transition temperature (T_g), while for semicrystalline polymers above the melting temperature (T_m). A cooling step is needed for the polymer to retain the shape prior to removing it from the mould, then the scaffold is soaked in an appropriate solvent to leach out the porogen [57]. This technique allows the filling of scaffolds with reinforcement or bioactive molecules.

Melt Spinning: Melt spinning is a technique for polymer fibres fabrication that is commonly used for sutures. Melt polymers are extruded from a spinneret, a wire is formed, then cooled with air, and wound onto spools. Polymers can be spun in monofilament or multifilament yarns, depending on the number of spinnerets, and fibres can be processed further, such as by texturizing, weaving, or braiding. Limit diameter of meltspun fibres fabrication is 10-12 μm .

Phase Separation: Phase separation is a potential technique to deliver drugs or bioactive molecules from a degradable tissue-engineering scaffold and prevent denaturation by harsh organic chemicals or temperatures. For example, a bioresorbable polymer is dissolved in an appropriate solvent and the bioactive molecules are added and dispersed by stirring. Mixture is cooled below solvent freeze

temperature until the liquid phases separate. The solvent is removed by sublimation, resulting in the formation of a porous scaffold with embedded bioactive molecules [58].

Fiber Bonding: Polymer fibers exhibit very high surface area to volume ratio, that greatly influence cell behaviour and enhance cell attachment. Non-bonded fibers lack in mechanical integrity for application in tissue engineering, but this problem was overcome by binding fibers together [59]. For example, PGA fibers are arranged in a nonwoven mesh and heated, hence fibers will bond at their contact points. To preserve the structure from collapse, PGA fibers are embedded in PLLA. PLLA is dissolved in methylene chloride, a non solvent for PGA, cast over the fibers and dried, resulting in a PGA-PLLA composite matrix. After fiber bonding, the PLLA is removed by dissolving it. Scaffold fabrication by fiber-bonding is simple, compatible with a wide range of materials, but it suffers of control over porosity and pore size.

Peptide Self-Assembly: Natural peptides such as collagen, gelatin, and fibrin self-assemble to form ECM. Many studies were conducted to develop synthetic peptides that can interact favourably to form self-assembled scaffolds that mimic ECM [60]. Self-assembling peptides are usually ionic and complementary sequences of alternating hydrophobic and hydrophilic domains with non-covalent bonds and ionic interactions within and between peptides. Peptide scaffolds have been tested in different *in vitro* cell culture, using for example osteoblasts, chondrocytes, and hepatocytes.

In Situ Polymerization: In situ polymerization offers a different strategy of scaffold fabrication. In this case a polymer or hydrogel is injected within a defect and polymerized or cured. This technique is useful in many orthopaedic procedures, when defects are of irregular or unpredictable shape. For example, polymeric bone cements are directly injected into bone fracture and they can also include an inorganic phase, such as β -tricalcium phosphate [61]. Hydrogels are usually used in soft tissue. The materials injected can be crosslinked to increase mechanical stability.

1.3.2 Electrospinning

Electrospinning (ES) is a processing technique that uses electrostatic forces to uniaxially stretch a viscoelastic jet derived from a polymer solution or melt. Continuous fibres with diameters ranging from tenth of nanometers to few micrometers are produced, typically assembled into a non-woven mat (Fig. 1.3). ES is mainly used for polymers, both synthetic and natural, although inorganic fibers can also be obtained. The first polymeric fiber production through ES was described by Anton Formhals in 1934 [62]; however, it was only in the 1990s that the technique raised the interest of academic research groups, first of all the Reneker's group at the University of Akron that contributed to its spreading in research institutes all around the world [63]. Since then, interest

about ES increased exponentially, for applications in several sectors such as filtration, textile, tissue engineering and composite materials [64].

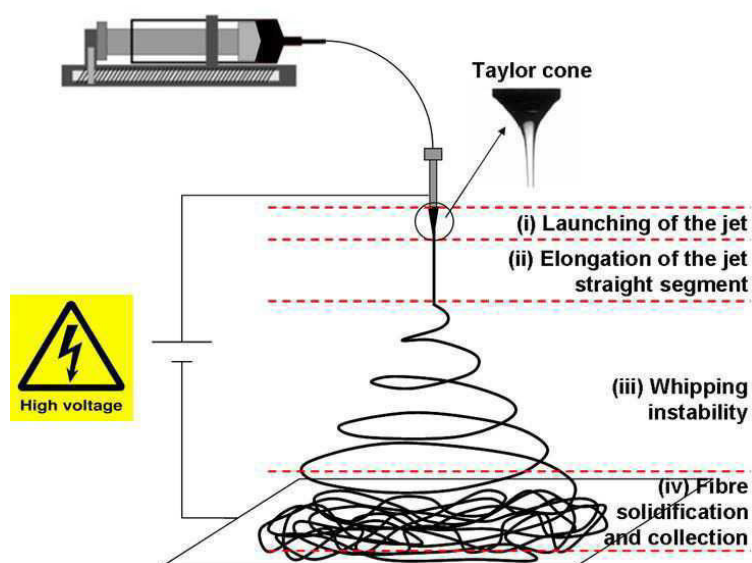


Figure 1.3 Schematic representation and description of the ES process

In principle, ES is a simple process where an electric field (usually of 10-30 kV) is applied to a polymeric solution that comes out from the tip of a metallic needle, which acts as one of the electrodes. The high voltage applied leads to deformation of the solution drop (called Taylor cone) and finally to the ejection of a charged polymer solution jet from the tip of the cone, accelerating towards a counter-electrode. The jet undergoes an instability and an elongation process, becoming very long and thin. Meanwhile, the solvent evaporates leading to the formation of continuous solid fibers (Figure 1.3). In a typical laboratory apparatus, the counter-electrode is placed at the distance of 10-30cm from the needle tip and fibers are collected on its surface as a nonwoven mat.

Feasibility of the ES process and morphology of the obtained fibers depend on many different parameters. These parameters include: (1) polymer properties (such as solubility, molecular weight, molecular-weight distribution, solid-state properties); (2) polymer solution properties (such as viscosity, viscoelasticity, polymer concentration, surface tension and electrical conductivity); (3) instrumental parameters (such as feed rate of the solution, applied voltage and needle-to-collector distance); (4) temperature and relative humidity of the surrounding environment.

The physical phenomena behind ES and fiber formation are related to interactions of different physical instability processes [65]. The first is the classical Rayleigh instability, which is axisymmetric with respect to the jet line and it is independent from the electric field; the second one is again an axisymmetric instability, related to a statistical variation of the jet's radius that causes a

modulation of the surface charge density; the third one is a non-axisymmetric instability, called “bending” (or “whipping”) instability and it is a consequence of charge repulsion. Bending instabilities occur at high charge densities and high electric fields, and they are typically enhanced by increasing the electrical conductivity of the polymer solution through the addition of additives or by using solvents with high dielectric constant. A straight jet that is subjected to these instabilities turns sideways and forms loops in the horizontal plane. The loop diameter increases during the motion towards the counter-electrode and during this path the jet is highly stretched and reduced in diameter.

Loosely interconnected fibrous mats with high porosity and high surface area are produced through the electrospinning technique. These meshes resemble the structure of the natural environment of cells, i.e. the extra cellular matrix, and for this reason electrospun mats are considered excellent candidates in the tissue engineering field as scaffolds for cell culture [66].

1.3.3 Electrospun fiber functionalization

Surface modification of electrospun fibers with suitable bioactive molecules and cell recognizable ligands is a common method used to obtain scaffolds with more desirable biological features for biomedical applications. Surface functionalized electrospun fibers can be employed in tissue regeneration processes or in drug delivery applications (e.g. biodegradable polymers can be loaded with anti-cancer drugs). In this chapter various functionalization strategies of electrospun nanofibers will be shortly described [67] (Figure 1.4).

Plasma treatment: Plasma treatment has been commonly used to change surface chemical composition of materials. By selecting the right plasma source and the correct gas of the plasma treatment, different functional groups can be introduced on fibers surface. The common plasma treatment with oxygen or air generates carboxyl groups at the surface of the material, whereas in the presence of nitrogen or ammonia, amine groups, among others, are formed. Carboxyl and amino groups are the desired ones for further conjugation reactions with bioactive molecules and drugs.

Wet chemical method: This procedure is mainly used for polyesters. For these polymers a chemical scission of the ester bonds in the chain results in the generation of carboxyl and hydroxyl groups. Typical reagents used in the wet chemical approach are NaOH or diamines and in the latter case the reaction is called aminolysis and it creates amine functionalized surfaces.

Surface graft polymerization: With this method a monomer is directly polymerized on the fiber surface through plasma or UV radiation. Free radicals are generated, that induce monomer polymerization. This method is often used to increase the surface hydrophilicity of synthetic

polymeric fibers and to introduce functional groups on the fiber surface for further immobilization of bioactive molecules.

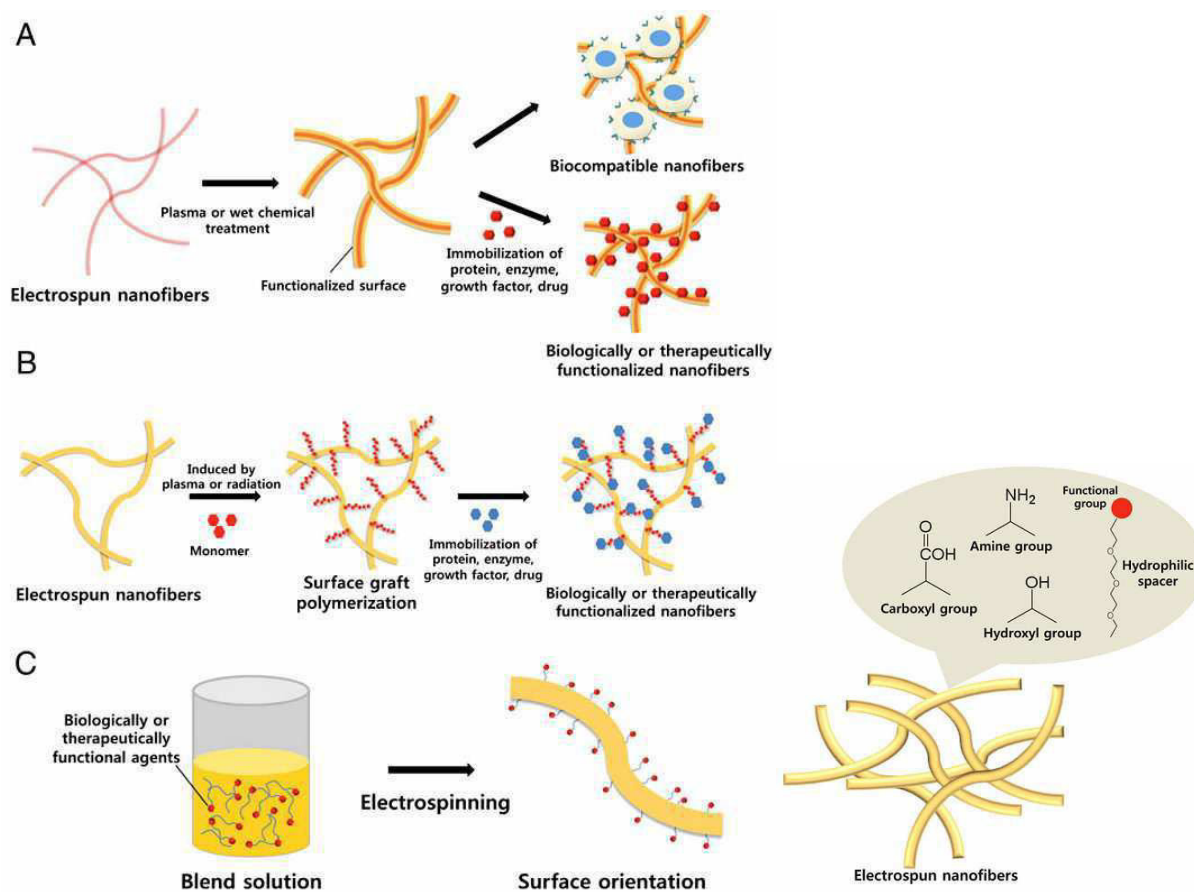


Figure 1.4 Surface modification techniques of electrospun nanofibers. (Left) (A) Plasma treatment or wet chemical method. (B) Surface graft polymerization. (C) Co-electrospinning. (Right) Surface functional groups used in chemical immobilization of bioactive molecules. Reprinted from [67], Copyright (2009), with permission from Elsevier: *Advanced Drug Delivery Reviews*.

Physical adsorption: The simplest approach for loading drugs or biomolecules at the surface of nanofibers is physical adsorption, that is driven by electrostatic interactions, hydrogen bonding, hydrophobic interactions and van der Waals forces. Electrospun fibrous mats can be used to physically adsorb molecules on their surface due to their high surface area to volume ratio, resulting in high amount of loaded drug per unit mass.

Chemical immobilization: Chemical immobilization of bioactive molecules through covalent bonds offers the advantage of higher stability with respect to physical immobilization. Primary amines and carboxyl groups are the most common functionalities used to immobilize molecules onto the

surface of nanofibers. This method is suitable for the attachment of small molecules, although polypeptides or proteins can also be grafted (Figure 1.4).

Blend electrospinning: While the above described surface modification methods are used for prefabricated electrospun nanofibers, bioactive molecules, nanoparticles, or functional polymer segments can be directly exposed at the surface of nanofibers during scaffold fabrication by means of the blend electrospinning method (or “co-electrospinning”). In this approach functional molecules or nanoparticles are blended with a carrier polymer and then electrospun. This method enables to exploit the properties of the carrier polymer in term of mechanical and structural stability and the properties of the added nanoparticles, biomolecules or functional polymer segments in term of favourable interactions with the surrounding environment or cell culture.

1.4 Synthetic and Natural Polymers

The previous paragraph reported common methods of scaffolds fabrication and functionalization, while this section will focus on materials. Although a wide range of materials can be employed, both inorganic and organic, in this paragraph only the major natural and synthetic polymeric materials used as biomaterials will be reported.

1.4.1 Synthetic polymers

Synthetic polymers are advantageous with respect to natural polymers since they possess controllable properties (e.g. mechanical and degradation properties), that can be tailored to meet the specific application required. The most common synthetic polymers used as biomaterials in tissue engineering are polyesters, but others polymers are also used such as: polyanhydrides, polycarbonates, polyphosphazenes and polyurethanes. One of the major drawbacks of the use of synthetic polymers is the release of polymer degradation products, that can result in adverse responses such as inflammation [68] (Figure 1.5).

Polylactic acid (PLA): PLA is a linear poly(α -hydroxy acid) that is synthesized by ring opening polymerization of lactide or condensation of lactic acid [69]. The monomer is derived from corn starch and it consists of two stereoisomeric forms: L-lactide and D-lactide, giving origin to the two homopolymers Poly-L-lactic acid (PLLA) and poly-D-lactic acid, respectively. Copolymers obtained from a mixture of D,L-lactides (poly-D,L-lactic acid) are amorphous when the D-lactide units are present in the copolymer in an amount higher than 15%. PLA has a melting point in the region of 170-180°C, a glass transition around 56-62°C and it can reach a crystallinity degree of

more than 40%. Despite PLA exhibits hydrophobic nature, it is suitable for cell culture and it is widely used in biomedical field for scaffold fabrication. Hydrolytic degradation of PLA occurs with lactic acid release, which is resorbed and metabolized, even if high concentrations can induce inflammation.

Polyglycolic acid (PGA): PGA, as PLA, is a linear aliphatic polyester of the poly(α -hydroxy esters) family and it is produced by ring-opening polymerization of cyclic diesters of glycolide. PGA is a semicrystalline polymer with a melting point between 185 and 225°C, a glass transition of 36-40°C and a low solubility in organic solvents. PGA is hydrophilic and undergoes bulk degradation with glycolic acid release, which is metabolized by the body. The drawback of glycolic acid is the possible inflammation reactions in the surrounding tissue.

Poly(lactic acid-co-glycolic acid) (PLGA): PLGA represent a family of random copolymers of LA and GA units. Copolymer having LA:GA ratio of 50:50 is amorphous, with much higher degradation rate compared to PLLA, and it usually undergoes bulk degradation by hydrolysis. The degradation rate of PLGA can be tailored by adjusting the LA:GA ratio.

Poly(ϵ -caprolactone) (PCL): PCL is a semicrystalline polymer prepared by ring-opening polymerization of cyclic ϵ -caprolactone. The glass transition temperature is around -60°C and the melting temperature is approximately at 59-64°C. PCL degrades very slowly, in a time scale of about 2 years, and it is therefore suitable for long-term implants. When it is copolymerized with different polymeric units (e.g. LA units), lower degradation rates are obtained [70].

Polyorthoester (POE): POE are polymers synthesized by reacting ketene acetals with diols. They have an hydrophobic nature and degrade through a surface erosion. Degradation rate can be tailored by incorporating glycolic or lactic acid units.

Polyanhydrides: Polyanhydrides are hydrophobic polymers containing anhydride bonds, synthesized by a dehydration reaction between diacids. Polyanhydrides are semicrystalline polymers with a melting temperature around 100°C. The labile anhydride bond allows polyanhydrides to rapidly degrade (degradation might occur within a few weeks).

Polyphosphazene: Polyphosphazenes are inorganic polymers containing nitrogen and phosphorous atoms in the backbone. They typically undergo surface hydrolytic degradation, with release of phosphate and ammonium as by-products. Polyphosphazenes properties can be tailored by acting on their chemical structure and in particular on the substituents on the phosphorous atoms.

Poly(ethylene glycol)/Poly(ethylene oxide) (PEG)/(PEO): PEG is linear polymer consisting of ethylene oxide repeating units. PEO backbone is the same as PEG, they differ for the molecular weight, which is higher in PEO with respect to PEG. PEG is often used as hydrogel, but its low mechanical stability limits its applications. Functional groups can be attached to the terminal units

of the PEG chain to achieve covalent cross-linking. PEG is a non-degradable polymer, however PEG degradation can be achieved by copolymerization with hydrolytically or enzymatically degradable polymers. PEG has received great attention because of its potential applications as biomaterial and as a hydrophilic polymer spacer that is easily chemically conjugated to various hydrophobic polymeric.

Polyurethanes (PU): Polyurethanes are elastomeric polymers usually non-degradable. PU are characterized by high flexibility and mechanical strength, together with very good biocompatibility.

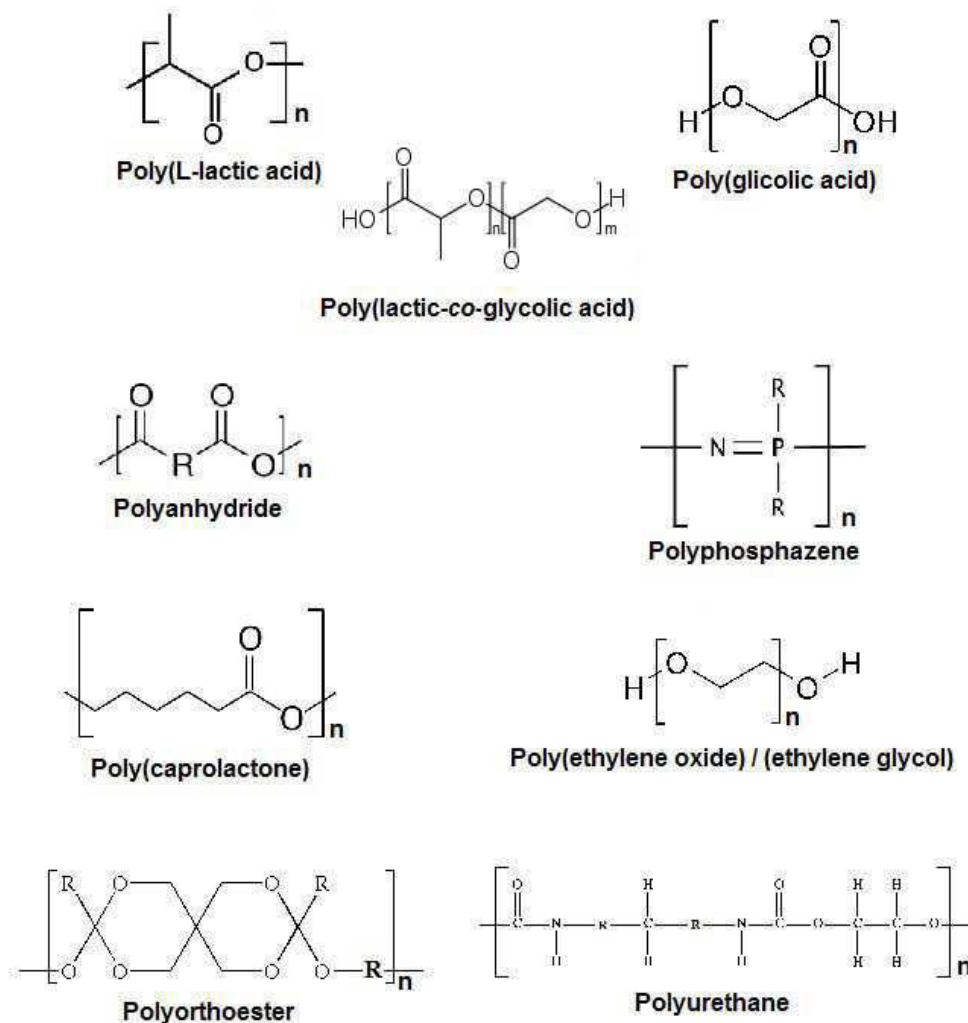


Figure 1.5 Repeating units of degradable synthetic polymers used for tissue engineering applications

1.4.2 Natural polymers

The two major classes of natural polymers used in tissue engineering are polypeptides and polysaccharides. The main advantages of using natural polymers instead of synthetic polymers are that natural polymers are highly biocompatible, they display unique bioactivity and excellent cellular affinity and they are enzymatically biodegradable. On the other hand, disadvantages of

using natural polymers are related to the poor control of their degradation rate and to the fact that their properties might not be consistent within different batches of materials. Additionally, natural polymers lack of mechanical strength, even if this is usually overcome by cross-linking to enhance their structural stability.

In Figure 1.7 the structures of the main natural polymers used in tissue engineering are reported.

Agarose: Agarose is a water soluble polysaccharide extracted from algae. It consists of an alternating linkage of 1,4-linked 3,6 anhydro- α -l-galactose and 1,3-linked β -d-galactose, Agarose is mainly used to prepare gels where cells grow in a three-dimensional suspension. In its native state it is enzymatically degraded by agarases.

Hyaluronic Acid (HA): Hyaluronic acid or hyaluronan is a natural polysaccharide with a $\beta(1-3)$ linkage of two sugar units: d-glucuronate and N-acetyl-d-glucosamine. HA is a glycosaminoglycan highly abundant within the extracellular matrix, it is non-immunogenic thus it is very attractive for biomedical applications. The major disadvantages of HA are its highly solubility in water and the rapid degradations by enzymes, such as hyaluronidase.

Chitosan: Chitosan is chitin partially deacetylated and it is found in the exoskeleton of crustaceans and insects. It is a linear polysaccharide composed of $\beta(1-4)$ linked d-glucosamine with randomly dispersed N-acetyl-d-glycosamine groups. Chitosan is used as sponges or hydrogels, that can be crosslinked (usually with glutaraldehyde) to improve structural stability. Like other polysaccharides, chitosan is degraded by enzymes, in this case chitosanase and lysozyme.

Collagen: The most abundant proteins in the extracellular matrix and the major structural constituents of the connective tissues are collagens. Nowadays, 26 different types of collagen are known. Collagen consists of three polypeptide α -chains assembled through hydrogen bonds to form a triple helix. These chains have a repeating triplet of glycine-X-Y, where X and Y are usually proline and hydroxyproline. Collagens can be divided into different families such as fibril-forming collagens, fibril-associated collagens (FACIT), network-forming collagens and others, but fibril-forming collagen represents about 90% of the total collagen [71]. Collagen types I, II, III, V and XI are fibril forming collagens. Type I collagen is the most abundant, it is found in bones [72], tendons, skin, ligaments, cornea, and many interstitial connective tissues. Collagen is able to assemble into highly orientated supramolecular aggregates (collagen quaternary structure), with fibril diameters ranging between 25 and 400 nm (Figure 1.6). These fibrils have a characteristic banding pattern with a periodicity of about 70 nm, called the D-period. Fibrils are stabilized by intra-chain disulphide bonds, that make collagen non soluble in water. Collagen is widely used as

scaffold in form of sponges, hydrogels or sheets, that can be crosslinked by different methods, such as glutaraldehyde, genipin or EDC/NHS.

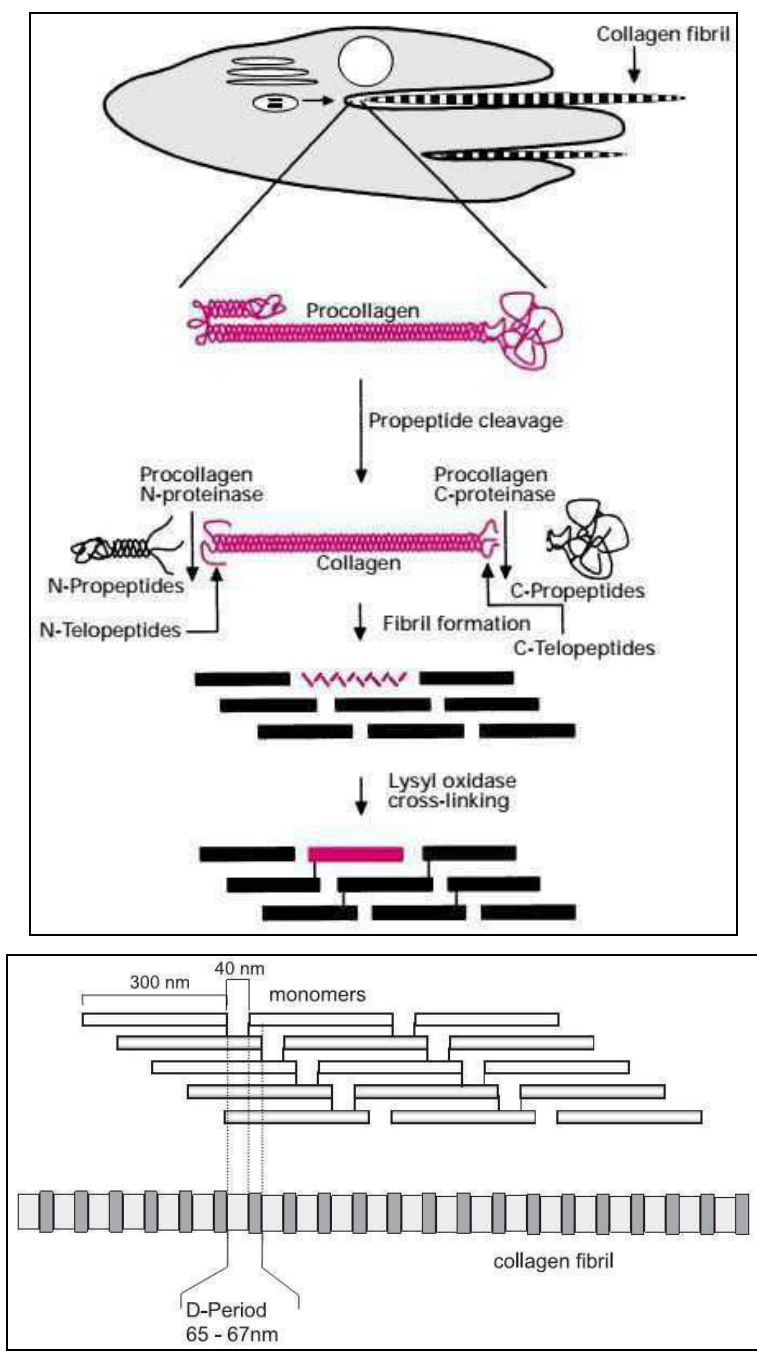


Figure 1.6 (Top) Extracellular events of collagen synthesis and fibril formation. Reprinted from [73], Copyright (1996), with permission from Portland Press Limited: Biochemical Journal; (below) Schematic representation of the supramolecular assembly of the collagen fibrils. Reprinted from [71], Copyright (2003), with permission from Elsevier: Advanced Drug Delivery Reviews

Gelatin: Gelatin derives from collagen denaturation, through breaking of collagen triple-helix structure into random coils of single α -chains. This can be done by thermal denaturation or physical

and chemical degradation. Gelatin is water-soluble and it forms gel through temperature changes, depending on the concentration. This occurs when aqueous solution of gelatin (sol state) are cooled and a physical thermo-reversible gels is formed. During the gelling process the α -chains undergo a conformational transition from disorder to order and the collagen triple-helix structure is partially recovered. Gelatin is broken down enzymatically by various collagenases. Stabilization of gelatin hydrogels, as for collagen, can be obtained through cross-linking with chemical agents, mostly glutaraldehyde [74], but EDC/NHS [75] and genipin [76] are also used.

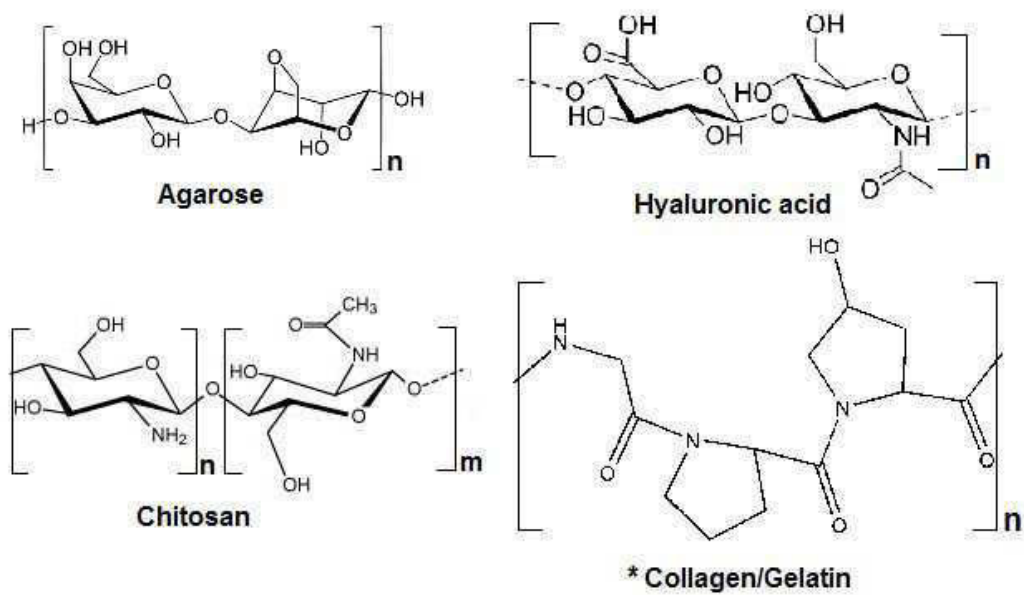


Figure 1.7 Repeating unit of natural polymers used for tissue engineering applications. (*Collagen and gelatin have variable sequences, but they are predominately constituted by glycine, proline, and hydroxyproline)

2 Materials and Methods

2.1 Materials

The following polymeric materials were used for scaffold fabrication:

- PLLA Lacea H.100-E ($M_w=8.4 \times 10^4$ g/mol, PDI = 1.7), supplied by Mitsui Fine Chemicals (Dusseldorf, Germany)
- Type A Gelatin (280 Bloom, Italgelatine SpA) from porcine skin [77].
- Acid soluble collagen type I (Coll) extracted from bovine skin, supplied by Kensey Nash Corporation (Exton, USA)
- Polysophorolipid - p(SL) ($M_n=60000$ g/mol and PDI = 1,6) - kindly provided by Prof. R.A. Gross, Dept. of Chemistry & Chemical Biology of the Rensselaer Polytechnic Institute (Troy, NY, USA). The p(SL) was synthesized by Ring Opening Metathesis Polymerization (ROMP) of the lactonic sophorolipid (LSL) with Grubb's catalysts [78]. The polymer, in the form of powder obtained by precipitation in ethanol, was kept in vacuum under P_2O_5 for 48 hours at room temperature (RT) prior to analysis. The LSL was produced by a fermentation process with the yeast *Candida bombicola* [79]. More detailed information are provided in part D of the Results and Discussion chapter.
- The oligopeptide used for p(SL) fibers functionalization was also provided by Prof. R.A. Gross (Figure 3.4.12)

The following solvents were used: Chloroform (CLF), Dichloromethane (DCM), N,N-dimethylformamide (DMF), Tetrahydrofuran (THF), Acetic acid (AcOH), 2,2,2-Trifluoroethanol (TFE) and Ethanol (EtOH).

The following reagents were used: Rhodamine B, Fluorescein isothiocyanate (FITC), Genipin, 1,4-butanediol diglycidyl ether (BDDE), 1-Ethyl-3-(3-dimethylaminopropyl)carbodiimide (EDC), Sodium Periodate ($NaIO_4$), Sodium Cyanoborohydride ($NaCNBH_3$), Cysteamine (CA).

All chemicals were purchased from Sigma-Aldrich, except Genipin that was purchased from Wako Chemicals USA Inc., and they were used without further purification.

2.2 Scaffold fabrication by electrospinning

The electrospinning (ES) apparatus used is made in house and the setup, with the main components, is schematically illustrated in Figure 2.1 and Figure 2.2. The system is composed of a high-voltage power supply (Spellman, SL 50 P 10/CE/230), a syringe pump (KD Scientific 200 series), a glass syringe containing the polymeric solution, a stainless-steel blunt-ended needle (Hamilton) that is vertically placed on an aluminium collector at a distance of 10 to 20 cm, depending on the experimental conditions used (see Results and Discussion section). The power supply electrode is connected to the needle, while the collector is connected to the ground. The apparatus is placed into a glove box (Iteco Eng., Ravenna, Italy) to enable temperature and humidity control.

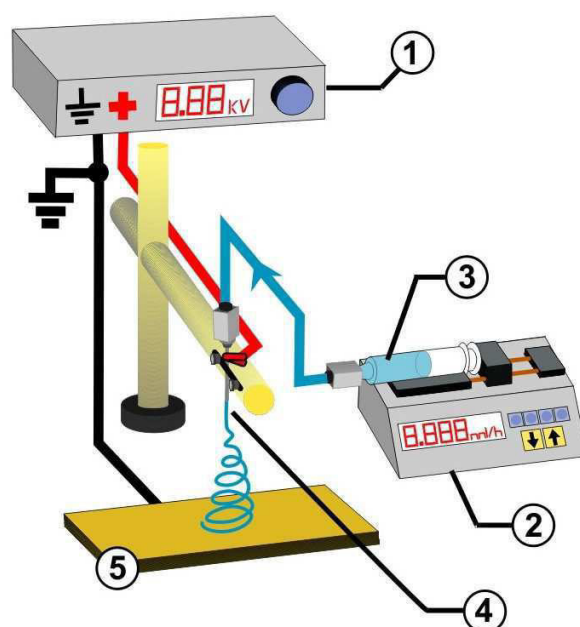


Figure 2.1 Scheme of the electrospinning setup: (1) high voltage power supply, (2) syringe pump, (3) syringe, (4) stainless-steel needle, (5) rotating cylindrical collector.

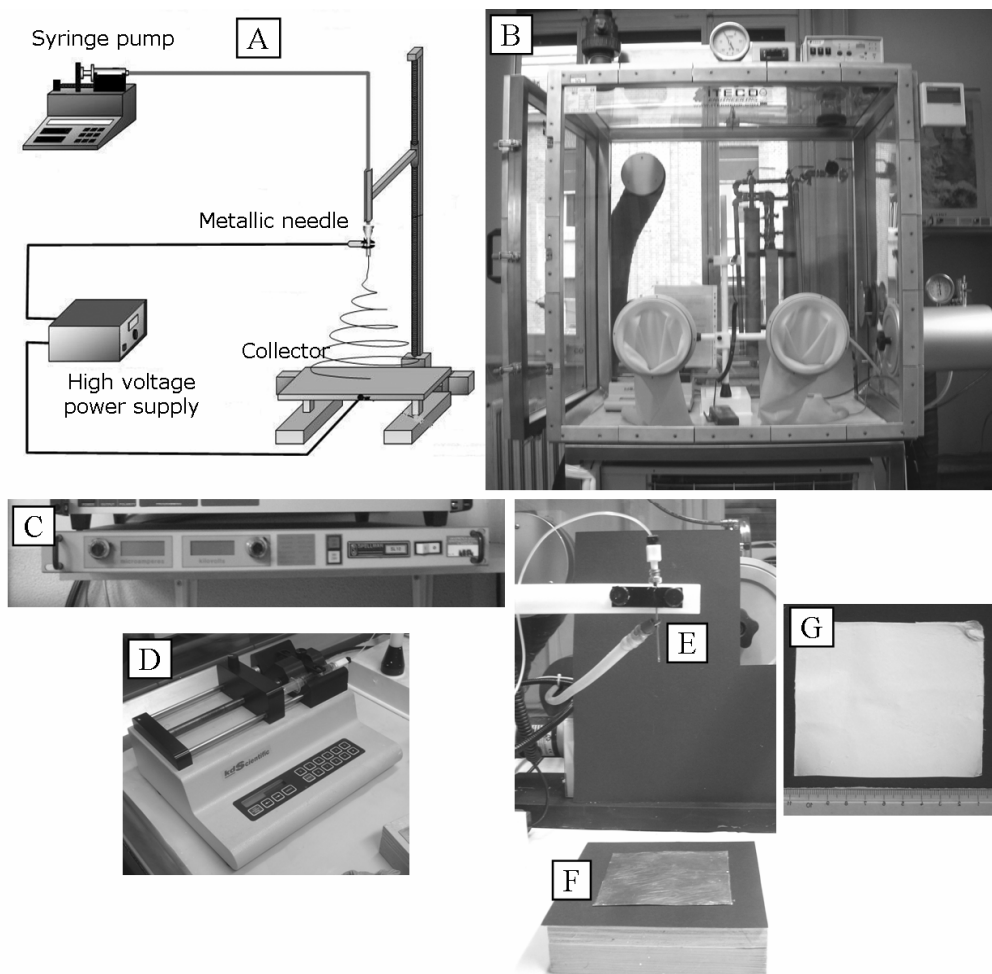


Figure 2.2 A) Scheme of the ES process, B) glove box containing the ES apparatus composed of: C) high voltage power supply, D) syringe pump, E) metallic needle and F) collector. G) picture of ES mat deposited on aluminium plate collector (10 x 10 mm).

2.2.1 Co-electrospinning

The apparatus to perform co-electrospinning (co-ES) is shown in Figure 2.3. An aluminium rotating mandrel (length = 12 cm, diameter = 5 cm, rotational speed 2.1 m/s) is used as the collector. Two polymeric solutions, whose feed rates are independently controlled by two syringe pumps (KD Scientific 200 e 100 series), are dispensed through a Teflon tube to two needles that are positioned on opposite sides of the collecting mandrel. Needle-to-collector distance is fixed at 15 cm.

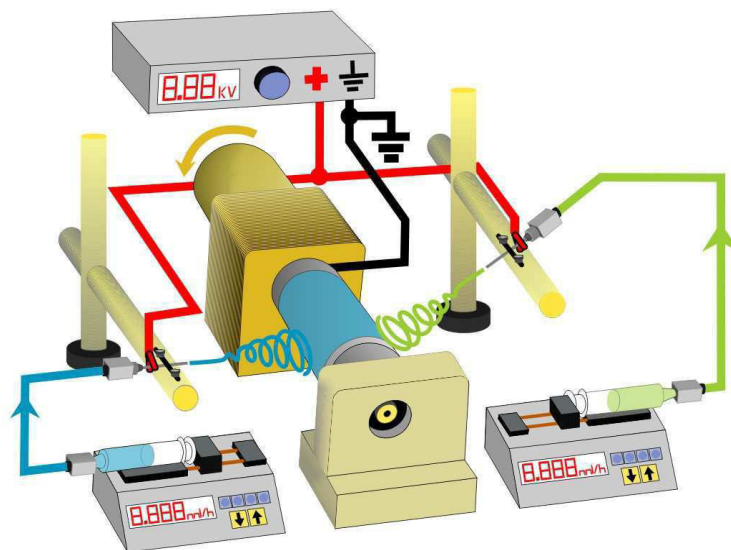


Figure 2.3 Scheme of the co-electrospinning setup arrangement

2.3 Scaffold Functionalization

Part of the research work of the present Thesis deals with surface post-functionalization of the electrospun fibres to enhance their biomimetic properties. Surface functionalization was achieved by means of two different methods: (i) non-thermal atmospheric plasma treatment and (ii) chemical reaction to covalently functionalize the fibres surface.

2.3.1 Non-thermal atmospheric plasma treatment

Plasma treatment of electrospun PLLA (ES-PLLA) scaffolds and PLLA films was carried out at the Industrial Engineering Department (DIN) of the University of Bologna by the group of Prof. Vittorio Colombo, by means of a Linear Corona (LC) plasma source mounted on a shaft moved at a controlled speed by a motorized linear stage (Figure 2.4). The LC plasma source is composed of a housing made of dielectric material and a sharp stainless steel blade, 36 mm wide and 0.1 mm thick, as the high-voltage electrode; the housing is provided of a gas inlet, a compensation chamber and two parallel gas channels to feed a uniform gas flow to the electrode region. In order to generate a uniform glow discharge and deliver a uniform treatment of ES-PLLA scaffolds and PLLA-film, the LC plasma source was driven by a nano-second pulsed generator (FID GmbH–FPG 20–1NMK) having peak voltage (PV) 7–20 kV into a 100–200 Ohm load, pulse repetition frequency (PRF) 83–1050 Hz, pulse width 12 ns and rise time 3 ns. Plasma treatment results described in this study were performed at PV 20 kV, PRF 1 kHz; N₂ (Air Liquide, 99.8% purity, O₂ impurities <100 ppm v/v, H₂O impurities <40 ppm v/v) was employed as the plasma gas with a 5 slpm flow rate; the

treatments were performed after flushing the gas line for 5 min. The distance between source and substrate was kept constant at 2 mm and the plasma source was moved at 1 mm s^{-1} speed; plasma treatment time was 20 s. After plasma treatment all materials were kept at RT in air.

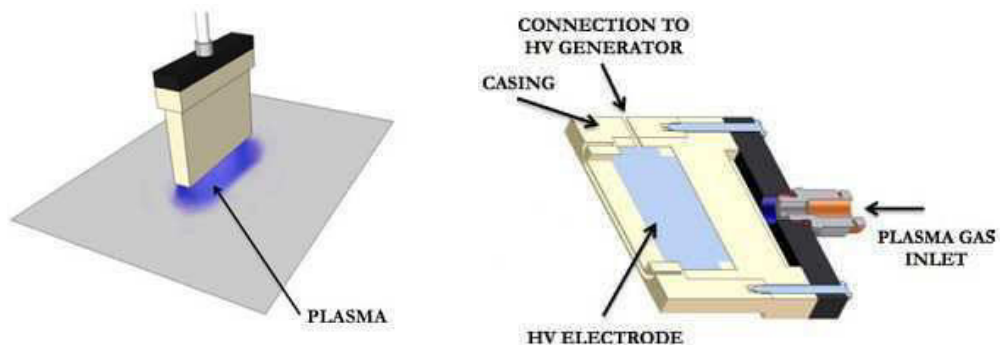


Figure 2.4 Schematic representation of plasma treatment of ES-PLLA scaffold and PLLA-film (left) and 3D section of the LC plasma source (right). Reprinted from [80], Copyright (2013), with permission from John Wiley and Sons: Plasma Processes and Polymers.

2.3.2 Chemical functionalization

Chemical functionalization was performed on electrospun p(SL) fiber mats, in order to covalently link an oligopeptide at the fiber surface, through the following steps:

Oxidation of p(SL) mats. The 1,2 diol moiety of sophorose unit was oxidized with periodate to form two aldehyde groups. Mats were cut and fixed on polycarbonate rings (Scaffoldex cell crown 24), then they were immersed in PBS 0,1 M (pH 4,5) and NaIO_4 10 mg/ml for 2 hours at 30°C in a shaking incubator. The oxidized p(SL) mats were rinsed in distilled water three times and dried.

Reductive amination. Oxidized p(SL) mats were reacted with cysteamine (CA) (22 mg) and sodium cyanoborohydride (18 mg) in PBS 0,1 M (pH 7,5) for 2 hours at 30°C in a shaking incubator. Aminated p(SL) mats were rinsed in distilled water three times and dried. A non-oxidized mats was incubated with CA and sodium cyanoborohydride and used as control for CA adsorption.

Oligopeptide “click” reaction. Oligo leu-glu (13 mg) was dissolved in 4 ml of double-distilled water and an aminated pSL mat was added. The radical photoinitiator 2,2-dimethoxy-2-phenyl acetophenone (DMPA) was added in the proportion 0.3% mol respect to oligopeptide mol. The solution was UV irradiated at 365 nm for 1 hour at RT under stirring. Oligo leu-glu clicked p(SL) mats were rinsed in distilled water three times and dried. An aminated mat was treated in the same conditions of oligo leu-glu click reaction, but without UV irradiation and used as control for oligo leu-glu adsorption.

2.4 Characterization Methods

Thermogravimetric analysis (TGA)

TGA measurements were carried out using a TGA2950 thermogravimetric analyzer (TA Instruments). Analysis were performed on samples weighing 2-10 mg, from RT to 600 °C, at a heating rate of 10°C/min, under N₂ or air flow.

Differential Scanning Calorimetry (DSC)

DSC measurements were carried out in helium atmosphere by using a Q100 DSC apparatus (TA Instruments) equipped with a liquid nitrogen cooling system (LNCS) low-temperature accessory. Samples were placed in aluminium pans and subjected to heating scans at 20 °C/min from –80 °C to a temperature higher than glass transition temperature (T_g) for completely amorphous polymers, or higher than melting temperature (T_m) when semicrystalline polymers were analysed. Quench cooling was applied between heating scans. T_g values were taken at half-height of the glass transition heat capacity step while crystallization temperatures (T_c) and T_m were taken at the maximum of exotherm and endotherm peaks respectively.

Scanning Electron Microscopy (SEM)

Samples were fixed with a carbon conducting bi-adhesive tape on aluminium stubs and they were sputter coated with gold. SEM observations were carried out by using a Philips 515 microscope at an accelerating voltage of 15 kV. Images were acquired and analysed with EDAX Genesis software.

Stress-strain analysis

Tensile stress–strain measurements were carried out on electrospun scaffolds using an Instron Testing Machine 4465, with a cross-head speed of 0,5 mm/min or 2 mm/min. Eight rectangular specimens (width = 5 mm, gauge length = 20 mm) for each electrospun scaffold were analyzed. The average specimen thickness, measured by using a digital micrometer, was used to obtain the stress–strain curves from the raw load–displacement data. Therefore the cross sectional area of the porous samples was used to calculate the macroscopic stress at break (σ_b) and the apparent tensile moduli (E) of electrospun specimens. Mechanical characterization data E, σ_b and deformation at break (ϵ_b) were given as the average value \pm standard deviation.

Tensile stress-strain measurements on collagen samples were carried out by using a DMA Q800 Dynamic Mechanical Analyzer (TA Instruments), with a cross-head speed of 0.5 mm/min. Five rectangular specimens cut from each mat (width = 5 mm, gauge length \approx 10 mm) were analyzed. The average specimen thickness was measured by using a digital micrometer and it was used to obtain the stress-strain curves from the raw load-displacement data. Tensile elastic modulus (E) and stress at break (σ_b) were given as the average value \pm standard deviation.

Wide Angle X-Ray Diffraction (WAXS)

WAXS measurements were carried out at RT with a X'Pert PRO diffractometer (PANalytical) equipped with an X'Celerator detector. Cu anode was used as X-ray source (K radiation at $\lambda = 0.15406$ nm, 40 kV, 40 mA) and 1° divergence slit was used to collect data in the range $2\theta = 3 \div 60^\circ$.

FTIR analysis

FTIR analysis was carried out using a Thermo Nicolet 380 FT-IR directly on as spun scaffolds. In the case of electrospun scaffolds of PLLA/gelatin, they were dissolved in TFE (20 mg in 0.5 ml) and few drops of solution were casted on KBr disk that was dried for 30 min prior to FTIR analysis. The spectra were collected in the range $4000\text{--}400$ cm^{-1} with 32 scans and 4 cm^{-1} resolution. Thermo Nicolet 380 FT-IR spectrometer was equipped with an attenuated total reflectance (ATR) sampling accessory (ATR single reflection with Germanium crystal) for FTIR-ATR analysis. Spectra were acquired at RT in absorbance mode, from 4000 to 400 cm^{-1} with a resolution of 2 cm^{-1} and a total of 192 scans were recorded for each spectrum.

Biuret Assay

The Biuret reagent [81] was prepared by dissolving 0.375 g of cupric sulfate (Sigma Aldrich) and 1.69 g of potassium tartrate hemihydrate (Sigma-Aldrich) in 100 ml distilled water. Subsequently, 100 ml of 10.5% (w/v) KOH was added to the solution. The resulting solution was then diluted up to 250 ml and stored at $2\text{--}8$ $^\circ\text{C}$. Each as-spun scaffold was immersed in 5 ml of distilled water at 37 $^\circ\text{C}$ in a shaking thermostatic bath (SW22 Julabo). After 1 h, 1 ml of solution was mixed with 4.5 ml of Biuret assay solution and kept at room temperature for 10 min. UV absorbance at 545 nm was measured with a Cary 1E (Varian) spectrophotometer and converted to gelatin concentration through a calibration curve obtained by measuring absorbance of gelatin standard solutions. Experiments were performed five times and results were provided as average value \pm standard deviation.

Confocal laser scanning microscopy (CLSM)

A Nikon Eclipse Ti microscope with A1R confocal laser system (CLSM) was used to obtain images of fluorescent fibers of the electrospun scaffolds. In particular, PLLA fibers containing Rhodamine B at a concentration of 0.01% w/w and Gelatin fibers containing FITC at a concentration of 0.1% w/w were analyzed.

X-Rays photoelectron spectroscopy (XPS)

Chemical functionalization reactions on p(SL) were monitored by X-ray photoelectron spectroscopy, VG Scientific Escalab, with a Mg $K\alpha$ X-ray source, 1.2 (1253.6 eV).

Circular dichroism spectroscopy (CD)

CD measurements were carried out by using a Jasco 715A spectropolarimeter, scanning from 190 to 350 nm at 100nm/min. CD was performed on collagen samples (see Chapter 3.2) in order to evaluate the amount of triple helix in the sample. A resolution of 0.1 nm was used and 3 scans were recorded for each spectrum.

Static Water Contact Angle (WCA)

WCA measurements were performed soon after plasma treatment and after selected ageing times at RT as specified in Chapter 3.3, under ambient conditions by using an optical contact angle and surface tension meter KSV's CAM 100 (KSV, Espoo, Finland). Milli-Q water was used for measurements. The water drop profile images were collected in a time range of 0–90 s, every 1 s. Optical contact angle and pendant drop surface tension software was used for image processing. Results were averaged on at least five measurements obtained at different areas of the sample.

Water adsorption

Water adsorption was determined by weighing the scaffold before and after soaking in deionized water for 24 h at RT. Prior to weighing, excess of adsorbed water was removed from the scaffold by gently blotting with filter paper. Scaffolds were immediately weighted in wet conditions with an electronic balance, to avoid water evaporation. The percentage water adsorption was calculated according to the following equation:

$$\text{Water adsorption (\%)} = \frac{W_e - W_d}{W_d} \times 100$$

where W_e is the wet weight and W_d is the dry weight of the scaffold. In order to improve the statistics, the experiments were performed using scaffolds with standard size (2.5cm × 2.5 cm) and with thickness between 30 and 60mm. Five replicate specimens were run for each sample and the average value±SD was taken as the percentage of water adsorption.

3. Results and Discussion

3.1. Part A

Co-electrospun gelatin-poly(L-lactic acid) scaffolds: Modulation of mechanical properties and chondrocyte response as a function of composition

3.1.1 Introduction

The development of scaffolds that address tissue specific needs is critical for the success of many tissue engineering strategies. Most of the scaffolds designed for tissue engineering applications are homogeneous porous constructs possessing uniform composition and, as a consequence, uniform properties. However, in the natural extracellular microenvironment complex gradients in tissue composition, structure and properties are usually present. Fabrication of scaffolds with tailored composition, chemical and mechanical properties, as well as a proper bioresorbability profile, is essential to mimic the native extracellular matrix and to positively influence cell behavior. This aspect is particularly important when scaffolds are designed to support the growth of an interfacial tissue, such as in the case of ligament–bone interface [82,83] or other interfacial tissues [83,84].

The combination of synthetic and natural polymers in a single scaffold is a convenient strategy widely used to modulate its chemical-physical, mechanical and degradation properties with the aim of addressing the specific requirements of the tissue to be regenerated [85].

Advantages of this approach include improvement of mechanical and degradation properties, as well as biological properties of the scaffold, in comparison with individual components. Synthetic bioresorbable polymers provide structural functionalities to the scaffold, whereas natural polymers display unique bioactivity and excellent cellular affinity [85].

Given its ability to create three-dimensional non-woven porous scaffolds mimicking the length scale of the native extracellular microenvironment, electrospinning has been increasingly used in recent years, for several tissue engineering applications [86,87,88], from vascular constructs [89,90], to wound healing [91,92,93], bone and cartilage regeneration [94,95,96,97,98], muscle tissue engineering [99] and drug delivery [100]. This technique is also useful in the fabrication of hybrid scaffolds made of different polymers with a controlled chemical composition and complex structure [89, 94, 99,101,102]. In particular, the co-electrospinning (or dual-electrospinning) approach, i.e. the concomitant electrospinning from two or more spinnerets, has been employed to produce interspersed fibers from different polymers [82,84,103,104,105,106,107,108,109,110,111]

and it has found an increasing number of applications in recent years, due to its flexibility in creating hybrid scaffolds with tailored properties [82]. In contrast to other approaches, the co-electrospinning strategy has the advantage of controlling scaffold chemical composition through the use of polymers with different chemical and physical properties that can be selectively incorporated in the scaffold in the desired amount. The different polymeric components maintain their individual properties, and contribute to the overall properties of the scaffold in a tailored and controlled way. In addition, co-electrospinning can be used to fabricate scaffolds with continuously graded chemical–physical, mechanical and degradation properties, mimicking biological interfacial tissues. In this work a synthetic polymer, poly(L-lactic acid), and a natural polymer, gelatin, were co-electrospun from two distinct spinnerets to obtain a composite scaffold made of randomly-oriented interspersed fibers of the two polymers. Scaffolds in the whole range of composition were obtained by adjusting fabrication parameters. A natural crosslinking agent, genipin, was used to stabilize the soluble component, gelatin. Scaffold chemical–physical and mechanical properties were investigated as a function of composition. The response of cells to the scaffolds was tested using a normal human primary chondrocyte cell culture.

3.1.2 Electrospun scaffold

The present study describes the fabrication of artificial scaffolds with tailored chemical–physical and mechanical properties, through the co-electrospinning technique. Co-electrospinning of PLLA and gelatin was performed in order to obtain a bio-synthetic scaffold that combines the mechanical properties and mechanical integrity of the synthetic PLLA polymer, with the very good biocompatibility and favorable cellular interaction of the natural gelatin polymer.

Scaffolds containing different amounts of PLLA and gelatin (nominal PLLA/gelatin weight ratio: 0/100, 30/70, 50/50, 70/30, 100/0) were fabricated by changing the feed rate of the two polymer solutions appropriately¹. The collecting time for each scaffold was set to reach a mat weight of about 0,3 g (the two polymeric solutions were electrospun contemporary for the same time) in order to obtain mats with good mechanical integrity. The obtained scaffolds were labeled: GEL, PLLA30GEL70, PLLA50GEL50, PLLA70GEL30 and PLLA.

Table 3.1.1 lists the electrospinning process parameters used for scaffold fabrication.

¹ PLLA was dissolved in DCM/DMF (65/35 v/v) at a concentration of 13% (w/v) and stirred for 2 h at room temperature (RT). Gelatin was dissolved in AcOH/double distilled water (60/40 v/v) at a concentration of 30% (w/v) and stirred for 60 min at 50 °C.

Nanofibrous scaffolds of the two plain polymers, PLLA and gelatin, were composed of bead-free and randomly arranged fibers, with similar morphology and similar fiber diameter distribution: PLLA fiber diameter = 560 ± 140 nm; gelatin fiber diameter = 500 ± 90 nm.

Table 3.1.1 Electrospinning process parameters used for scaffold fabrication.

Electrospun scaffold	Gelatin feed ratio [ml/min]	PLLA feed ratio [ml/min]	Voltage [kV]
GEL	0.005	-	15
PLLA30GEL70	0.01	0.01	20
PLLA50GEL50	0.005	0.012	20
PLLA70GEL30	0.004	0.0215	20
PLLA	-	0.015	16

The similar morphology of PLLA and gelatin fibers made them indistinguishable in the composite scaffolds by SEM observations (SEM images not shown). For this reason fluorescent dyes were added to the two polymeric solutions to demonstrate the presence of the different fiber populations within the scaffold, through Confocal Laser Scanning Microscopy (CLSM) analysis (Figure 3.1.1). The gradual change of color from green (scaffold of pure gelatin) to red (scaffold of pure PLLA) provided evidence of the variation of scaffold chemical composition in line with solution feed rates and demonstrated that fibers could be successfully interspersed by co-electrospinning.

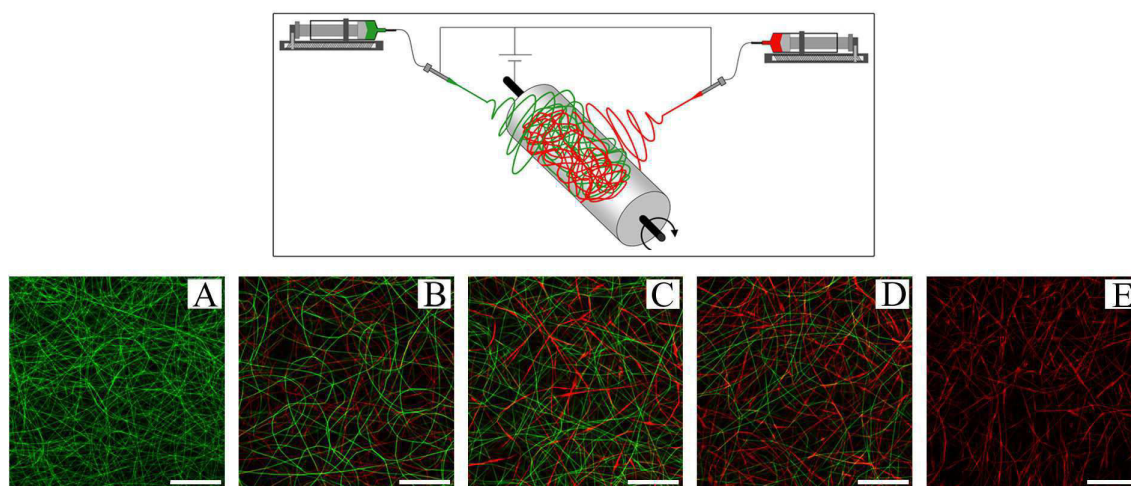


Figure 3.1.1 Top: diagram of PLLA and gelatin co-electrospinning process. Bottom: CLSM images of as-electrospun mat A) GEL, B) PLLA30GEL70, C) PLLA50GEL50, D) PLLA70GEL30 and E) PLLA. (Scale bars: $50\mu\text{m}$). Reprinted from [112], Copyright (2014), with permission from Elsevier: Materials Science and Engineering: C.

3.1.3 Electrospun scaffold composition

Qualitative evaluation of PLLA and gelatin content in the electrospun scaffolds was performed through FTIR analysis on scaffolds dissolved in TFE (Figure 3.1.2A). It is noteworthy that additional FTIR analysis performed on as-spun scaffolds showed the same bands as those reported for the scaffold dissolved in TFE. The characteristic PLLA band, corresponding to the C=O stretching, was located at 1760 cm^{-1} (see Figure 3.1.2A) whereas gelatin showed Amide I (C=O double stretching mode) and Amide II (deformation of N-H bonds and C-H stretching) bands at 1651 cm^{-1} and 1537 cm^{-1} , respectively [113,114] (see GEL FTIR spectra in Figure 3.1.2A). In composite scaffolds the intensity of the band at 1760 cm^{-1} decreased with decreasing PLLA feed rate and, concomitantly, the characteristic bands of gelatin increased, consistent with the expected chemical composition of the electrospun scaffolds.

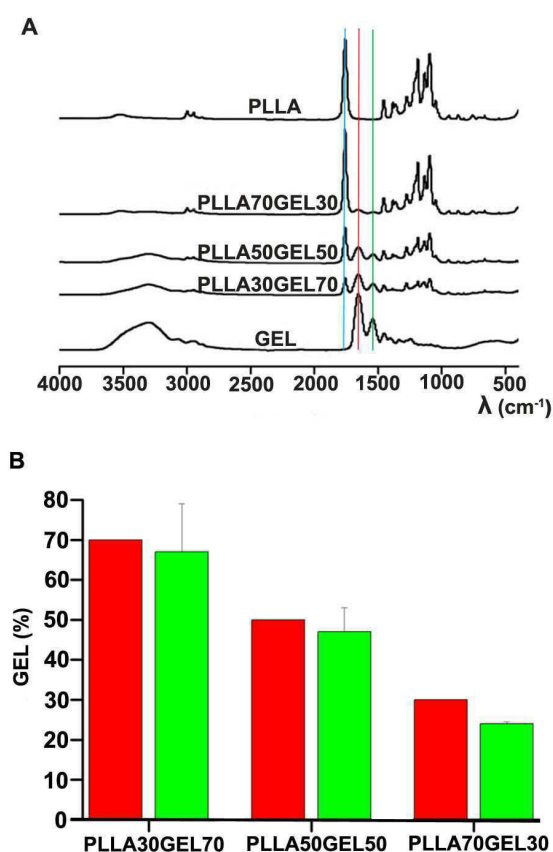


Figure 3.1.2 (A) FTIR spectra of electrospun mats dissolved in TFE. (B) Percentage of GEL in as electrospun mats: theoretical gelatin content (red); gelatin content determined by the Biuret assay (green) Reprinted from [112], Copyright (2014), with permission from Elsevier: Materials Science and Engineering: C.

In addition to the qualitative evidence of gradual change of scaffold composition provided by FT-IR measurements (Figure 3.1.2A), gelatin content in the composite scaffolds was determined after immersing as-spun scaffolds in water, through quantitative evaluation of dissolved gelatin by the Biuret assay. The measured gelatin content in the composite scaffolds ($67 \pm 12\%$ in PLLA30GEL70; $47 \pm 6\%$ in PLLA50GEL50 and $24 \pm 1\%$ in PLLA70GEL30) was found to be consistent with that expected according to the solution flow rate in the electrospinning process (Figure 3.1.2B).

3.1.4 Scaffold crosslinking

Cross-linking of as electrospun scaffolds was required in order to prevent dissolution of gelatin fibers in aqueous solutions. To this aim, the low toxicity agent genipin was used, according to an optimized procedure [115]. that allowed for the maintenance of the original high-quality nanofiber morphology after exposure to cell culture medium, as well as to water.

In order to perform the crosslinking procedure, the electrospun scaffolds were fixed to plastic rings ($\varnothing = 10$ mm, CellCrowns™12, Scaffoldex) and soaked in ethanol containing genipin (5% w/v) for 7 days at 37 °C. Subsequently the scaffolds were rinsed in 0.1 M PBS, pH 7.4, dried overnight at 37 °C, then rinsed in ethanol and dried again.

Figure 3.1.3 shows SEM images and respective photographs of crosslinked scaffolds. After the crosslinking with genipin, fiber morphology and fiber diameter distribution of pure PLLA scaffold did not appear to be significantly modified (average fiber diameter changed from 560 ± 140 nm to 480 ± 100 nm), whereas in pure gelatin scaffold average fiber diameters slightly increased: 750 ± 120 nm vs. 500 ± 90 nm of the non-crosslinked scaffold, as previously observed for plain gelatin electrospun scaffolds [115]. This increase of average diameter can be ascribed to the steric hindrance provoked by the penetration of genipin into gelatin nanofibers to form crosslinks with primary amino groups of the protein.

As illustrated in the photographs reported in Figure 3.1.3, after crosslinking gelatin containing scaffolds acquired a blue coloration, whose intensity variation was consistent with gelatin content of the scaffolds [116]. No coloration was observed for PLLA scaffolds.

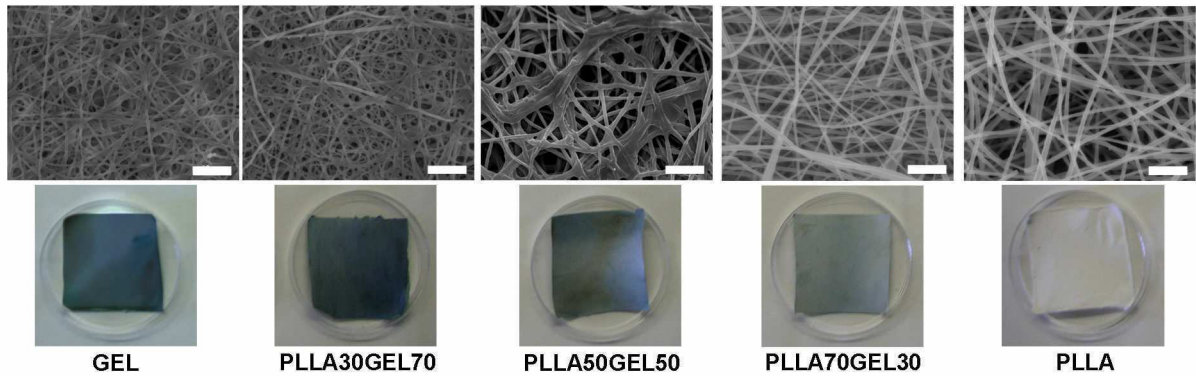


Figure 3.1.3 SEM images and photographs of crosslinked mats. (Scale bars: 10 μ m). Reprinted from [112], Copyright (2014), with permission from Elsevier: Materials Science and Engineering: C.

3.1.5 Mechanical properties

In order to explore the relationship between composite scaffold composition and tensile properties, stress–strain measurements were performed on crosslinked scaffolds.

The results of the tensile stress–strain measurements carried out on the crosslinked hybrid scaffolds are reported in Figure 3.1.4. The pure gelatin scaffold was the most rigid and fragile one, with the highest value of elastic modulus E , the highest stress at break σ_b , and the lowest strain at break ϵ_b , as a consequence of cross-junction between macromolecular chains. Conversely, the pure PLLA scaffold displayed the lowest values of E and σ_b and the highest ϵ_b .

Tensile properties of composites scaffolds were intermediate between those of the pure components, according to PLLA to gelatin ratio. This is particularly evident for E and σ_b values. The elastic modulus of the PLLA scaffold was 130 ± 10 (MPa), increasing progressively to 253 ± 13 MPa, 334 ± 50 MPa and 621 ± 76 MPa when 30 wt%, 50 wt% and 70 wt% of GEL fibers were added respectively to the scaffold and it reached its maximum value for the GEL mat (820 ± 100 MPa). A similar trend is displayed by σ_b that progressively increased from 3.4 ± 0.2 MPa of PLLA to 6.0 ± 0.3 MPa, 7.4 ± 0.9 MPa, 14 ± 2 MPa of PLLA70GEL30, PLLA50GEL50 and PLLA30GEL70, respectively, up to a value of 22 ± 4 MPa for GEL scaffold. The trend of ϵ_b as a function of scaffold composition is less evident given the high standard deviation associated with these values (see Figure 3.1.4). It is known that fiber arrangement changes in the course of a stress–strain analysis. In particular, fibers tend to align in the direction of the applied force before getting thinner and finally breaking [117]. Therefore, the high variability of ϵ_b can be related both to the complex phenomena of fiber rearrangement that occurs during the scaffold deformation and to the presence in the composite scaffolds of fibers made of two polymers characterized by very different intrinsic mechanical resistance.

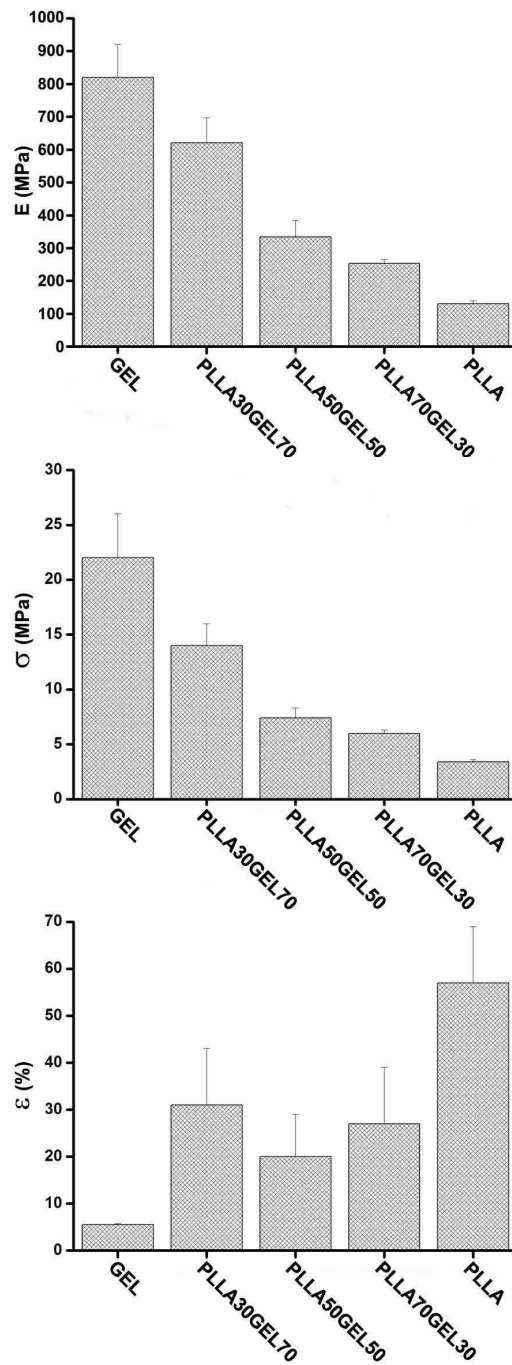


Figure 3.1.4 Tensile moduli (E), stress at break (σ_b) and strain at break (ϵ_b) of composite electrospun scaffolds and pure PLLA and gelatin mats after crosslinking treatment. Reprinted from [112], Copyright (2014), with permission from Elsevier: Materials Science and Engineering: C.

It has been previously demonstrated that combination, through co-electrospinning, of two individual fiber components with dissimilar mechanical properties has an influence on the mechanics of the composite scaffold which displays properties of both fiber components [82,104,105]. This finding was demonstrated for different pairs of polymers such as polyurethane (PU) and polycaprolactone (PCL) loaded with nanohydroxyapatite [82], PCL and gelatin [104], PU and gelatin [105]. In agreement with these results, the tensile properties of the composite scaffolds were found to be

intermediate between those of the pure PLLA and gelatin components. Moreover, they were found to depend on the amount of PLLA in the composite (Figure 3.1.4).

3.1.6 Cell proliferation, viability and differentiation

Cell culture studies were performed to assess the biological response to the composite scaffolds. These studies were performed by the group of dr. Milena Fini at the a Preclinical and Surgical Studies Laboratory and at the Laboratory of Biocompatibility, Innovative Technologies and Advanced Therapies of the Rizzoli Orthopaedic Institute (Bologna, Italy).

Water Soluble Tetrazolium salts (WST1) assay was used to measure cell proliferation and viability². Chondrocytes seeded on composite scaffolds were viable and proliferated from baseline conditions (mean of seeded cells 2.5×10^5 /ml) to 7 and 14 days, as shown in Figure 3.1.5A. At 7 days no differences were observed among any groups, while at 14 days chondrocytes cultured on PLLA50GEL50 and PLLA70GEL30 showed significant higher values of WST1 than GEL, PLLA30GEL70, PLLA, and CTR. PLLA values were significantly greater than PLLA30GEL70 values at 14 days. Lactate dehydrogenase (LDH) levels in cell culture supernatant were measured to evaluate cytotoxic effects on chondrocytes cultured on PLLA, GEL and their composites up to 24 h. No differences of LDH values were found between experimental groups and CTR, demonstrating that no membrane damage affected cell cultures (Table 3.1.2).

Common markers of chondrocyte differentiation and activity were evaluated after 7 and 14 days of culture on different PLLA and GEL composites, to assess cell activity. The concentrations of Cathepsin B (CTSB), collagen type II (COLL II), and Aggrecan (AGC) produced by chondrocytes are reported in Figure 3.1.5B–D. CTSB is considered a marker of chondrocyte differentiation, because its level was found to decrease when cells are differentiated [118]. COLL II and AGS are the major components of articular cartilage extracellular matrix, synthesized by chondrocytes.

At 7 days no differences were found between groups for all studied parameters. CTSB level (Fig. 5B) significantly decreased from 7 to 14 days in all experimental groups; CTSB value decreased also in CTR group, but it did not reach a significantly lower value. At 14 days COLL II production

² A normal human primary chondrocyte culture derived from the human knee articular cartilage (NHAC-kn, Clonetics™ Cell System, Lonza Milano srl, BG, Italy), was used for the experiment. Cells were expanded in monolayer cultures, using Chondrocyte Growth Medium (CGM, containing FBS 5%, gentamicin sulfate-amphotericin B 0.1%, bFGF-B 0.5%, R3-IGF-1 0.2%, insulin 0.2%, transferrin 0.1%). When the cells reached 70–80% confluence, they were detached from culture flasks by trypsinization, and centrifuged; cell number and viability were checked with Trypan Blue dye exclusion test (Sigma, UK). A cell suspension of 2.5×10^5 cells/ml at the first passage was used for experiment. A differentiating medium to activate chondrocytes (Chondrocyte Differentiation Medium (CGM supplemented with TGFβ-1 0.5%, R3-IGF-1 0.2%, insulin 0.2%, transferrin 0.2% and ascorbic acid 2.5%) was used. Cultures were maintained in standard conditions at $37^\circ\text{C} \pm 0.5$ with 95% humidity and 5% $\text{CO}_2 \pm 0.2$ up to 14 days. The same concentration of cells was also seeded on polystyrene of the culture plate as a control (CTR).

(Figure 3.1.5C) was significantly higher in PLLA50GEL50 and PLLA70GEL30 in comparison with CTR group. As shown in Figure 3.1.5D, AGC synthesis in GEL, PLLA, and in all PLLA/GEL composites at 14 days was greater than CTR, although with different degrees of significance. Additionally, PLLA70GEL30 was higher when compared also to GEL, PLLA30GEL70 and PLLA.

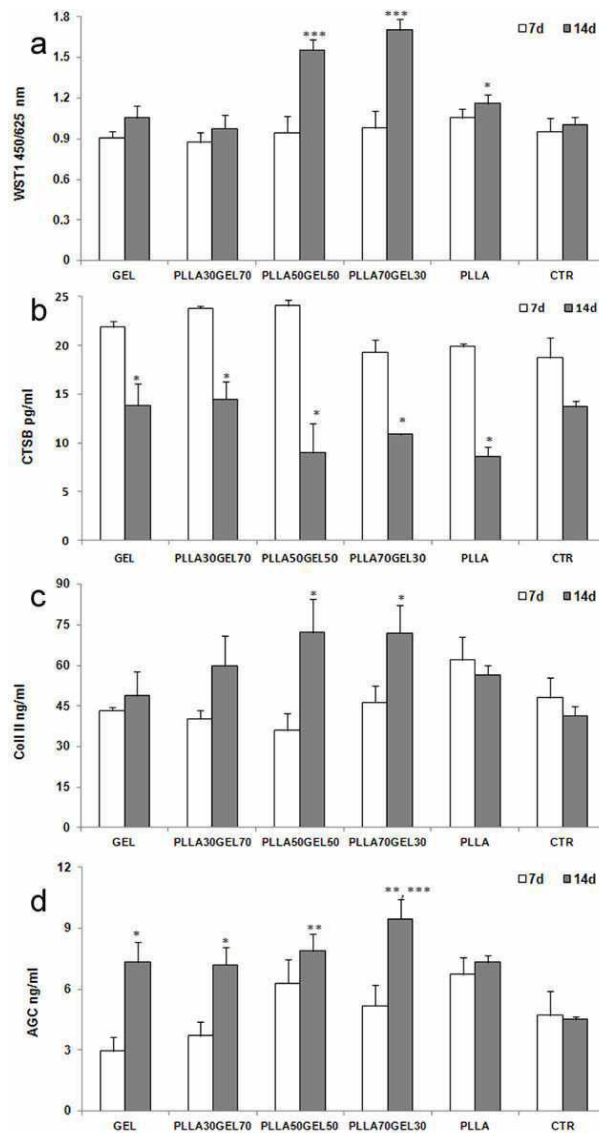


Figure 3.1.5 Cell proliferation and activity of chondrocytes cultured on GEL, PLLA30GEL70, PLLA50GEL50, PLLA70GEL30, PLLA and CTR for 7 (white bar) and 14 (gray bar) days (* $p < 0.05$; ** $p < 0.005$; *** $p < 0.0005$). A) WST1. 14 days: PLLA50GEL50, PLLA70GEL30, vs GEL, PLLA30GEL70, PLLA, CTR ($p < 0.0005$); PLLA vs PLLA30GEL70 ($p < 0.05$). B) CTSB. GEL, PLLA30GEL70, PLLA50GEL50, PLLA70GEL30, PLLA: 7 vs 14 days ($p < 0.05$). C) COLL II. 14 days: PLLA50GEL50, PLLA70GEL30 vs CTR ($p < 0.05$). D) AGC. 14 days: GEL, PLLA30GEL70 vs PLLA70GEL30, CTR ($p < 0.05$); PLLA50GEL50 vs CTR ($p < 0.005$); PLLA70GEL30 vs PLLA ($p < 0.005$), CTR ($p < 0.0005$). Reprinted from [112], Copyright (2014), with permission from Elsevier: Materials Science and Engineering: C.

Table 3.1.2 LDH measurement at 24 h on GEL, PLLA30GEL70, PLLA50GEL50, PLLA70GEL30, PLLA culture. CTR–(medium) and CTR + (phenol solution 0.5% in medium) were added for LDH evaluation. No differences were found among groups and CTR–, while CTR+ showed a highly significant difference.

	LDH	<i>p</i>
GEL	0.95±0.08	0.551
PLLA30GEL70	0.91±0.11	0.776
PLLA50GEL50	0.97±0.04	0.088
PLLA70GEL30	0.85±0.07	0.063
PLLA	0.89±0.07	0.313
CTR–	0.92±0.01	-
CTR+	1.87±0.10	<0.0001

SEM imaging was performed to evaluate the morphology of human chondrocytes grown on the different scaffolds after 7 days of culture. The cells were observed to attach and spread on all the surfaces, regardless of the scaffold composition. They generally appeared well flattened and rich in filopodia, as can be observed in Figure 3.1.6A,B for PLLA50GEL50 and PLLA70GEL30 scaffolds respectively. Moreover, chondrocytes were seen to penetrate into the scaffolds, within the polymer fibers, as shown in the representative Figure 3.1.6C for PLLA scaffold. This aspect is important in view of the formation of tissue engineering constructs.

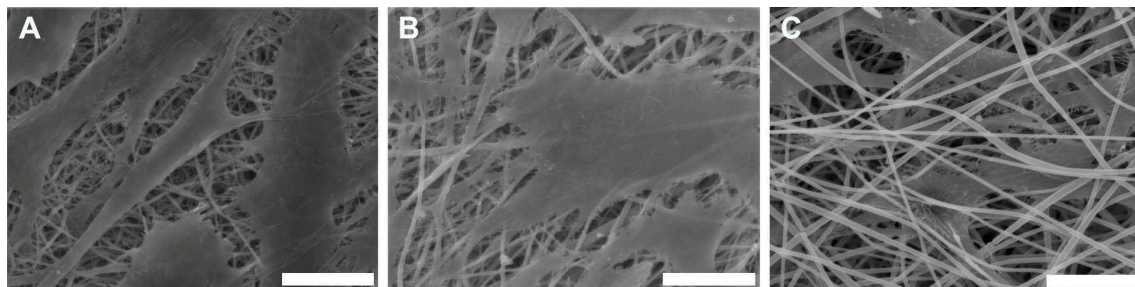


Figure 3.1.6 SEM images of human chondrocytes grown on electrospun scaffolds: (A) PLLA50GEL50, (B) PLLA70GEL30, and (C) PLLA. (Scale bars: 20µm). Reprinted from [112], Copyright (2014), with permission from Elsevier: Materials Science and Engineering: C.

Summarizing the cell culture results, we can conclude that chondrocytes seeded on composite scaffolds showed good viability and proliferation rate. In addition to supporting chondrocyte growth, the electrospun composite scaffolds studied in this work promote their differentiation, as evidenced by reduced CTSB levels in all experimental groups. Furthermore, the composites PLLA50GEL50 and PLLA70GEL30 seem to be the two best compositions that enhance significantly not only cell proliferation, but also both COLL II and AGS production. Collectively,

all results on chondrocyte growth and differentiation markers indicate that the scaffolds are suitable for cartilage tissue engineering applications.

3.1.7 Scaffold mineralization

Electrospun scaffolds obtained from PLLA/gelatin blends have been previously proposed also for bone tissue repair [119,120,121] and the capability of the scaffolds to promote apatite deposition was tested through immersion in simulated body fluid (SBF) a solution with anionic composition similar to that of blood plasma.

In particular, in order to accelerate mineralization, 5xSBF and 10xSBF solutions were utilized onto electrospun scaffolds of PLLA/gelatin blends [119,120]. In vitro mineralization tests were performed using a slightly supersaturated CaP solution, which was prepared as previously reported [122].

In brief, the reagent grade chemical $\text{CaCl}_2 \cdot 2\text{H}_2\text{O}$ was dissolved in double distilled water and buffered at pH 7.2 with Hepes (Ca solution). The reagent grade chemicals $\text{Na}_3\text{PO}_4 \cdot 12\text{H}_2\text{O}$, and NaHCO_3 were dissolved in double distilled water and buffered at pH 7.2 with Hepes (P solution). CaP supersaturated calcifying solution was freshly prepared by mixing 500 ml of the Ca solution and 500 ml of the P solution at 37 °C. The final ionic concentration of the CaP solution was 2.5 mM Ca^{2+} , 2.5 mM PO_4^{3-} , and 18 mM HCO_3^- . Mineralization was performed by immersion of the crosslinked scaffolds, which were fixed to plastic rings (CellCrowns™12, Scaffoldex), in the CaP calcifying solution at 37 °C for 6 h, with solution refreshment after 3 h. Mineralized samples were carefully rinsed in double distilled water, and dried at 37 °C overnight. Immersion of the scaffolds into the calcifying CaP solution resulted in the deposition of a uniform mineralized layer onto all composite scaffolds. No significant differences were observed among the scaffolds.

Figure 3.1.7A,B shows representative SEM images of PLLA30GEL70 and PLLA scaffolds respectively. The deposits consisted of almost spherical aggregates with mean diameter of 1–2 μm. Moreover, single gelatin and PLLA fibers appeared covered with a mineralized layer (Figure 7A,B). The XRD patterns (Figure 3.1.7D) of mineralized scaffolds show the presence of a broad band centered at about 32° of 2θ and of a reflection at about 25.9° of 2θ, characteristic of poorly crystalline apatite [122]. Accordingly, the EDS spectra recorded on the mineralized fiber surface of PLLA30GEL70 scaffold (Figure 3.1.7C) indicate a Ca/P molar ratio of 1.45, commensurate with the presence of poorly crystalline apatite.

These results show that composite PLLA/GEL scaffolds are able to promote mineralization from slightly supersaturated solutions and that osteo-conductivity can be enhanced through the incorporation of a mineral phase, while maintaining the fibrous structure of the scaffold.

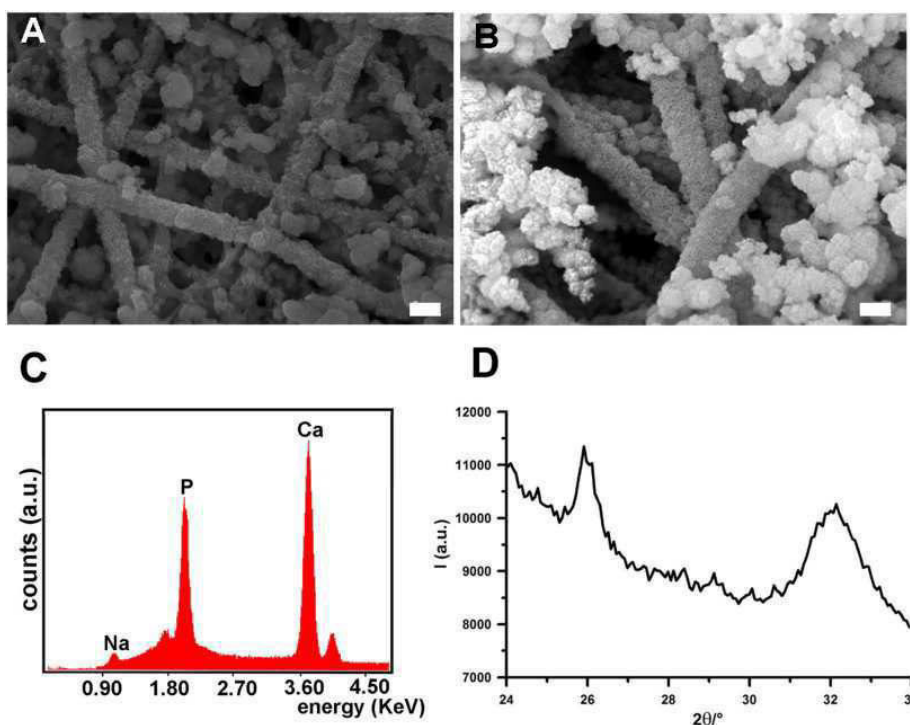


Figure 3.1.7 SEM images of mineralized electrospun mats: (A) PLLA30GEL70 and (B) PLLA (Scale bars: 2 μ m). (C) EDS spectra of mineralized PLLA30GEL70 mat and (D) relative XRD diagram. Reprinted from [112], Copyright (2014), with permission from Elsevier: Materials Science and Engineering: C.

3.1.8 Conclusions

The results of this work demonstrated that co-electrospinning technique can be usefully applied to tailor the relative amounts of interspersed PLLA and gelatin fibers in bio-synthetic scaffolds. Composition was found to affect the tensile mechanical properties of the composite scaffolds that were intermediate between those of the pure PLLA and gelatin scaffolds, and varied as a function of PLLA relative content. Results on chondrocyte growth and differentiation markers indicated that the scaffolds are suitable for cartilage tissue engineering applications, with PLLA50GEL50 and PLLA70GEL30 providing the best cellular response. Mineralization experiments suggested that potential applications of the scaffolds can be extended to cartilage-bone interface tissue engineering.

3.2 Part B

Comparative performance of collagen nanofibers electrospun from different solvents and stabilized by different crosslinkers

3.2.1 Introduction

The need of biocompatible scaffolds mimicking the functions of the native extracellular matrix (ECM) in aiding cell attachment, proliferation and differentiation, has promoted a great deal of research aimed to design and develop collagen-based scaffolds [123,124,125,126]. Collagen is indeed the major constituent of ECM fulfilling functional and structural key roles in many biological tissues such as ligaments and tendons, bone, cartilage, skin, blood vessels and muscles. It can be extracted from biological tissues by different methods, the most common ones being dissolution in dilute acid or by means of proteolytic enzymes to obtain tropocollagen and atelocollagen, respectively [127]. The extracted collagen, under appropriate conditions of temperature, ionic strength and pH, can spontaneously self-assemble to generate fibrils with the typical D periodicity found in native tissues, thus making its use extremely attractive for the production of collagenous scaffolds with desired morphology.

Electrospinning is a scaffold fabrication technique that, starting from a polymeric solution, enables to obtain micrometric and nanometric fibers assembled in the form of non-woven mat, thus resembling the fibrous morphology of native ECM more than any other scaffold technology presently available [128,129]. Therefore, collagen electrospinning is believed to be a suitable way to obtain highly biomimetic scaffolds for cell culture and tissue engineering applications.

Electrospinning of collagen has been firstly carried out in blend with poly(ethylene oxide) in acid solution [130]. Pure collagen was then electrospun from fluoroalcohol solutions by Matthews et al. in 2002 [131]. Afterwards tens of papers dealt with collagen electrospinning, mostly by dissolving it in fluoroalcohols as well as in acidic solutions [132]. A peculiar aspect, which was systematically taken into account for the first time in 2008, is that the resulting electrospun scaffolds, fabricated starting from a non-water soluble collagen, are always readily soluble in water if not crosslinked. Zeugolis et al. [133] explained this finding by demonstrating that collagen dissolved in fluoroalcohols and then electrospun into fibers was completely denatured and contained no trace of insoluble triple helices, even suggesting that collagen electrospinning “is an expensive way to make gelatin”. In latest years several conflicting results have been reported in the literature concerning the structure that collagen assumes in electrospun fibers (i.e. fibrils, triple helix, single helices) [131, 134, 135, 136, 137, 138, 139]. The process of collagen dissolution, especially in

fluoroalcohols, as well as the high shear forces acting during the electrospinning process, have been suggested to hinder the natural folding of collagen into triple helix [136,139], that is almost absent in the resulting electrospun fibers. It was demonstrated that fluoroalcohols denature the molecular structure of collagen via hydrophobic and hydrophilic interactions that unfold the triple helix and produce an “open-helical structure”, having the hydrophobic segments mostly exposed to the solvents [140]. On the other hand, contrasting results are reported on the presence of triple helix in the final fibers when collagen is electrospun from acid solutions [135, 136, 137, 138, 139].

In spite of these concerns it was demonstrated that electrospun collagen induces a better cellular response than electrospun gelatin [141, 142]. For instance, Telemeco et al. [141] demonstrated that scaffolds of electrospun collagen implanted *in vivo* were infiltrated by cells and by functional capillaries whereas scaffolds of electrospun gelatin did not support cell infiltration and initiated fibrosis, although a more recent study reported good *in vitro* cell response to electrospun gelatin [115].

As above mentioned, crosslinking of electrospun collagen is necessary to stabilize the scaffolds in water and to use them for tissue engineering applications. Several methods have been applied to increase the dimensional, mechanical and water stability of electrospun collagen, most of which utilized glutaraldehyde vapors [131, 143, 144] and N-[3-(dimethylamino)propyl]-N'-ethylcarbodiimide hydrochloride (EDC) in the presence of N-hydroxysuccinimide (NHS) [145,146,147], but also genipin and enzymes [148]. The choice of the crosslinking agent must take into account its effectiveness in stabilizing the fibrous morphology that can be completely lost leading to a non-porous structure, if crosslinking conditions are not optimized as well as costs and cytotoxicity. In this work electrospun collagen fibers were produced from both fluoroalcohol solution and acid solution, using respectively trifluoroethanol (TFE) and diluted acetic acid (AcOH), and differences were highlighted in terms of scaffold morphology and structural properties of collagen electrospun from the two different solvents. Moreover, for the first time the collagen fibrous morphology was stabilized by using 1,4-butanediol diglycidyl ether (BDDE), a crosslinking agent that was demonstrated to be less toxic than glutaraldehyde, and water-soluble carbodiimide [149]. In parallel EDC was used, which is extensively employed in the literature for electrospun fiber crosslinking, and the performances of electrospun collagen crosslinked was compared with the two different systems in terms of fibrous morphology retain, mechanical properties and mesenchymal stem cells response.

3.2.2 Electrospinning of Collagen

Electrospinning conditions employed for the production of collagen fibers from the two different solvents TFE and AcOH were set after a series of experiments aimed at optimizing polymer concentration and electrospinning process parameters³. Collagen was successfully electrospun to produce es-TFE (electrospun collagen from TFE) and es-AcOH (electrospun collagen from AcOH) membranes made of fibers with smooth surface and free of bead defects with diameter of 320 ± 80 nm and 150 ± 30 nm, respectively (Figure 3.2.1a and 3.2.1b).

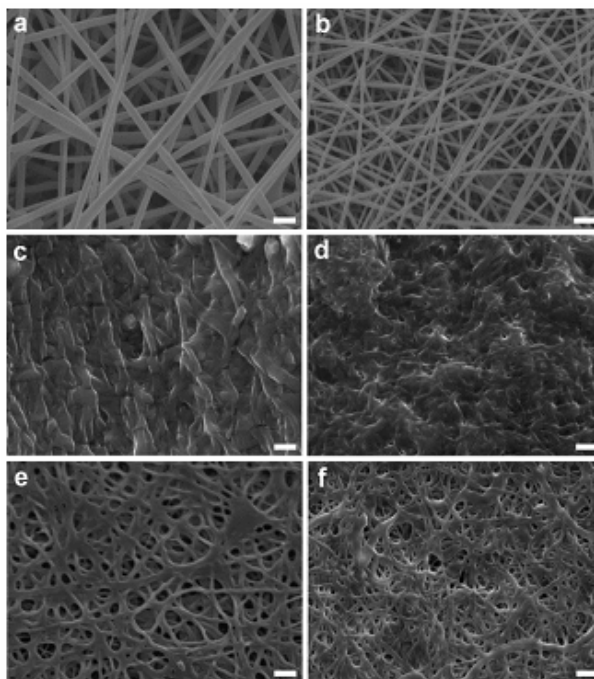


Figure 3.2.1 SEM micrographs of as-spun and crosslinked scaffolds: a) es-TFE, b) es-AcOH, c) es-TFE-EDC, d) es-AcOH-EDC, e) es-TFE-BDDE and f) es-AcOH-BDDE. Scale bar A and B = 1 μm ; scale bar C-F= 2 μm

3.2.3 FTIR-ATR, Circular Dichroism and WAXD characterization

The structure of electrospun collagen, processed from both fluoroalcohol and acidic solutions, was investigated by means of ATR-FTIR, CD spectroscopy and WAXD analysis.

Figure 3.2.2a shows ATR-IR spectra of pristine collagen (Coll), es-TFE and es-AcOH samples. Spectra are similar and display the typical absorption bands of collagen. Coll sample showed the absorption bands characteristic of amide A at 3310 cm^{-1} , amide I at 1654 cm^{-1} , corresponding to stretching vibrations of peptide C=O groups, amide II at 1542 cm^{-1} , deriving from N-H bending and

³ Electrospinning was performed at room temperature (RT) and relative humidity $RH = 40 \div 50\%$. Collagen was dissolved in TFE at a concentration of 10% (w/v) and the solution was stirred overnight at RT before electrospinning. Non-woven collagen mats electrospun from TFE (es-TFE) were obtained under the following processing conditions: applied voltage = 18 kV, feed rate = 0.015 mL/min. Mats electrospun from AcOH (es-AcOH) were produced by dissolving collagen in AcOH/ddH₂O (20/80 v/v) at a concentration of 30% (w/v). The solution was stirred for 2 hours at RT and electrospun at 24 kV with a feed rate of 0.001 mL/min.

C-N stretching, and amide III at 1235 cm⁻¹, assigned to C-O stretching and N-H bending vibrations. Es-AcOH showed amide A at 3300 cm⁻¹, amide I at 1647 cm⁻¹, amide II at 1540 cm⁻¹ and amide III at 1250 cm⁻¹, while es-TFE showed amide A at 3317 cm⁻¹, amide I at 1650 cm⁻¹, amide II at 1538 cm⁻¹ and amide III at 1245 cm⁻¹.

A shift to lower wavelength of Amide I, that is evident in the case of es-TFE with respect to Coll, indicates a partially unfolded structure of triple helix [150]. Amide I of es-AcOH occurred at lower wavelength (1647 cm⁻¹) that indicates the presence of unfolded structures similarly to es-TFE. A further evidence of collagen denaturation in electrospun fibers is the decreased intensity of Amide III [151]. This band had a high intensity in Coll sample, while its intensity was lower in esAcOH and in es-TFE.

A more detailed characterization of collagen triple helix structure of pristine and electrospun samples was carried out by means of CD spectroscopy. CD was performed on es-TFE, es-AcOH, Coll as a positive control and collagen denaturated at 90°C for 2 h (90°C-Coll) as a negative control. CD spectra were acquired after dissolution of the samples in AcOH 2,5 mM at a concentration of 0,005 mg/ml. The amount of triple helix was calculated according to the following equation [152]:

$$\%_{\text{TH}} = \frac{\theta_{\text{obs}} - \theta_{\text{D}}}{\theta_{\text{H}} - \theta_{\text{D}}} \times 100$$

Where %_{TH} is the percentage of folded protein, θ_{obs} , θ_{H} , and θ_{D} represent the ellipticities values measured at 221 nm of the sample, of pristine collagene and of completely denaturated collagene, respectively. Native collagen displays a characteristic CD spectrum with a negative peak at around 198 nm, a cross-over at 214 nm and a positive peak at around 220 nm, the latter corresponding to the triple helix structure, whose intensity decreases upon denaturation. As a consequence, thermally denatured collagen only exhibited the negative peak, which is characteristic of randomly arranged α -chains. Accordingly, in Figure 3.3.2b Coll sample showed a positive and intense peak at 221 nm, that completely disappeared in Coll sample after denaturation at 90°C (90°C-Coll). Es-TFE and es-AcOH displayed intermediate intensity values corresponding to a retention of triple helix fraction of 16% and 18%, respectively, with respect to the Coll sample.

This data demonstrate that collagen was extensively denaturated after the electrospinning process and that fibers preserved only a very small amount of triple helix.

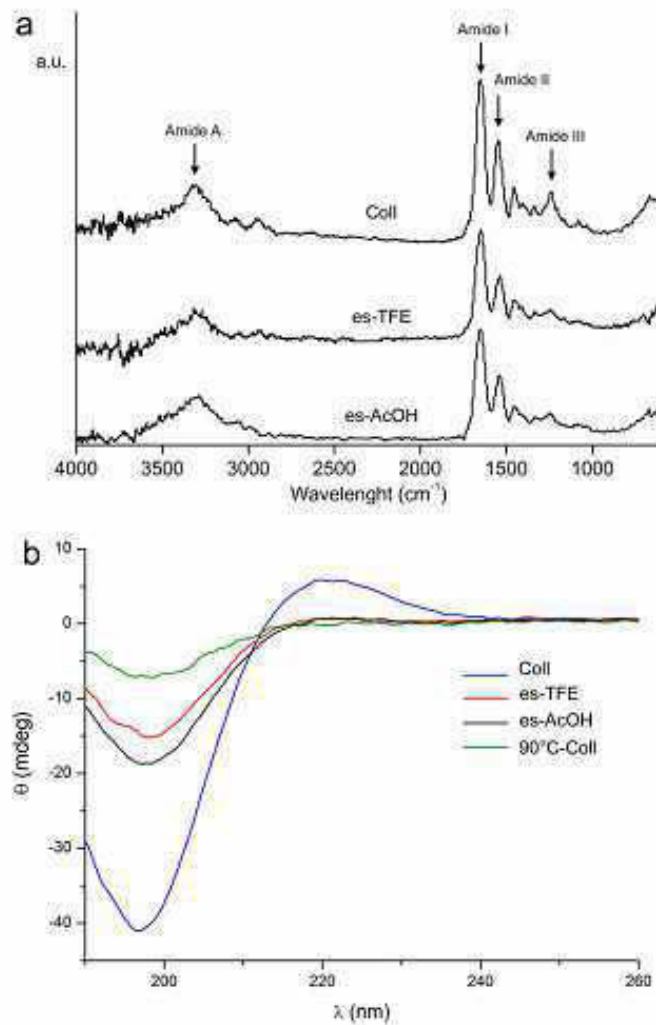


Figure 3.2.2 a) ATR-IR spectra and b) CD spectra

Furthermore, in order to highlight what prevents the formation of collagen triple helix in electrospun fibers, the collagen structure was investigated by separating the two steps of fiber production (i.e. collagen dissolution process and electrospinning process) to distinguish their independent contribution. To this aim collagen films were prepared by solvent casting the TFE and AcOH collagen solutions used in electrospinning and investigated collagen molecular structure by wide angle X-ray diffraction analysis. WAXD patterns of Coll sample, film-TFE and film-AcOH are reported in Figure 3.2.2 The characteristic peaks of collagen are found at at about 8° of 2θ , corresponding to a periodicity of about 1.1 nm, which is related to the distance between adjacent triple helical molecules, and at about 22° of 2θ corresponding to a periodicity of about 0.45 nm and related to the distance between adjacent polypeptide strands [153]. The relative intensity of the 1.1 nm diffraction peak is quite high in the pattern from Coll sample while it is very weak in the WAXD patterns of films obtained from solvent casting.

WAXD analysis thus indicates that there is a strong contribution of the solvent in collagen triple helix denaturation, so that collagen molecules do not fold into triple helix even when they slowly solidify from TFE and AcOH solutions during the solvent casting process. The fast solvent evaporation and fiber solidification occurring during the electrospinning process should further hinder triple helix renaturation. This hypothesis is confirmed by comparing the results of WAXD analysis on films and CD data on electrospun samples: it emerges that collagen, which is highly denaturated in solutions, during the electrospinning process does not spontaneously fold and the fraction of triple helix in the final fibers is very low. Figure 3.2.3 shows that the intensity of 1.1 nm peak was slightly higher for film-AcOH than for film TFE, suggesting that collagen casted from dilute AcOH might contain a higher amount of triple helix fraction than film obtained after dissolution in TFE. This is in line with CD spectra of electrospun samples that suggested a slightly higher content of triple helix in fibers obtained from AcOH with respect to TFE and our results agree with those reported by previous authors [136,139].

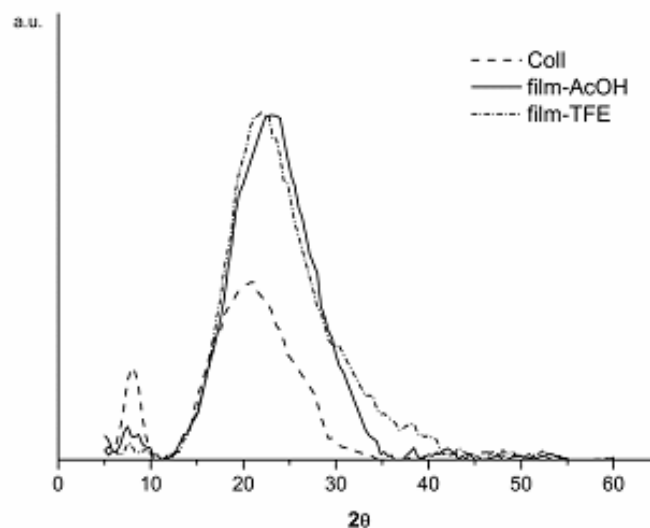


Figure 3.2.3 X-Rays diffractogram of Coll and films obtained from solvent evaporation of electrospinning solutions

3.2.4 Crosslinking of electrospun collagen

As a consequence of triple helix denaturation as spun collagen readily dissolves in aqueous media. Therefore, crosslinking of electrospun collagen nanofiber is necessary prior to use the scaffolds for cell culture experiments. Chemical crosslinking treatments, applied to generate stable intra- and intermolecular chemical bonds between collagen molecules, can be performed by using either bifunctional reagents to bridge the amino functions of lysine and hydroxylysine residues or reagents activating the carboxylic acid groups of glutamic and aspartic acid residues followed by their

reaction with free amine groups of another polypeptide chain [154]. The first category includes glutaraldehyde, diisocyanates and polyepoxies. Acyl azide and carbodiimides belong to the second category where EDC is the most used one and it is often coupled with NHS which helps in preventing the formation of side products and in increasing the reaction rate [155].

Among the above cited methods, glutaraldehyde is the most used and well characterized reagent because of its low cost and quick reaction time. However its cytotoxic effects and induced calcification associated to its persistence as residual traces in the device are well-documented [154]. Nonetheless, it has been largely employed in the crosslinking of electrospun collagen scaffolds [130,143,156]. EDC and NHS in water solution have also been recently applied [146,147,148]. Recently Barnes et al. [157] have crosslinked electrospun collagen with EDC in ethanol to better preserve the fibrous morphology by preventing scaffold immersion in aqueous solution during the crosslinking treatment. Polyepoxies, such as BDDE, have been proposed as valuable, cheap and low cytotoxic crosslinking agents [149, 158, 159] but their effectiveness has never been proven on electrospun fibers. Here the effectiveness of BDDE was tested as electrospun collagen fibers crosslinking agent in comparison with EDC which, conversely, has been largely employed as low cytotoxic crosslinker for electrospun collagen.

The crosslinking conditions applied to the scaffolds⁴ derived from a set of optimization experiments carried out by varying crosslinker concentration and crosslinking time. In particular, crosslinker concentrations of 3, 5 and 10 wt% were tested as well as 3 and 7 days of crosslinking time. Crosslinked scaffolds were labeled: es-TFE-EDC, es-TFE-BDDE, es-AcOH-EDC and es-AcOH-BDDE. Fiber morphology after immersion in phosphate buffer (PBS) was investigated to select the optimized crosslinking conditions. If short crosslinking time was applied fiber morphology was lost after PBS rinsing, even when a high concentration of crosslinker (10 wt%) was used. On the other hand, one week of crosslinking gave better results in terms of fiber morphology at all crosslinker concentrations tested. In addition, crosslinker concentration had a remarkable effect on porous structure retention: a 3 wt% concentration was too low to preserve collagen fiber structure after immersion in PBS, while both 5 and 10 wt% values were effective in maintaining the scaffold porous structure. The above results were observed for both BDDE and EDC reagents. For these reasons, collagen scaffolds were crosslinked for 7 days by using a reagent concentration of 5 wt%. Es-TFE and es-AcOH were both crosslinked by EDC and BDDE and SEM images are reported in Figure 3.2.1c-f. When EDC was used the scaffolds electrospun from both solvents did not retain

⁴ Crosslinking of electrospun collagen fibers was carried out either in EDC or in BDDE solution at 5% w/v in EtOH. Mats of collagen were fixed at CellCrown®24 (Scaffdex, Finland) plastic rings and immersed in crosslinking solution at 37°C for 7 days. Mats were then rinsed in PBS 0,1 M (pH 7,4) three times and stored one day at 37°C in oven.

their porous morphology as a consequence of fiber swelling and pore occlusion. By using BDDE, fibers electrospun from both solvents retained their morphology even if a certain degree of swelling occurred leading to an increase of fiber diameter and decrease of pore dimension (compare first row with last row of Figure 3.2.1). SEM inspection demonstrated that, overall, BDDE was more effective in preserving porous structure than EDC. However, by comparing Fig. 1e and 1f it emerges that es-TFE-BDDE had a more open porous structure than es-AcOH-BDDE. Indeed the original es-AcOH had smaller pore dimensions compared to es-TFE. Pore dimensions became even smaller as a consequence of crosslinking treatment leading to partial pore occlusion in es-AcOH-BDDE sample.

3.2.5 Mechanical characterization

The effect of crosslinking on scaffold mechanical properties was assessed by stress-strain measurements carried out on as spun and crosslinked collagen scaffolds (Table 3.2.1). It is pointed out that it is somewhat difficult to make direct comparison among stress–strain data of non-woven electrospun fibrous matrices. Indeed, for this kind of samples, mechanical data depend not only on type of polymeric material and on single fiber features. As already mentioned, many parameters related to structural arrangement of the fibers in the non-woven matrices, such as fiber arrangement in the mat, fiber curvature, fiber interconnections and mat porosity [160, 161], can influence electrospun mat mechanical properties.

All as spun scaffolds showed similar mechanical properties in terms of elastic modulus while a difference was observed for stress at break. As expected, crosslinked scaffolds exhibited a huge increasing of tensile elastic modulus and higher stress at break compared to as spun scaffolds [144]. Among the crosslinked scaffolds the ones treated with EDC showed the highest moduli and stresses. Both elastic modulus and stress at break decrease in es-AcOH-BDDE and their assumed the lowest values in the case of es-TFE-BDDE sample. These findings might be related to the different porosities of the crosslinked electrospun samples. Indeed, it was previously observed that scaffolds crosslinked with EDC lost their porous structure, es-AcOH-BDDE underwent partial pore occlusion as a consequence of crosslinked treatment while es-TFE-BDDE maintained a good porous structure (see Figure 3.2.1). It is thus reasonable that stress-strain data of crosslinked samples, calculated by considering the apparent mat section, are influenced by the specimens microstructure.

Table 3.2.1 Mechanical data of as spun and crosslinked collagen scaffolds

Sample	E (MPa)	σ (MPa)
Es-AcOH	84 \pm 8	2.3 \pm 0.2
Es-TFE	88 \pm 14	1.5 \pm 0.2
Es-AcOH-BDDE	780 \pm 130	6.6 \pm 0.8
Es-AcOH-EDC	870 \pm 160	12.3 \pm 0.1
Es-TFE-BDDE	160 \pm 30	2.8 \pm 0.6
Es-TFE-EDC	890 \pm 110	12 \pm 3

3.2.6 In vitro cell culture

Preliminary in vitro study was performed⁵ (in collaboration with Dr Silvia Panseri of Laboratory of Biomechanics and Technology Innovation, Rizzoli Orthopaedic Institute, Bologna and Institute of Science and Technology for Ceramics, National Research Council of Italy ISTECCNR, Faenza, Italy) to test the biocompatibility of es-AcOH-BDDE and es-TFE-BDDE samples resulted to be the most promising samples from the previous investigations.

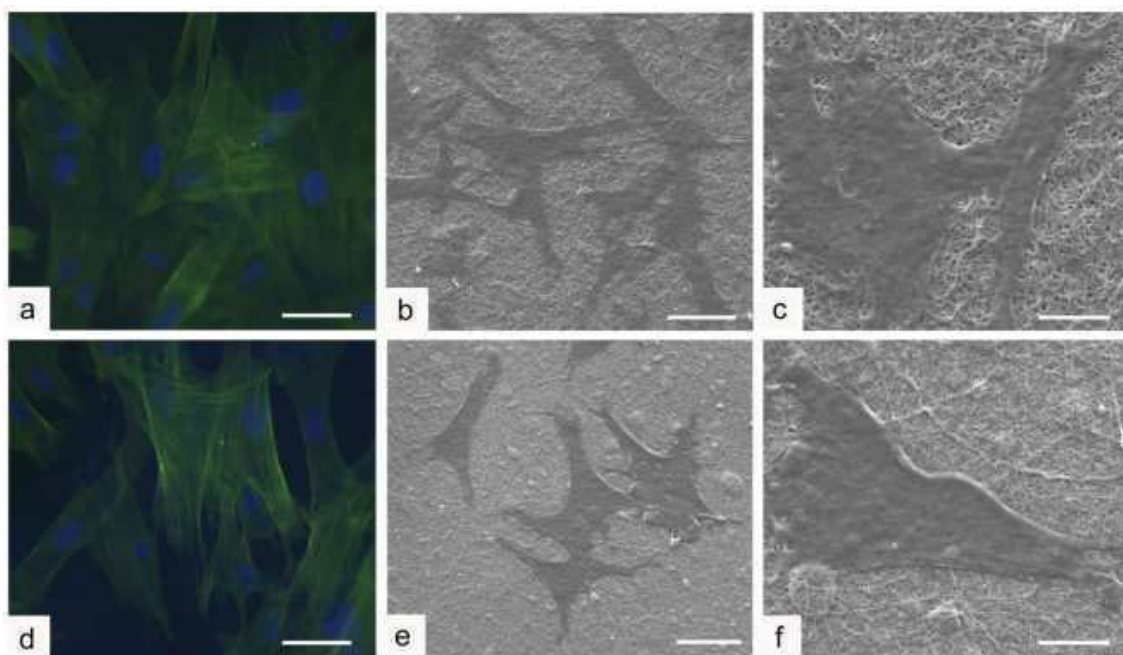


Figure 3.2.4 Cell morphology analysis by immunofluorescence and SEM. a, d: Cells were spread with good morphology and firmly attached to the surface of es-TFE-BDDE and es-AcOH-BDDE sample respectively at 24 h. Phalloidin in green stains for actin filaments and DAPI in blue stains for cell nuclei. Detailed analysis by SEM showed typical cell morphology on es-TFE-BDDE sample (b, c) and es-AcOH-BDDE sample (e, f). Scale bars: 30 μ m (a, d); 50 μ m (b, e); 20 μ m (c, f)

⁵ Rabbit mesenchymal stem cells were isolated from the rabbit bone marrow and cultured in α -MEM medium plus 10% Fetal Bovine Serum and 1% Penicillin-Streptomycin (100 U/ml - 100 μ g/ml). MSCs were detached from culture flasks by trypsinization and were centrifuged; cell number and viability were assessed with trypan -blue dye exclusion test. Samples were placed one per well in a 24-well plate and a drop of 50 μ l containing 1.00×10^4 cells was seeded on the center of the upper sample surface allowing cell attachment for 30 min in the incubator, before addition into each well of 2.0 ml of cell culture medium. Moreover a group of cells cultured directly on tissue culture plastic was used as control (cells only group). All cell-handling procedures were performed in a sterile laminar flow hood. All cell-culture incubation steps were performed at 37°C with 5% CO₂.

Immunofluorescence and SEM morphological analysis showed good results in term of cell adhesion and morphology 24 h after cell seeding. Cell–surface interaction and cell adhesion are complex processes involving the reorganization of cytoskeleton proteins like actin, and it is used as a measure of biocompatibility [162, 163].

Attachment phase of cell adhesion occurs rapidly and involves physicochemical linkages between cells and material. Cell spreading is an essential function of a cell which has adhered to a surface and precedes the function of cell proliferation to finally provide a cell covered surface. Analysis of phalloidin staining did not reveal differences in cell morphology between the groups (Figure 3.2.4 a, d). Detailed cell morphology was also analysed by SEM. After 24 hours, cells were firmly attached to samples surface showing their typical morphology (Figure 3.2.4 b, c, e, f).

These preliminary results proved the biocompatibility of both es-AcOH-BDDE and es-TFE-BDDE samples; further investigations are needed to verify if these samples could enhance cells proliferation and/or cell differentiation in order to obtain an in vitro tissue-engineered construct useful for regenerative medicine applications.

3.2.7 Conclusions

Collagen electrospun from TFE and AcOH can be collected in form of sub-micrometric fibers free of beads defects. However, electrospun collagen fibers are in both cases readily soluble in water in spite of being obtained starting from a non-water soluble collagen. Structural characterization of electrospun fibers demonstrated that collagen is collected in denatured form and that the triple helix content is very low in the electrospun fibers. In particular CD spectra enabled to calculate an amount of triple helix of 18% and 16% in the fibers produced from AcOH and TFE, respectively. WAXD analysis performed on films casted from electrospinning solutions demonstrated that collagen triple helix is destroyed in both AcOH and TFE, consistently with CD results. Given the water solubility of electrospun collagen, crosslinking treatment was carried out in order to perform further cell culture experiments. By comparing scaffolds crosslinked with EDC and BDDE it was demonstrated for the first time that the latter crosslinking agent can be successfully used to stabilize electrospun fibers and that it is more effective in preserving fiber morphology than EDC. The biocompatibility of BDDE crosslinked electrospun fibers was also demonstrated, that supported mesenchymal stem cell adhesion.

3.3. Part C

Carboxyl Surface Functionalization of Poly(L-lactic acid) Electrospun Nanofibers through Atmospheric Non-Thermal Plasma Affects Fibroblast Morphology

3.3.1 Introduction

In the rapidly evolving field of tissue engineering, biomaterials should interact with cells to emulate the complexity of the extracellular matrix in terms of topographical, mechanical, as well as molecular features, to elicit controlled response from the biological system [164]. Surface modification of artificial polymeric biomaterials has been extensively studied as a useful strategy to improve material biocompatibility, bio-integration, and to promote cell adhesion, proliferation, and differentiation, without altering the main bulk properties (e.g., mechanical strength) of the material [165,166].

Among the various techniques available for surface modification and functionalization of biomaterials, non-thermal plasma treatment has been proved to enhance biomaterial cellular acceptance and to increase cell viability and proliferation [167,168,169]. This solvent-free versatile process can provide a uniform physical and chemical modification of the scaffold surface without altering its bulk properties; indeed, the typical thickness of the region affected by plasma treatment ranges from several hundred Angstrom to several hundred nanometers [170]. Historically, plasma modification of polymeric materials has been limited to low pressure technologies such as ion implantation [171] and RF glow discharges [172], but recent technological advancements have enabled to sustain uniform glow discharges even at atmospheric pressure [173] with an evident cost reduction and process simplification. Moreover, in atmospheric pressure non-equilibrium discharges, the temperature can be limited to $<40^{\circ}\text{C}$, minimizing the risk of damaging thermo-sensitive materials. These advantages have led to explore several new fields of application of plasma treatment, such as the medical field [174], plasma interaction with liquids [175], and prompted to reconsider established processes like plasma decontamination [176] where atmospheric pressure non-equilibrium plasmas are being studied as an alternative to low pressure plasmas.

Potentialities of non-thermal atmospheric pressure plasma are greatly expressed in surface modification of polymers and biomaterials, where successful use of this versatile process has been reported by several authors [168,177,178,179,180,181,182,183]. However, only few reports describe atmospheric plasma functionalization of porous nanofibrous scaffolds fabricated through the electrospinning technology [184,185,186,187,188]. Indeed, most of the available data in this field are related to low-pressure plasma processes [189,190,191,192,193,194,195,196,197,198,199].

Electrospun assemblies are ideal candidates for the production of scaffolds to be used for tissue engineering, since they mimic the fibrillar arrangement of the extracellular matrix, fulfilling specific topographical, morphological, and mechanical requirements of different tissues and organs [200]. The introduction of hydrophilic functional groups on the nanofiber surface through plasma processes, that can be followed by immobilization of bioactive molecules, allows to couple scaffold physical (e.g., mechanical, topographic, etc.) and biological properties, thus enhancing biocompatibility, cell-biomaterial interactions, and wettability. Hydrophobicity is in fact responsible for some undesired effects related to practical use of biomaterials, such as unspecific protein adsorption, adhesion of bacterial agents, and reduced water wetting.

Among polymeric materials typically used in the fabrication of bioresorbable scaffolds for tissue engineering, poly(L-lactic acid) (PLLA) has been proven successfully in wound dressings [201], neural tissue engineering [202], cardiac repair [203], and other tissue-engineered implants [204]. PLLA, and polyesters in general, are hydrophobic materials. Moreover, electrospun polyester constructs display enhanced hydrophobicity compared to planar films of the corresponding material, given their highly porous structure and their high surface/volume ratio, which increases air entrapment.

This study investigates atmospheric plasma surface functionalization of PLLA scaffold fabricated by electrospinning technique using a linear corona (LC) discharge; the LC source is driven by a nanosecond pulsed high voltage generator and can be operated with various gases (He, Ar, air, and N₂). In order to increase the treatment area with respect to the typical pin-to-plate configuration of corona discharges [205], in the LC plasma source a sharp blade is used as the high-voltage electrode. The effect of LC non-thermal atmospheric pressure nitrogen plasma treatment on electrospun scaffolds is evaluated through morphological and thermo-mechanical characterization, as well as by measuring the changes of the static water contact angle (WCA) on the scaffold and the water absorbance percentage after scaffold exposure to plasma source. In order to estimate the relative amount of COOH functional groups created during the treatment with atmospheric plasma, a conjugation with fluorescein isothiocyanate (FITC) is performed. In view of biomedical applications, the effect of LC plasma treatment of electrospun PLLA (ES-PLLA) scaffold is evaluated by a morphological assay using mouse embryonic fibroblast (MEF) cells.

3.3.2 Electrospun Scaffold: fabrication and characterization

SEM micrographs of Figure 3.3.1 show morphology of pristine electrospun PLLA untreated (ES-PLLA-untreated) and plasma-treated PLLA fibers (ES-PLLA-LC) (plasma treatment provided by the group of Prof. Vittorio Colombo of Advanced Mechanics and Materials, Interdepartmental

Center for Industrial Research (AMM-ICIR) and Department of Industrial Engineering (DIN), University of Bologna, Italy). After optimization of the experimental electrospinning conditions⁶, smooth and beadless fibers were obtained. Both ES-PLLA-untreated and ES-PLLA-LC showed uniform diameter (820 ± 200 and 730 ± 200 nm, respectively), and no morphological modifications occurred in fiber shape and diameter of ES-PLLA-LC compared with ES-PLLA-untreated scaffold (see Figure 3.3.1).

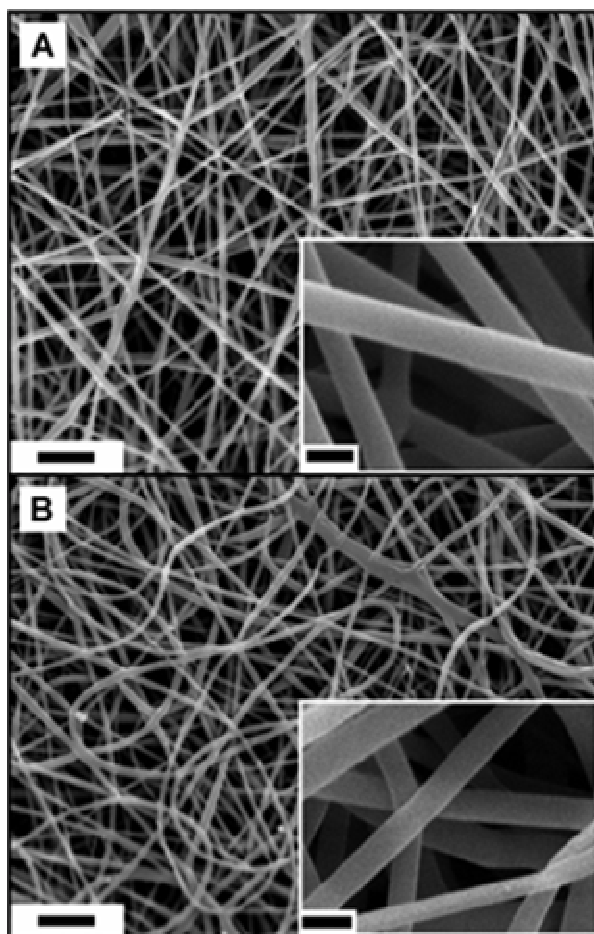


Figure 3.3.1 SEM micrographs of: A) ES-PLLA-untreated and B) ES-PLLA-LC (scale bar: $10\ \mu\text{m}$). Insets: higher magnification (scale bar: $1\ \mu\text{m}$). Reprinted from [80], Copyright (2013), with permission from John Wiley and Sons: Plasma Processes and Polymers.

In order to verify if the plasma treatment induced possible bulk modification, thermal and mechanical properties of PLLA electrospun scaffold before and after LC treatment were studied and

⁶ PLLA was dissolved in a mixed solvent, DCM:DMF 65:35 v/v at a concentration of 13% w/v. The polymer solution was dispensed, through a teflon tube, to the needle (inner diameter: 0.84 mm). ES-PLLA scaffolds were fabricated using the following conditions: applied voltage 18 kV, needle to collector distance 15 cm, collector rotational speed 40 rpm, solution flow rate 0.015 ml/min, at room temperature (RT) and relative humidity (RH) 40-50%. Electrospun mats (30-60 μm thick, measured by microcaliper) were kept under vacuum over P_2O_5 at RT overnight in order to remove residual solvents.

compared. The as-spun PLLA scaffold showed a glass transition at a temperature (T_g) around 65°C and a cold crystallization process (centered at a temperature, T_c , of 126°C) followed by a melting process (melting temperature, T_m , around 163°C) of the same entity ($\Delta H_m=40$ J/g). This result indicates that the melting phenomena regards only the PLLA crystal phase developed in the cold crystallization process during the heating scan, thus demonstrating that completely amorphous PLLA mats were obtained through the electrospinning process, as previously reported [206,207]. The plasma treatment did not modify thermal properties of the polymer (Table 3.3.1) that remained amorphous, showing that the plasma treatment was mild enough to preserve the structure and mechanical properties of the bulk material.

Table 3.3.1 Thermal and mechanical properties of ES-PLLA-untreated and ES-PLLA-LC

Sample	T_g (°C)	ΔC_p (J/g.°C)	T_c (°C)	ΔH_c (J/g)	T_m (°C)	ΔH_m (J/g)	σ_b (MPa)	ϵ_b (%)	E (MPa)
ES-PLLA-untreated	65.4	0.73	126.3	40.5	162.8	40.8	3.4±0.5	56.1±5.3	86.0±12.8
ES-PLLA-LC	64.7	0.75	126.1	38.7	162.1	39.7	2.3±0.3	71.2±9.1	63.8±7.9

As expected, similarity of thermal properties led to mechanical properties not significantly different for the two scaffolds, as demonstrated by the data in Table 3.3.1. The only appreciable effect of the plasma treatment was a slight decrease of the elastic modulus (E) associated with a small increase of deformation at break (ϵ_b), attributing to a slight loss of rigidity.

3.3.3 Surface properties: hydrophilicity

It is well known that PLLA electrospun scaffolds are materials with intrinsic high hydrophobicity, that impairs their wettability as well as cell adhesion. One of the most advantageous applications of non-thermal plasma processes is to improve surface hydrophilicity of intrinsically hydrophobic polymers such as polyesters, by forming oxygen containing groups at the surface of the materials [167,168,169].

Water contact angle measurements were performed on ES-PLLA-untreated and ES-PLLA-LC to investigate the surface hydrophilicity of the scaffolds. LC plasma treatment dramatically lowered the contact angle of the scaffold and its wettability with respect to the untreated scaffold, (Figure 3.3.2A). In the plasma-treated scaffold, the water drop was spread out instantaneously and immediately penetrated into the mesh, resulting in a change of the WCA from about 120° to about 20° (or lower) within 60 s, as revealed by the evolution of water drop profile reported in Figure 3.3.2B. WCA values obtained for electrospun scaffolds were compared with those obtained for PLLA compression molded films, both untreated and subjected to the same plasma treatment

performed on electrospun scaffolds. Data listed in Table 3.3.2 show that untreated ES-PLLA fibrous meshes display enhanced hydrophobicity compared to PLLA planar films given their porous structure that increases air entrapment. The porous structure of the electrospun scaffolds is also responsible for the rapid penetration of the water drop inside the plasma treated construct, that was observed over an ageing time of at least 48 h at RT (Table 3.3.2). Such rapid water penetration did not occur for films. In the case of PLLA-film-LC, the decrease of WCA was not so pronounced as in the case of the fibrous meshes; however data confirm an increase of hydrophilicity also for PLLA-film-LC, which is maintained for at least 48 h.

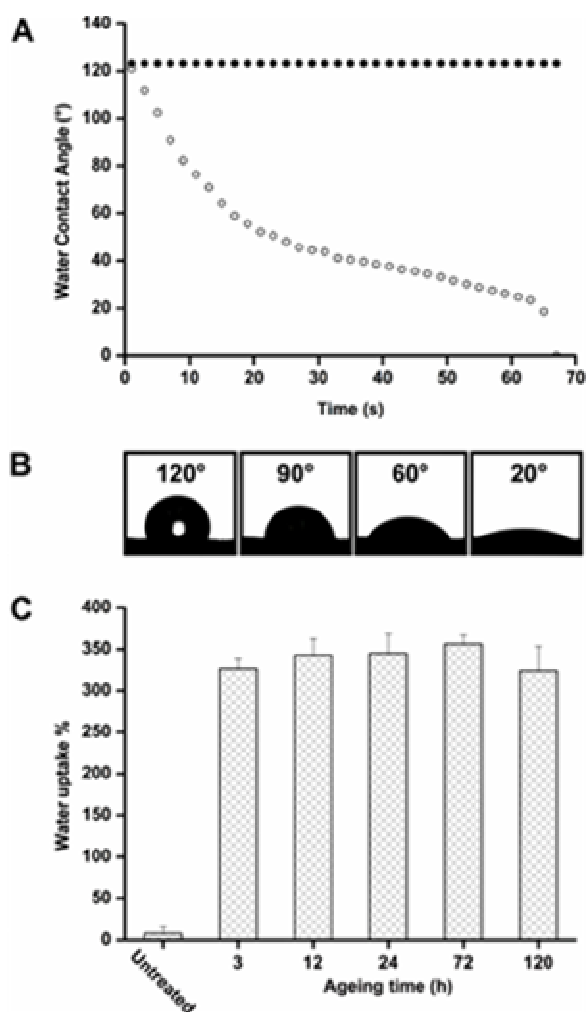


Figure 3.3.2 A) Water contact angle behavior of ES-PLLA-untreated (black circles) and ES-PLLA-LC soon after plasma treatment (white circles); B) evolution of water drop profile obtained on ES-PLLA-LC with time; C) percentage of water uptake for ES-PLLA-untreated and ES-PLLA-LC at different ageing times at RT after plasma treatment. Reprinted from [80], Copyright (2013), with permission from John Wiley and Sons: Plasma Processes and Polymers.

Table 3.3.2 Effect of ageing time at RT on WCA values of PLLA electrospun scaffolds and films

Sample	Time after plasma treatment [h]	WCA [°]
ES-PLLA-untreated	-	121,5±1,7
ES-PLLA-LC	3	a
	24	a
	48	a
PLLA-film-untreated	-	90,3±5,8
PLLA-film-LC	3	46,4±3,9
	24	48,6±3,4
	48	45,8±4,0

a) Instantaneous water penetration

It is well documented that surface chemical composition and therefore surface properties of plasma-treated polymeric materials undergo changes with material storage time [208,209]. The ageing phenomenon can be reasonable interpreted in terms of: (i) post-plasma oxidation processes caused by the radicals still present on the material surface after plasma treatment; (ii) polymer chain rearrangements from the surface into the bulk of the materials, given the much greater mobility of the polymer chains at the surface than in the bulk, allowing the surface to rearrange in response to the environment [208]. The ageing effects on electrospun samples exposed to LC plasma and stored for different periods of time in air at RT were also studied through water uptake measurements, as described in the Materials and Methods section.

Figure 3.3.2C shows that LC plasma treatment dramatically increased the ability of retaining water into ES-PLLA-LC mats: the average percentage of water uptake was around 10% and around 400% for ES-PLLA-untreated and ES-PLLA-LC, respectively. In addition, this ability was preserved for different ageing times, up to at least 120 h.

The obtained results demonstrate that the applied treatment is an effective method to increase the surface hydrophilicity and wettability of ES-PLLA. The increase of hydrophilicity of the plasma-treated PLLA scaffolds can be interpreted considering that oxygen containing functionalities are introduced on the scaffold surface, enhancing its hydrophilic behavior. It is well known that the common treatments to introduce oxygen based groups onto polymeric material surface are oxygen or air plasma treatments, where the oxidation is mainly caused by radical reactions between the polymer chain and the atomic oxygen in the plasma, or inert gases plasmas followed by a post-plasma exposure to air [208]. In all cases, the introduction of oxygen-containing functionalities leads to various functionalities such as hydroxyl, hydroperoxides, carbonyls, carboxylic acids, and peracids [208].

Atmospheric pressure nitrogen plasma treatment implemented in this work was performed in open air and therefore it is reasonable to assume that air entrainment in the plasma region causes the formation of reactive oxygen species responsible of the introduction of oxygen-containing functionalities at the material surface; this effect can be also partially attributed to the reaction, taking place after the treatment, between the free radicals at the surface created during the plasma treatment and the oxygen existing in the air.

3.3.4 Surface properties: chemical modification

The presence of carboxyl (COOH) functional groups, introduced on the surface of PLLA fibers by LC plasma treatment, was studied by means of chemical conjugation reactions via the FITC fluorophore.

The interest toward carboxyl groups is also related to the possibility of further exploitation of such functionalities through conjugation reactions to introduce specific bioactive molecules on the biomaterial surface.

The protocol reaction is illustrated in Figure 3.3.3A. Carboxyl groups were activated with water-soluble carbodiimide to covalently attach FITC molecules using a diaminobutane as a crosslinker, according to classical and well known chemical conjugation reactions [210]. Briefly, the ES-PLLA-LC scaffold was incubated with diaminobutane in carbonate buffer 0.1 M pH 9.8 for 1 h at RT with shaking. In Figure 3.3.3B, signal/background ratio of fluorescence intensity is reported as a function of FITC concentration.

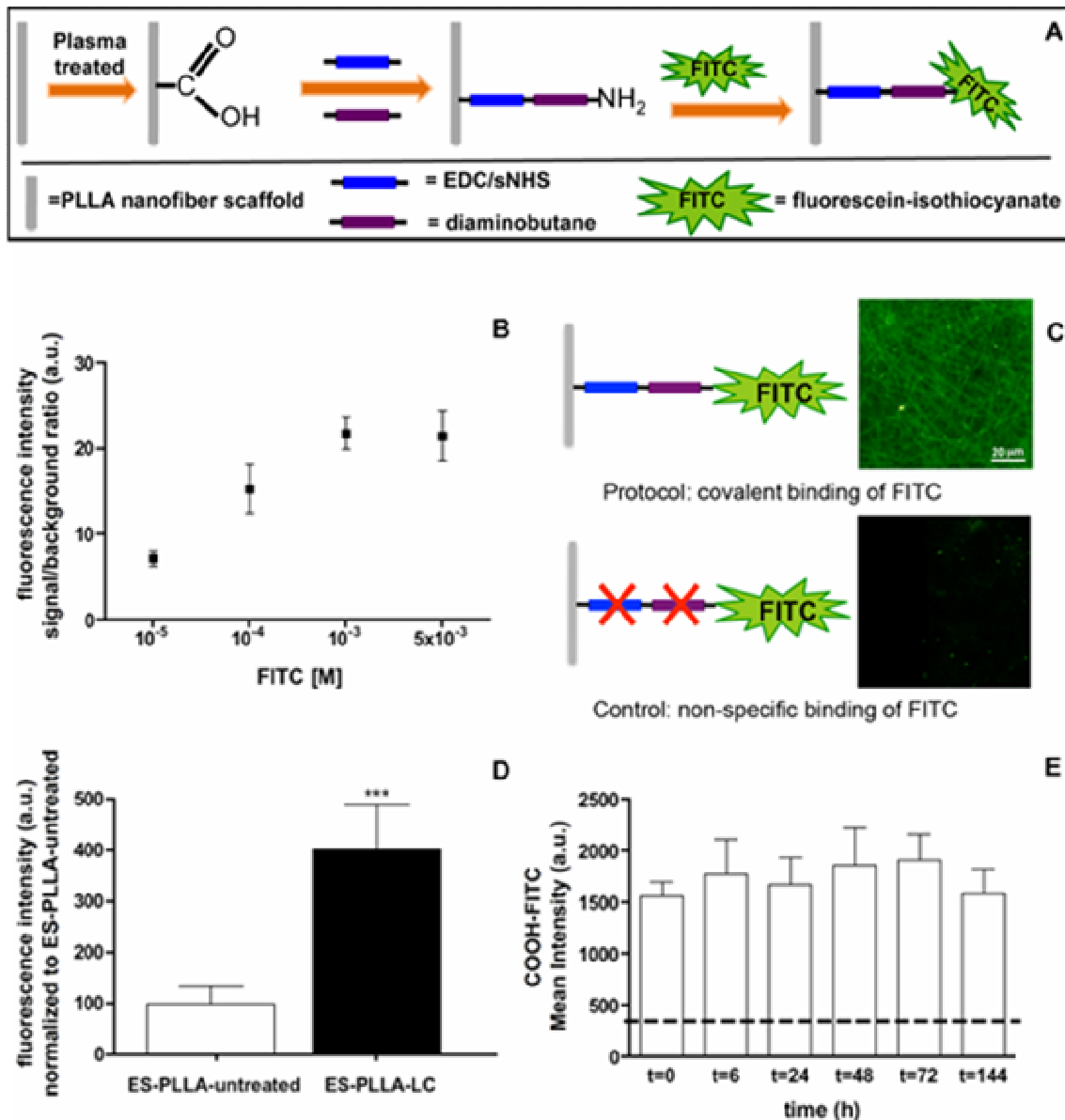


Figure 3.3.3 A) Scheme of chemical conjugation reaction; B) fluorescence intensity (signal-to-background ratio) measured on ES-PLLA-LC. FITC concentration ranging from 5 to 0,01 mM from left to right error bars=mean value \pm SD; C) scheme of reaction for complete and control-protocol (FITC 1 mM) and relative fluorescence microscope images; D) mean fluorescence intensity normalized to ES-PLLA-untreated, using optimal FITC dilutions error bars as expressed as mean \pm SD of four independent measurements ($p < 0.0001$); E) COOH-FITC mean fluorescence intensity response as a function of storage time at RT after plasma treatment compared with that of ES-PLLA-untreated indicated with dashed line. Reprinted from [80], Copyright (2013), with permission from John Wiley and Sons: Plasma Processes and Polymers.

As expected, the fluorescence intensity progressively increased with FITC concentration, up to 1 mM. Further increase of FITC concentration did not bring to significant improvement of the fluorescence intensity (Figure 3.3.3B). The 1 mM concentration was therefore selected for the subsequent scaffold characterization.

Parallel to this reaction protocol, a control-reaction was performed on ES-PLLA without EDC/sNHS and diaminobutane cross-linker reagents (Figure 3.3.3C), to evaluate nonspecific binding of FITC to the fiber surface. No appreciable fluorescence was observed in the absence of the conjugation reagents, indicating that FITC non-specific binding was negligible.

Results obtained from this control-reaction also demonstrated that no significant amount of primary amino groups (NH₂) were formed on the fiber surface during LC plasma treatment.

Figure 3.3.3D displays the mean fluorescence intensity after background subtraction (signal-background normalized to ES-PLLA-untreated) of both ES-PLLA-untreated and ES-PLLA-LC subjected to conjugation reaction. The signal of ES-PLLA-LC increased more than five times if compared with that of ES-PLLA-untreated (Figure 3.3.3D. $p < 0.0001$). It is worth noting that fluorescence signal of ES-PLLA-untreated is not completely lacking, possibly due to the presence of terminal carboxyl groups in the macromolecular chains of PLLA. Finally, fluorescence intensity of ES-PLLA-LC was measured as a function of time at RT. Figure 3.3.3E shows that the fluorescence intensity, and thus the concentration of carboxyl groups, remained almost constant over a period of 6 days of ageing at RT, demonstrating that no ageing effect was present, in agreement with results of WCA and water uptake reported above. The intra-assay CVs across the entire range were $< 20\%$ ($n=15$), while interassay CVs, evaluated by comparing the six time point using the PLLA scaffold after functionalization was below 17%.

3.3.4 Cell Culture on Scaffold

In order to understand if the plasma-induced modification of the PLLA-scaffold surface produced biological consequences, the survival and morphology of MEF was investigated on ES-PLLA-untreated and ES-PLLA-LC⁷ (by the group of Prof. Laura Calzà of Health Sciences and Technologies, Center for Industrial Research (HST-ICIR), University of Bologna and IRET Foundation). Cells were seeded on glass, BME-coated glass, ES-PLLA-untreated, and ES-PLLA-

⁷ *Mouse fetuses at Day 12.5–14.5 were dissected from the uteri and separated from placental tissue. In brief, the head, heart, liver, and alimentary track were aseptically removed from the corpse and the remaining tissue mechanically minced into very small pieces, washed with PBS Life and digested with 0.1% trypsin/EDTA (Gibco) in a shaking water bath at 37°C for 20 min. After trypsin neutralization with 10% FBS (fetal bovine serum) (Gibco), 103 U of DNase (Sigma, St. Louis, MO, USA) were added to digest DNA. Non-digested tissue was discarded and the resulting cell suspension washed by centrifugation. Mouse embryonic fibroblasts were cultured in DMEM-F12 containing 10% FBS-ES, 1% MEM-NEAA, 100 U/ml penicillin and 100 mg/ml streptomycin in a humidified atmosphere at 37°C and 5% CO₂. For passage, cells were incubated with a solution of 0,05% trypsin/EDTA for 5 min at RT. After neutralizing trypsin (MEF medium), cells were washed and seeded. Cultrex Basement Membrane Extract (BME) (Trevigen, Gaithersburg, MD, USA) was used to coat a cover glass at 0.25 mg/ml concentration for at least 2 h. The coating solution was removed just before cell seeding. MEF were cultured in DMEM-F12 containing 10% FBS-ES, 1% MEMNEAA, 100 U/ml penicillin (Sigma) and 100 mg/ml streptomycin in a humidified atmosphere at 37°C and 5% CO₂. MEF were seeded on different surfaces (glass, BME coated glass, ES-PLLA untreated, and ES-PLLA-LC) at a density of 7×10^3 cells/well; each sample was repeated in duplicated.*

LC, for 24, 48, and 72 h. To analyze cell morphology, the actin staining was used and the cell field-to-body ratio and shape-factor were measured. These parameters allow to evaluate fibroblast stretching and were obtained as previously described [204]. Briefly, the cell body area is defined as the outline of the cell's cytoplasm excluding cell processes and the cell field area is defined as the outline that contains the cell including cellular processes. A cell process is defined as an extension of a cell's cytoplasm longer than $2\mu\text{m}$ and $<2\mu\text{m}$ in width at any portion of its length (Figure 3.3.4D). The field/body area ratio was calculated as the ratio of cell field area to cell body area. The shape-factor, assumes values ranging from 0 (=line) to 1 (=circle). Results obtained from cells seeded on glass and on BME-coated glass were overlapping, therefore the BME-coated glass was chosen as the control substrate.

At all investigated times the cell body of fibroblasts seeded on BME-coated glass showed the classical round and "spread" shape (Figure 3.3.4A) and no significant time-dependent variation of shape factor was observed (Figure 3.3.4E). Conversely, fibroblast shape factors were mostly different when cultured on ES-PLLA-untreated (a: $p<0.001$ compared to cells seeded on BME-coated glass) and ES-PLLA-LC (a: $p<0.001$ compared to cells seeded on BME coated glass). Noteworthy, fibroblasts seeded on ES-PLLA-untreated (Figure 3.4.7D) were small, rounded, and star-like with short cell processes, while those grown on ES-PLLA-LC (Figure 3.3.4C) were elongated and with "dendritic" morphology. Shape factor of cells cultured on ES-PLLA-untreated and treated was different at all investigated times (24 h c: $p<0.001$; 48 h b: $p<0.01$; 72 h c: $p<0.001$) (Figure 3.3.4E).

Field/body area ratio was also analyzed to investigate the distribution and the length of cell processes. Cells with "spread" and round shape and with short processes present a low field/body area value (close to 1), while cells with elongated and with "dendritic" morphology with long processes present a high field/body area value. The field/body area ratio of MEF cultured on different substrates are shown in in Figure 3.3.4F. At all investigated times, MEF cultured on ES-PLLA-untreated and ES-PLLA-LC presented a higher field/body area ratio compared to cells cultured on BME-coated glass (c: $p<0.001$ Figure 3.3.4F). A significant difference was observed by comparing the field/body ratio obtained for MEF cultured on the ES-PLLA-untreated and on ES-PLLA-LC (24 h c: $p<0.001$; 48 h b: $p<0.01$; 72 h c: $p<0.001$).

Finally, in order to study the effect of plasma treatment on viability of MEF cultured on PLLA, percentage of apoptotic cells was determined by counting pyknotic and fragmented nuclei at each time point (24, 48, and 72 h). The number of pyknotic nuclei is presented as % of the total number of nuclei, and expressed as mean \pm SEM (Figure 3.3.4G). A lower percentage of pyknotic nuclei was found for fibroblasts cultured on BME-coated glass compared with those cultured on ES-PLLA-

untreated and ES-PLLA-LC for each time. There was about a threefold increase in pyknotic nuclei for MEF cultured on ES-PLLA-untreated ($a:p<0.001$). Notably, plasma treatment significantly reduced the percentage of apoptotic nuclei at 48 and 72 h ($b:p<0.01$).

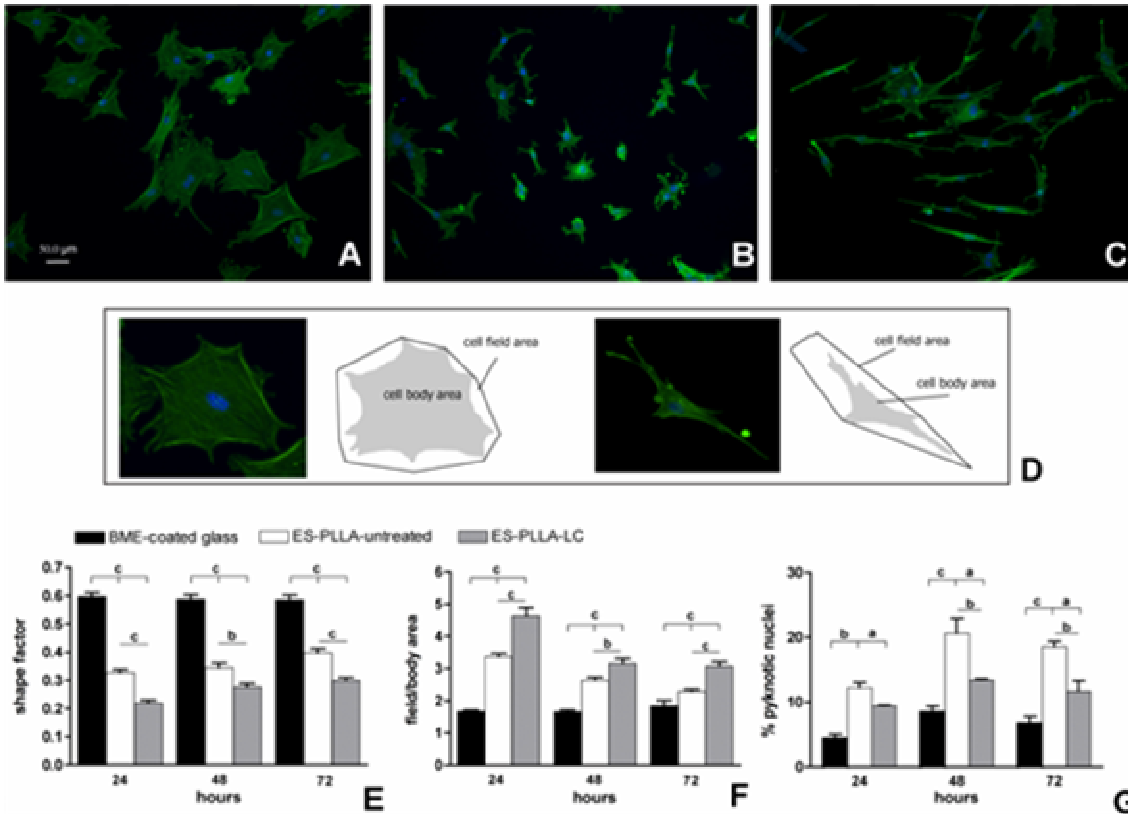


Figure 3.3.4 Mouse embryonic fibroblast cells (MEF) cultured on A) BME-coated glass, B) ES-PLLA-untreated and C) ES-PLLA-LC; D) examples of profiles for fibroblasts cultured on BME-coated glass (left) and on ES-PLLA-LC (right); E) shape-factor statistical differences of ES-PLLA-untreated and ES-PLLA-LC compared to controls for each time point ($c: p < 0.001$); statistical difference between ES-PLLA-untreated and ES-PLLA-LC ($b: p < 0.01$ and $c: p < 0.001$); F) field/body area ratios statistical difference of ES-PLLA-untreated and ES-PLLA-LC compared to controls for each time point ($c: p < 0.001$); statistical difference between ES-PLLA-untreated and ES-PLLA-LC ($b: p < 0.01$ and $c: p < 0.001$). G: analysis of percentage of pyknotic and fragmented nuclei from total cells visualized by Hoechst 33258 staining at 24, 48, and 72 h. Statistical difference were obtained between ES-PLLA-LC and ES-PLLA-untreated compared with BME-coated glass (two-way ANOVA, Bonferroni posttests $c: p < 0.001$, $b: p < 0.01$, and $a: p < 0.05$) and between ES-PLLA-LC compared with ES-PLLA-untreated at 48 and 72 h, $b: p < 0.01$. Data are shown as mean \pm SEM obtained from two duplicates.

A main result of this study is that plasma-treatment significantly improved the biocompatibility of ES-PLLA. In fact, while fibroblasts seeded on untreated-PLLA were characterized by a high cell death (three times higher than standard culture conditions) as indicated by percentage of pyknotic and fragmented nuclei, plasma treatment significantly improved fibroblast viability. Moreover, cell morphology was also deeply modified by culturing conditions. In particular, while fibroblasts

cultured in standard conditions were large, poorly polarized cells (shape factor >0.5), fibroblasts cultured on untreated ES-PLLA were largely polar with extended processes (shape factor <0.5). Notably, plasma treatment further exacerbated elongated shape of fibroblast, thus further confirming that a surface chemical modification could deeply affect cell biology. In fact, fibroblast shape is a complex phenomenon strictly regulated by transmembrane proteins (like integrins) linking binding domains of the extracellular matrix to the cell cytoskeleton [211], which is highly influenced by cell adhesion and mechanic forces [212]. The increase in carboxyl groups derived from plasma treatment, could be part in reshaping of fibroblast, as also suggested for silk fibroin surface treated with low energy plasma [213].

3.3.5 Conclusions

Non-thermal atmospheric pressure plasma was successfully applied for surface modification of ES-PLLA scaffolds that mimic the extracellular matrix. The plasma treatment was effective in modifying surface chemical properties of the scaffolds without altering their morphological characteristics and thermo-mechanical properties. A notable increase of scaffold hydrophilicity and wettability was observed and measured as a decrease of WCA and water absorbance capacity. Chemistry of the fiber surface was changed by introduction of carboxylic functional groups. Chemical derivatization and conjugation with FITC were used to evaluate the amount of carboxyl functional groups and a relevant increase of COOH concentration was registered. In vitro experiments were performed using MEF cells to assess the effect of plasma treatment on cells. Cells cultured on ES-PLLA-LC showed a more elongated and “dendritic” morphology than cells cultured on untreated ES-PLLA. Moreover, cells cultured on ES-PLLA-LC showed a higher vitality than cells grown on ES-PLLA-untreated. These results demonstrated that the treatment applied was successful to make the scaffold more compatible with fibroblast cells. In addition, carboxyl functionalities obtained through the atmospheric plasma approach, could be a useful platform for additional conjugation reactions with bioactive molecules and drugs, also in view of regenerative medicine and drug delivery purposes.

3.4. Part D

Fibrous mats of a sophorolipid polymer: fabrication by electrospinning and functionalization with biomolecules

3.4.1 Introduction

In recent years, polysophorolipids - p(SL) - attracted great interest for their properties and the wide range of possible applications. In addition to their intrinsic characteristics, p(SL) can be modified to improve or tailor their properties. Furthermore p(SL) can be successfully obtained from renewable sources [78].

The starting monomer for the synthesis of polysophorolipids is sophorolipid (SL). It is obtained by fermentation using a yeast such as *Candida bombicola*. The SL molecule is formed by two distinct moieties: the disaccharide sophorose, which is formed by two glucose molecules linked via glycosidic bond $\beta 1 \rightarrow 2$, and a fatty acid, containing from 16 to 20 carbon atoms [214]. The mostly present acid is oleic acid (C 18). The overall structure has an apolar part, the aliphatic fatty acid, and two polar residues, sophorose and the carboxyl group of the fatty acid. This structure makes sophorolipid an amphiphilic molecule that belongs to a class of compounds called bola-amphiphiles.

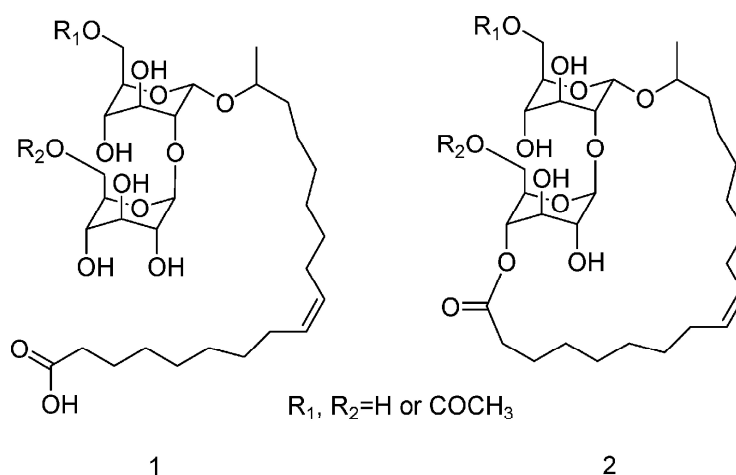


Figure 3.4.1 Sophorolipids from *Candida Bombicola* are synthesized as a mixture of ring-opened (1) and lactonic (2) molecules that are acetylated to variable degrees at sophorose 6'- and 6''-position. Reprinted from [78], Copyright (2007), with permission from American Chemical Society: Macromolecules.

The sophorolipid were isolated for the first time as a fermentation product by a yeast of the genus *Torulopsis* in 1960 [215] and are still produced in the same way [216,79] . Currently yeasts used are

mainly of the genus *Candida* [216]. The sophorolipid produced by the yeast can be in linear or in lactonic form (Figure 3.4.1). In fact, the carboxyl group can form an ester bond with one of the free hydroxyl groups of the sophorose.

Polymerization of a sophorolipid was reported in 2007 by Gross's group [78]. The reaction is a Ring -Opening Metathesis Polymerization (ROMP), based on ruthenium Grubb's catalyst (Figure 3.4.2). It was possible to obtain the p(SL), with yields of up to 89% and number average molecular weight $M_n = 103\ 000$ g/mol, with a polydispersity index between 1,8 and 2,2. H- NMR showed a 10 % of trans isomer in the polymer, whereas the double bond of lactonic diacetate sophorolipids is purely cis [217]. Other studies have been carried out recently to improve the polymerization and to study in detail the kinetics [218].

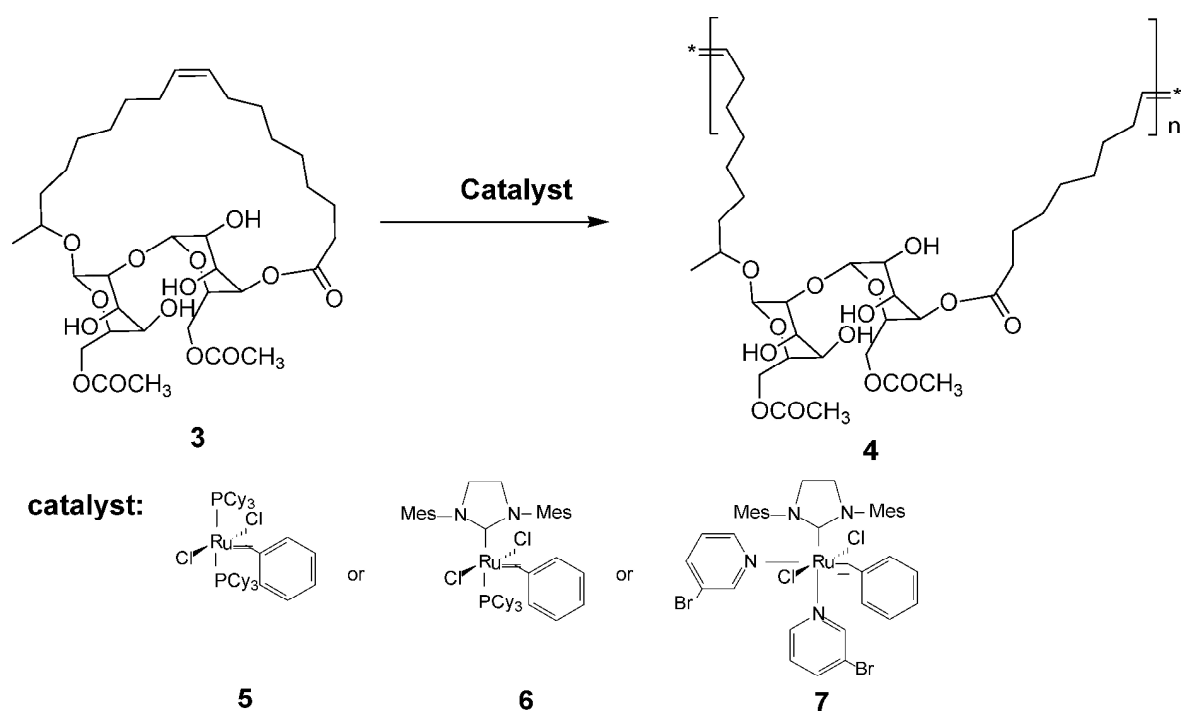


Figure 3.4.2 ROMP of lactonic sophorolipid (3) to yield p(SL) polymer (4). Grubb's catalyst of the first (5), second (6) and third (7) generation. Reprinted from [78], Copyright (2007), with permission from American Chemical Society: *Macromolecules*.

In this work, efforts have been made to electrospin the p(SL) and to functionalize the surface of electrospun fibers by covalently binding an oligopeptide.

The functionalization reaction exploits the reactivity of the hydroxyl groups of the sophorose, that is the oxidation of 1,2 diol with periodate [219,220], which leads to the formation of a di-aldehyde. Subsequently, the primary amine cysteamine was chosen to react with the aldehyde, in an amination reaction [222,221]. The thiol group of cysteamine was subsequently reacted with an alkene functionalized oligopeptide by UV "click" reaction [222].

3.4.1 Characterization of the polysophorolipid

The p(SL) was characterized both in its original ‘as received’ powdery form and after compression molding into a film.

The p(SL) powder was subjected to TGA analysis carried out under nitrogen and under air purge (Figure 3). TGA in nitrogen shows two main weight losses: first at 385°C with $\Delta m = 74\%$, second at 446°C with $\Delta m = 18\%$. Between room temperature and 200°C a small weight loss of 1 % is observed probably caused by adsorbed water. The residue at 600°C is 7%.

TGA in air shows two weight losses: first at 340°C with $\Delta m = 67\%$, second at 470°C with $\Delta m = 32\%$. The same weight loss between room temperature and 200°C is observed, with 1% loss, similarly to the previous case. The differences in TGA behavior are ascribed to the purge gases. The oxygen contained in air provides an oxidizing environment. For this reason, in air degradative phenomena are anticipated and usually the residue is very low, because all organic carbon is oxidizes to CO₂.

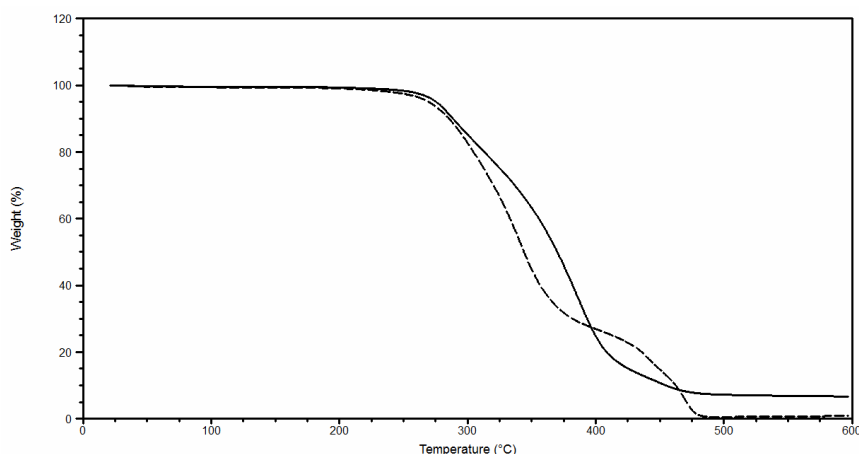


Figure 3.4.3 Thermogravimetric curves of the poly(SL) under nitrogen purge (solid curve) and under air purge (dashed curve); heating rate 10°C/min.

The first step at 340°C was associated [223].with degradation of the disaccharide moieties, because it is known that polysaccharides show thermal degradation around 350°C, 10 with cleavage of glycosidic bonds and the release of CO, CO₂, etc.[224] The second step around 450°C in Figure 3.3.3 can be attributed to thermal degradation of oleic acid chain. This temperature is typical of polyolefin thermal degradation, such as polyethylene [225]. Furthermore, the ratio between the steps weight loss roughly corresponds to the calculated weight ratio of oleic chain to sophorose groups in the repeating unit (34 to 66 wt %).

The calorimetric analysis performed on p(SL) powder (Figure 3.4.4) shows a glass transition and a melting endotherm. In the first scan an endothermic transition at 134°C, with a ΔH_f of 26 J/g,

associated at the melting of the p(SL) is observed, indicating that the polymer is semicrystalline. This is consistent with polymer purification by precipitation in non-solvent [78], because this method promotes the crystallization of polymers. The second scan, after controlled cooling at 10°C/min, only shows a clear glass transition at 62°C, $\Delta C_p = 0.45 \text{ J/g } ^\circ\text{C}$. The absence of a melting peak in the second scan confirms that the material is completely amorphous and that crystallization is hindered in the thermal cycle applied.

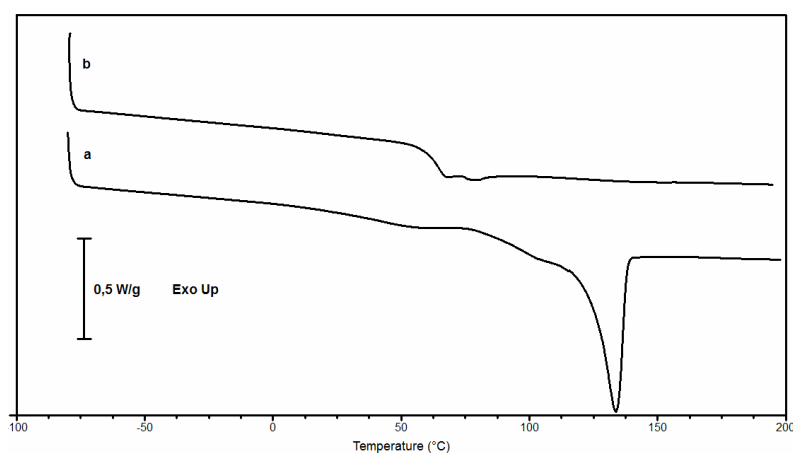


Figure 3.4.4 DSC curves (heating rate 20°C/min) of the polymer in the form of powder. a) First scan, b) second scan after controlled cooling at 10°C/min.

X-rays diffraction analysis was carried out on the original p(SL) powder in order to investigate the nature of the crystalline phase of the polysophorolipid and the diffractogram is reported in Figure 3.4.5.

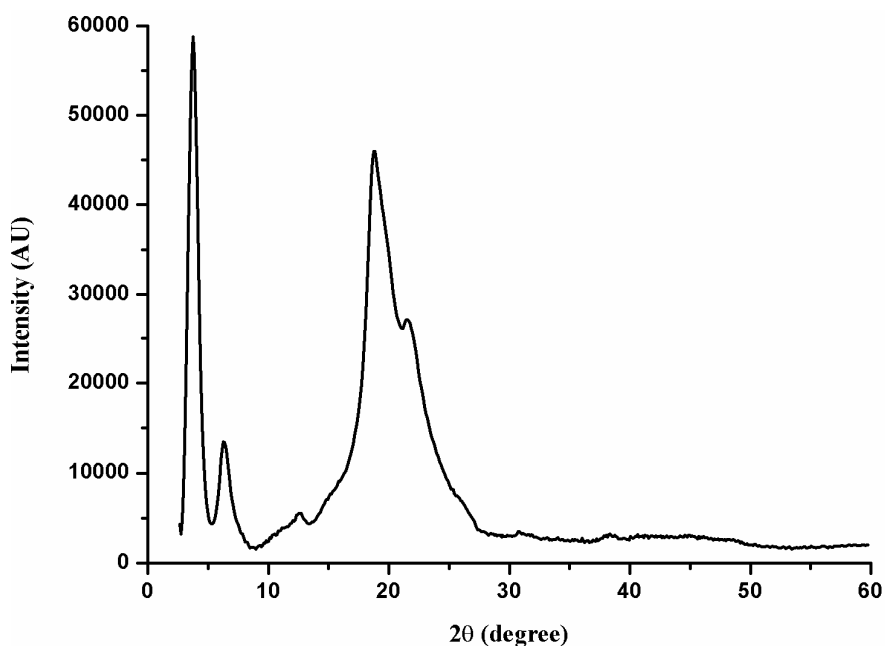


Figure 3.4.5. X-ray diffractogram of p(SL) powder.

With increasing 2θ values, the diffractogram shows an intense peak at $2\theta = 3.7^\circ$, a low intensity peak at $2\theta = 6.2^\circ$, then two higher-angle peaks at $2\theta = 18.7^\circ$ and 21.6° , that overlap the typical band of the amorphous phase centered at 20° . The reflections at 6.2° , 18.7° and 21.6° are typical of oleic acid crystal structure, which is the lipid part of the monomer. The oleic acid exists in three polymorphs, the α , β , and γ form, each characterized by a different crystal structure [226]. The reflection at $2\theta = 6.3^\circ$ is present in the diffractogram of the two polymorphs, α and γ [227]. The high angle peaks, at $2\theta = 18.7^\circ$ and 21.6° , are very close to those typical of the γ phase of oleic acid, then it is hypothesized that p(SL) develops a crystalline phase similar to that of oleic acid type γ [217] and that this is responsible for the fusion process shown at about 130°C in the DSC curve of Figure 3.4.4.

In the diffractogram of Figure 3.4.5, the first peak at $2\theta = 3.7^\circ$ is ascribed to sophorose groups periodicity along the p(SL) chain. This hypothesis is derived from the following data: the oleic chain of p(SL) is in the γ phase, from previous WAXS data, and the disaccharide unit is 0,74 nm long (length of pure crystalline sophorose). From these data is possible to calculate the distance between two sophorose groups in the polymer chain, which results to be 2,40 nm [217]. This value very closely matches the experimental value obtained from the peak at $2\theta = 3.7^\circ$ that corresponds to a periodicity of 2,39 nm.

The p(SL) in the form of a compression molded film was also subjected to thermal and structural characterization. TGA analysis showed no differences with respect to results obtained with the p(SL) powder and this confirms that degradation does not occur while compression molding the powder. On the other hand, DSC analysis yielded a curve is similar to that of Figure 3.4.4 (curve b) showing that p(SL) film was completely amorphous. This result is consistent with the quick cooling of the film after molding. The diffractogram of p(SL) film is shown in Figure 3.4.6, where the broad band of the amorphous phase, centered around $2\theta=20^\circ$ and the low angle reflection ($2\theta=4.1^\circ$, $d=2.15$ nm) are the only evident features.

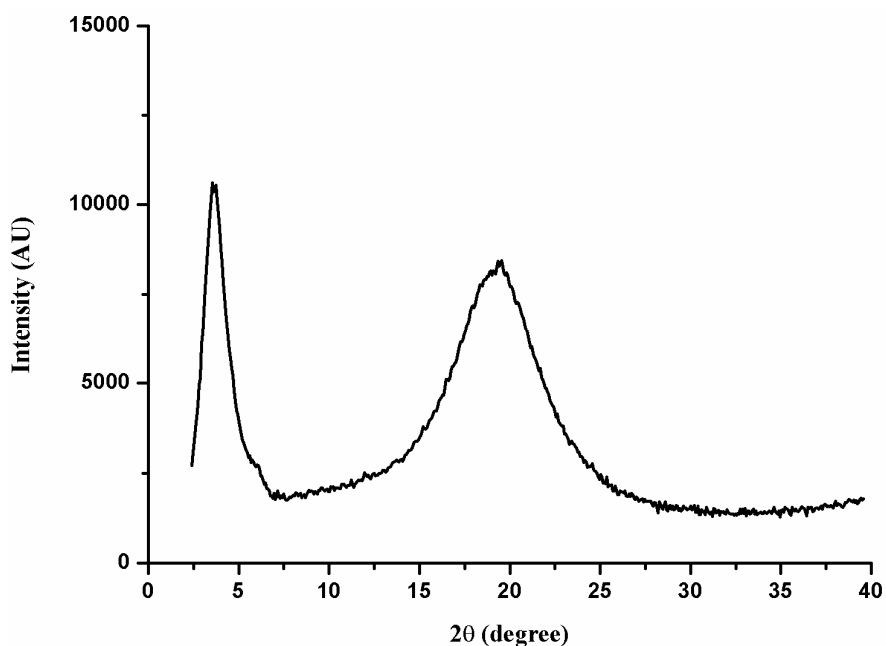


Figure 3.4.6. WAXS diffractogram of p(SL) film

This confirms the absence of oleic acid γ phase, the lipid chain is not organized in the crystalline structure, consistent with the DSC analysis, which does not show melting. Despite this, the presence of low angle signal indicates some degree of organization among the sophorose groups. It is worth noting that the position of this peak is slightly higher ($2\theta=4.1^\circ$) compared to that of the semi-crystalline polymer ($2\theta=3.7^\circ$). This finding suggests that when the lipid part of the polymer is in the amorphous state the sophorose groups come closer, probably in order to optimize the H-bond interactions [217].

The p(SL) films were also subjected to mechanical stress-strain measurements. The curves are reported in Figure 3.4.7 and the results are collected in Table 3.4.1.

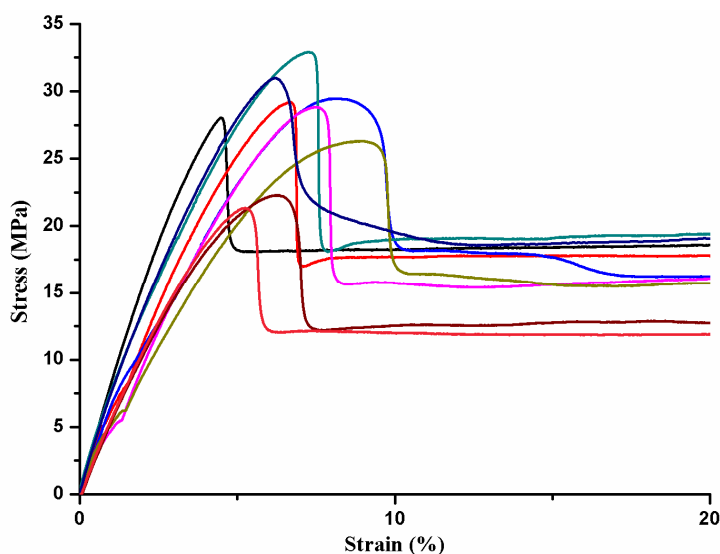


Figure 3.4.7 Stress-strain curves of several specimens of p(SL) film (curves reported only up to strain = 20%). Strain rate 2mm/min.

Table 3.4.1. Mechanical properties of p(SL) film: stress at yield (σ_y), strain at yield (ϵ_y) elastic modulus (E), strain at break (ϵ). Average values with calculated standard deviations are reported.

σ_y (Mpa)	ϵ_y (%)	E (Mpa)	ϵ (%)
27,7±3,8	7±2	681±136	>200%

It is interesting to note that the ϵ value is surprisingly high, despite the fact that the polymer is in the glassy state (T_g is higher than room temperature, where the measurements were performed). It is seen that the p(SL) film displays good mechanical properties.

Measurements of water contact angle (WCA) were also performed on p(SL) film as a function of time. Figure 3.4.8 shows the WCA behavior in a time frame of 60s as well as the picture of a water drop after 30s of contact with the film surface. The contact angle decreases by about 2° in 60s. Since the volume of the droplet does not change over the time, this phenomenon is ascribed to interactions of water with the material, a gradual absorption of the drop into the film with the consequent decrease of WCA.

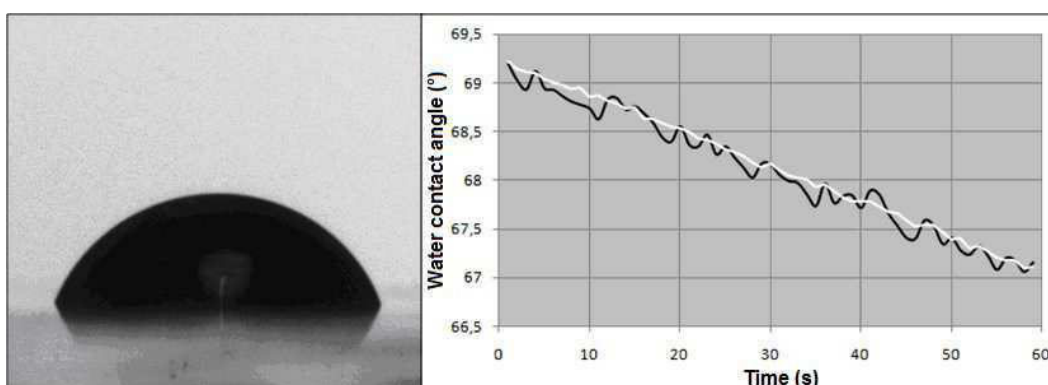


Figure 3.4.8. Left) Drop on the surface of the p(SL) film after 30s from drop deposition; right) WCA trend over 60s, for a single drop (black line) and for the average of 15 drops (white line).

The average WCA calculated over 15 drops at 30s is $68 \pm 2^\circ$ (value \pm sd). This value, lower than 90° , suggests that in p(SL) the hydrophilic nature of the sophorose moieties prevails over the hydrophobicity of the oleic chain.

3.4.2 Electrospinning of polysophorolipid and characterization of the fiber mats

Electrospinning of p(SL)⁸ results in good morphology fibres (Figure 3.4.9), beadless and circular shaped, with random orientation. Measured fibres diameter is $1,19 \pm 0,16 \mu\text{m}$.

⁸ A glass syringe containing the p(SL) solution was connected to a stainless-steel blunt-ended needle through a Teflon tube. The needle and an aluminium foil (2 mm thick) used as collector were connected to an high voltage power supply (Spellman SL 50 P 10/CE/230). Needle-to-collector distance was fixed at 20 cm and potential was 20 kV. Electrospinning solution was p(SL) 16 % by weight in THF/DMF (90/10 v/v). The p(SL) solution feed rate, controlled

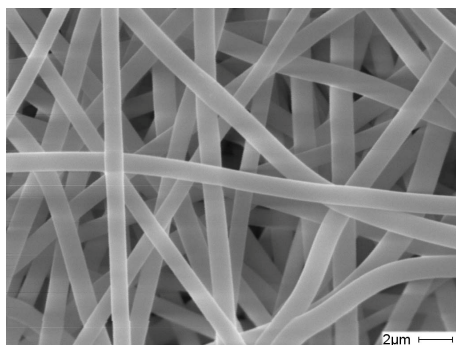


Figure 3.4.9 SEM micrographs of electrospun p(SL) fibers.

The non-woven mat of p(SL) obtained by electrospinning was subjected to thermal characterization by TGA and DSC. TGA analysis does not show differences compared to the TGA results on p(SL) powder (Figure 3.4.3), while the DSC curve (first scan) only shows the glass transition indicating that in the fibers the polymer is amorphous (Figure 3.4.10). This confirms that during electrospinning the solvent undergoes very fast evaporation and this does not allow polymer crystallization.

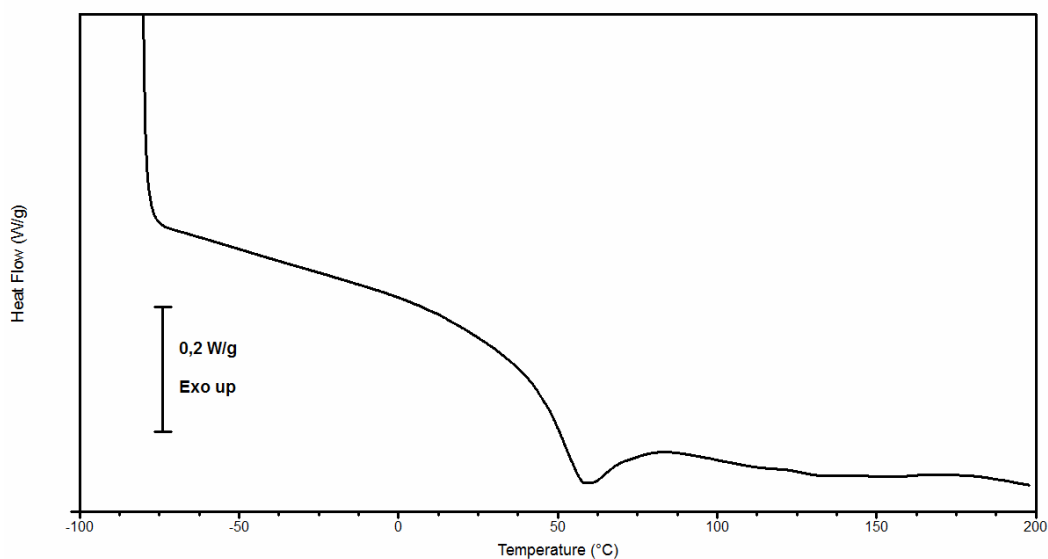


Figure 3.4.10. DSC analysis of an electrospun p(SL) fiber mat.

The electrospun p(SL) mat was subjected to tensile stress-strain measurements. The curves are shown in Figure 3.4.11 and Table 3.4.2 collects the results.

by syringe pump (KD Scientific 200 series), was 0.9 ml/h. During electrospinning, temperature and relative humidity were kept constant at 24-26°C and 47-50%, respectively.

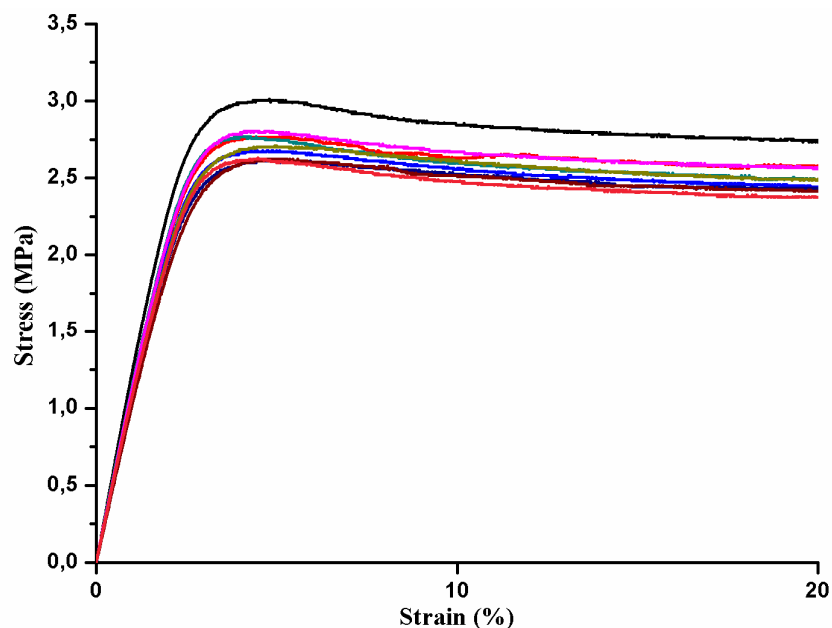


Figure 3.4.11 Stress-strain curves of several specimens cut from electrospun p(SL) mats (curves reported only up to strain = 20%). Strain rate 2mm/min.

Table 3.4.2 Mechanical properties of electrospun p(SL) mat: stress at yield (σ_y), strain at yield (ϵ_y) elastic modulus (E), strain at break (ϵ). Average values with calculated standard deviations are reported

σ_y (Mpa)	ϵ_y (%)	E (Mpa)	ϵ (%)
2,7±0,1	5±1	112±6	206±22

As expected, elastic modulus and strength at yield are lower than the corresponding values obtained for the p(SL) film (see Table 3.4.1). This result is expected and it can be ascribed to unavoidable overestimation of the specimen cross section area, because the mats are extremely porous. An additional reason for the low modulus and strength values obtained is that when mats are subjected to stress-strain measurements the applied force does not act on all fibers simultaneously, owing to the random orientation of the fibers in the mat.

3.4.3 Surface functionalization of electrospun p(SL) mat

The reactions carried out in order to ‘graft’ an oligopeptide at the fiber surface were conducted as described in the Materials and Method paragraph (2.4). In brief, the first reaction was an oxydation of the sophorose 1,2 diols to aldehyde using periodate, followed by a reductive amination using

cysteamine and a final click reaction between the thiol group on the sophorose and the terminal double bond of the 'ad hoc' synthesized oligopeptide (Figure 3.4.12).

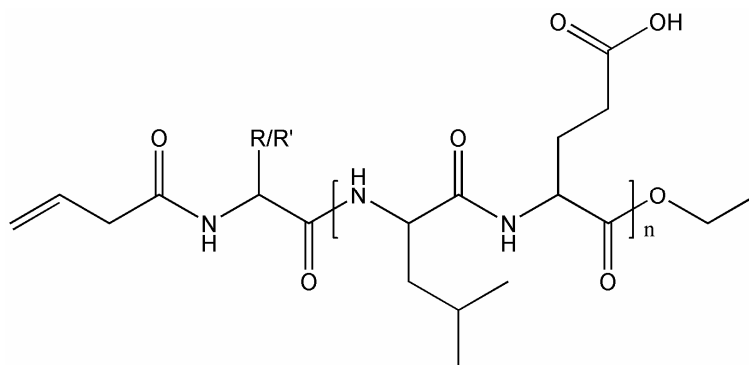
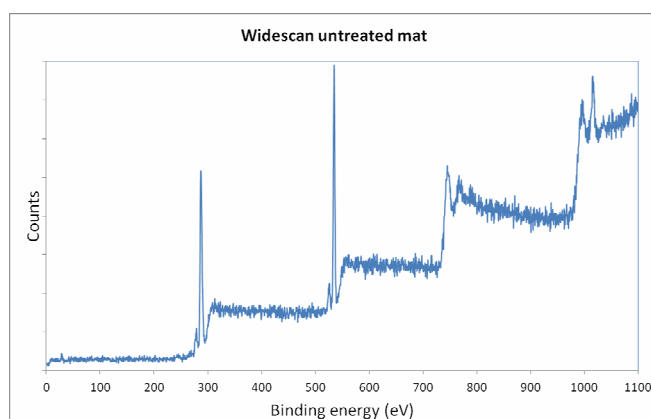


Figure 3.4.12 Oligo (γ -ethyl-L-glutamate-co-L-Leucine) R/R', sidechain of Glu ethyl ester or Leu, and $n \sim 7$.

In order to check the success of the various steps of the functionalization reaction on p(SL) mats, the characterization was carried out using XPS. First of all, non treated mats were analyzed (Figure 3.4.13). From the reported repeat unit structure of untreated p(SL) mats (Figure 3.4.2.4), and considering that hydrogen is not detected by XPS analysis, the expected atomic abundance of carbon and oxygen was calculated. Not considering the hydrogen atoms, the repeat unit formula would be $C_{34}O_{14}$. From this formula the expected atomic ratio O/C is 0.41. The result obtained from the surface analysis of Figure 3.4.13 a), i.e. $O/C = 0.39$, fits quite well with the expected one. The slightly higher carbon content can be due to the presence of hydrocarbon contamination usually observed in XPS analysis of polymeric systems.

More information, confirming the structure of the substrate surface, can be derived from the analysis of the C1s peak envelope, i.e. from the relative abundance of different functional groups.



a)

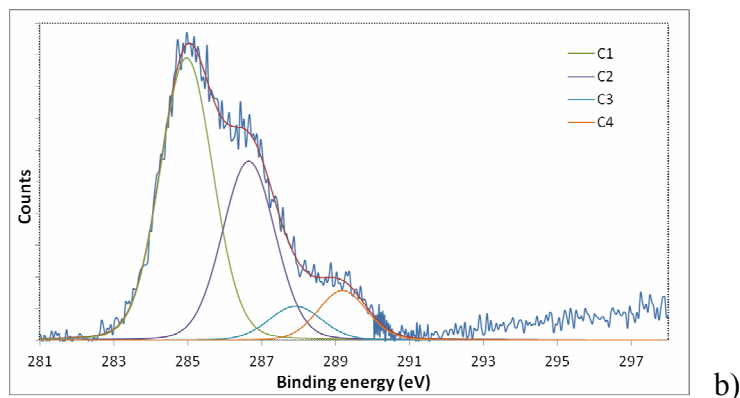


Figure 3.4.13 Untreated mat: widescan (a), C1s envelope and its components (b). Oxygen (~532 eV), carbon (~285 eV).

From the structure of the repeat unit four chemical states can be identified and their position and relative abundance can be predicted: C1 (285 eV), deriving from the 18 carbon atoms, present in the repeat unit, bound to other carbon or hydrogen atoms (C-C or C-H); C2 (286.6 eV), deriving from the 11 carbon atoms present in the repeating unit linked by a single bond to an oxygen atom (C-O); C3 (287.9 eV), deriving from the two carbon atoms linked via a single bond to two oxygen atoms O-C-O; C4 (289.2 eV), deriving from the 3 carbon atoms, present in the repeat unit, engaged in carboxylic functions (O-C=O).

The peak fitting elaboration of the C1s envelope (Figure 3.4.13b) perfectly matches the predictions both in terms of peak position and of relative abundance (Table 3.4.3) confirming the polymer structure.

Table 3.4.3 Relative abundance from C1s envelope deconvolution (untreated mat)

Components	C1	C2	C3	C4
Experimental (%)	52	33	6	9
Calculated (%)	53	32	6	9

An analogous XPS analysis was performed after the oxidation reaction with periodate (Figure 3.4.14).

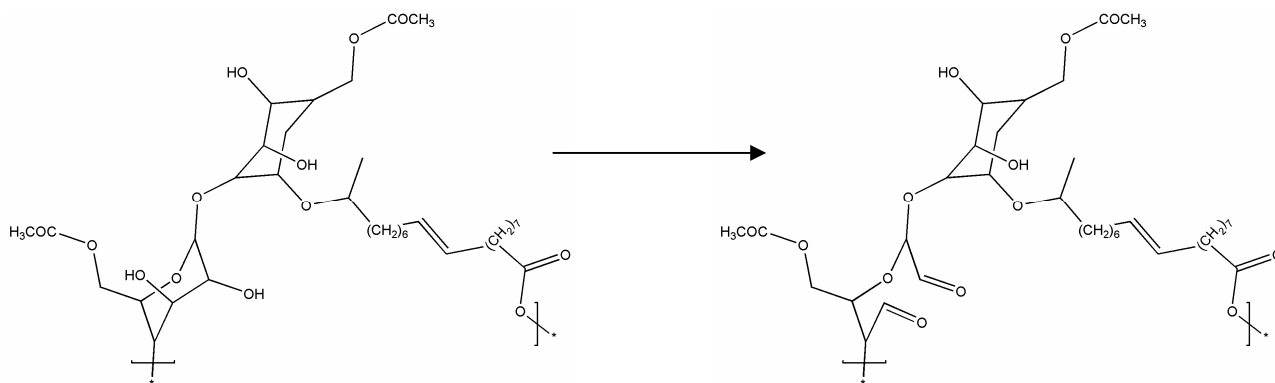


Figure 3.4.14. Sophorose 1,2 diol oxidation by periodate

Figure 3.4.15 shows the XPS widescan together with the C1s envelope deconvolution after the oxidation reaction.

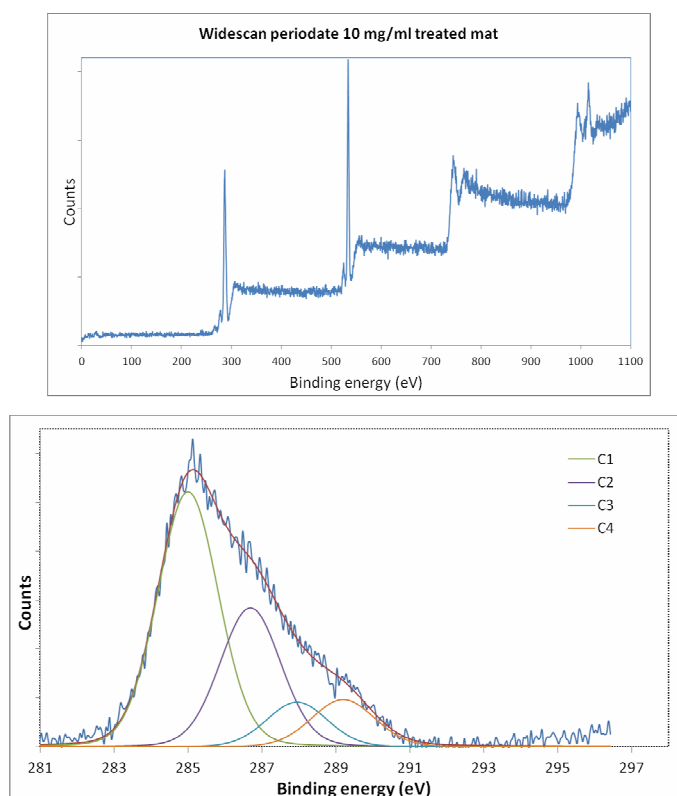


Figure 3.4.15 Oxidated mat: widescan (top), C1s envelope and its components (bottom)

From peak fitting analysis, the C2 component decreases (i.e. carbon atoms single bonded to oxygen), while the C3 peak intensity increases (carbon atoms double bonded to oxygen) due to substitution of 1,2 diols moieties with aldehydic functions. This is the result expected and from the quantitative point of view the variation of the relative abundance is summarized in Table 3.4.4.

Table 3.4.4 Experimental relative abundance from C1s envelope deconvolution (oxidized mat).

Components	C1	C2	C3	C4
Untreated (%)	52	33	6	9
Oxidized (%)	52	28	9	10

The conversion of alcoholic functions into aldehyde almost reaches 25% (expected values of C1s deconvolution in this hypothesis: C1=53%, C2=29%, C3=9% and C4=9%). In summary, out of the eight hydroxyls present on the sophorose of two repeating units, only 2 have been transformed into aldehyde groups.

Fibers morphology was observed after the oxidation of p(SL) mats (Figure 3.4.16) and fibres were not damaged, but the roughness increased.

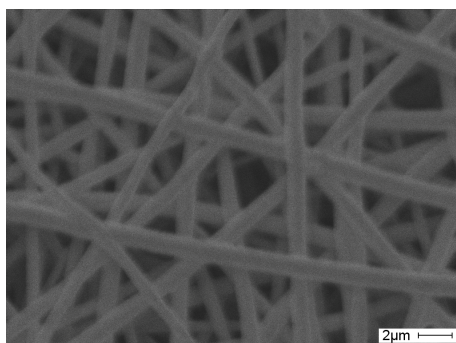


Figure 3.4.16 SEM micrographs of oxidized electrospun p(SL) fibers.

The oxidized mat was further reacted with cysteamine and sodium cyanoborohydride in the reaction of reductive amination (Figure 3.4.17). This step enables to covalently bind the amine to aldehydes, in order to obtain an available thiol group for the next functionalization reaction.

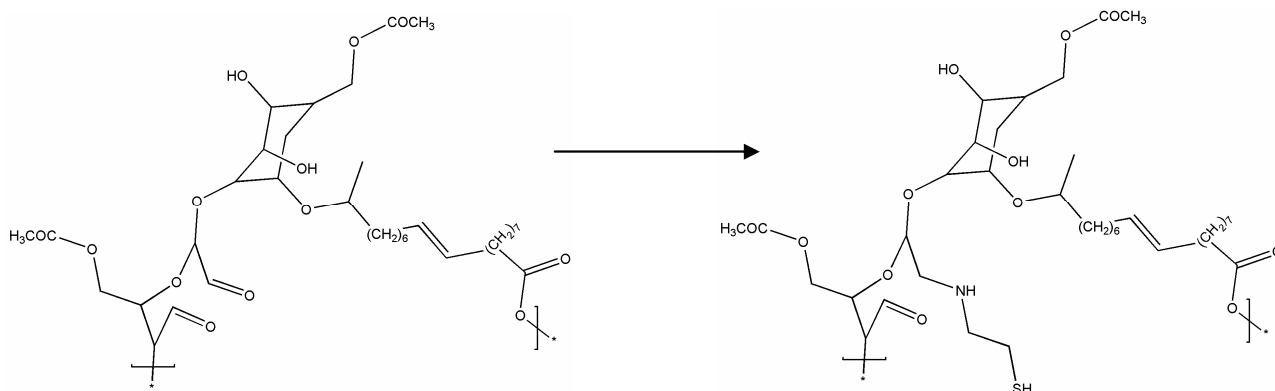


Figure 3.4.17. Reductive amination of aldehydes with cysteamine and sodium cyanoborohydride.

The results of XPS analysis on the aminated fiber mats are shown in Figure 3.4.18.

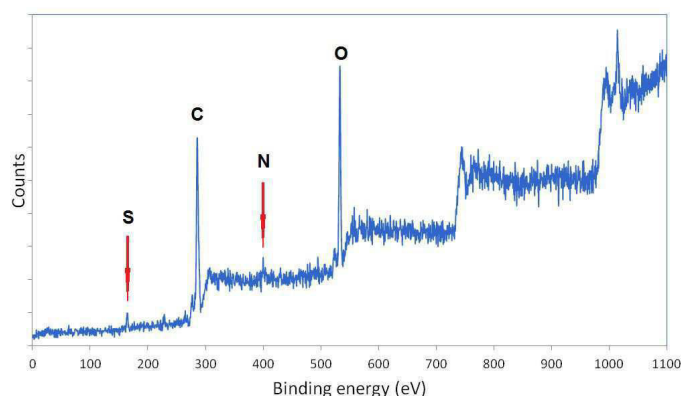


Figure 3.4.18. Amminated mat wide-scan. Atom binding energies are: sulfur (~ 164 eV), carbon (~285 eV), nitrogen (~400eV) and oxygen (~532 eV).

From the spectrum in Figure 3.4.18, the atomic ratios listed in Table 3.4.5 are observed at two different take off angles (t.o.a = 45° and 80°)

Table 3.4.5 Experimental atomic ratios of aminated p(SL) fiber mat.

t. o. a.	O/C	N/C	N/O	S/C	N/S	S/O
45°	0.364	0.0357	0.0900	0.0355	1.00	0.0895
80°	0.336	0.0327	0.0898	0.0345	0.95	0.0948

In order to determine the average number of aldehyde groups that have reacted with the amine, a theoretical correlation between this value and the various atomic ratios (O/C, N/C, N/O) to be expected from the change in chemical structure can be put forward. The following equations describe such a correlation and they are plotted in Figure 3.4.19.

For O/C ratio

$$n^{\circ} \text{ of cysteamine} = 30.552(\text{O/C})^2 - 42.681(\text{O/C}) + 12.429 \quad [\text{eq. 3.4.1}]$$

For N/C ratio

$$n^{\circ} \text{ of cysteamine} = 101.59(\text{N/C})^2 + 31.95(\text{N/C}) + 0.0348 \quad [\text{eq. 3.4.2}]$$

For N/O ratio

$$n^{\circ} \text{ of cysteamine} = -7.5367(\text{N/O})^2 + 12.866(\text{N/O}) + 0.0577 \quad [\text{eq. 3.4.3}]$$

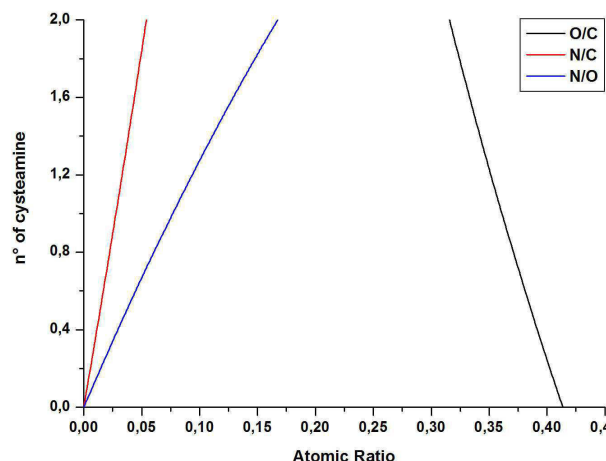


Figure 3.4.19 Calculated correlation between cysteamine groups present (i.e. aldehyde groups reacted) and the expected atomic ratios.

These functions enable the calculation (from the experimental atomic ratios of Table 3.4.5) of the number of cysteamine molecules reacted for each repeating unit of p(SL), as shown in Table 3.4.6.

Table 3.4.6 Number of cysteamine molecules reacted per repeat unit (calculated from the experimental atomic ratios, using equations 3.4.1, 3.4.2, and 3.4.3)

t.o.a	O/C	cysteamine	N/C	cysteamine	N/O	cysteamine
45°	0.364	0.94	0.0357	1.30	0.0900	1.15
80°	0.336	1.54	0.0327	1.19	0.0898	1.15

From these data an average value of cysteamine molecules for repeating unit can be calculated, yielding the following values: for take off angle of 45° = 1,13 and take off angle of 80° = 1,29. Taking into account that an average of one aldehyde group per repeating unit was formed during the first oxidation reaction, this result indicates that practically all aldehydic functions have reacted with cysteamine.

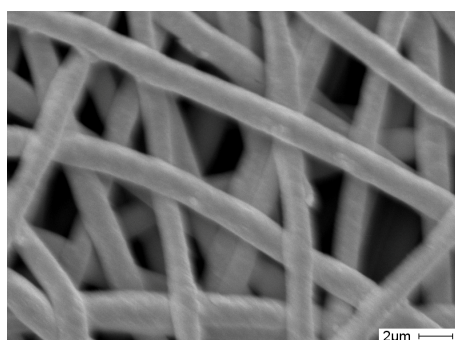


Figure 3.4.20 SEM micrographs of aminated electrospun p(SL) fibers.

The morphology of fibers was observed at SEM after the reductive amination reaction (Figure 3.4.20). Fibers were not damaged, but the roughness increased.

In order to exclude that the XPS cysteamine signals are due to the absorbed reactant, mats not subjected to the oxidation step were treated with cysteamine and sodium cyanoborohydride, in the same conditions adopted for the reductive amination reaction. The XPS spectra of the obtained samples are shown in Figure 3.4.21, where only negligible traces of sulphur and nitrogen are observed, thus confirming that the fiber mats do not physically adsorb cysteamine.

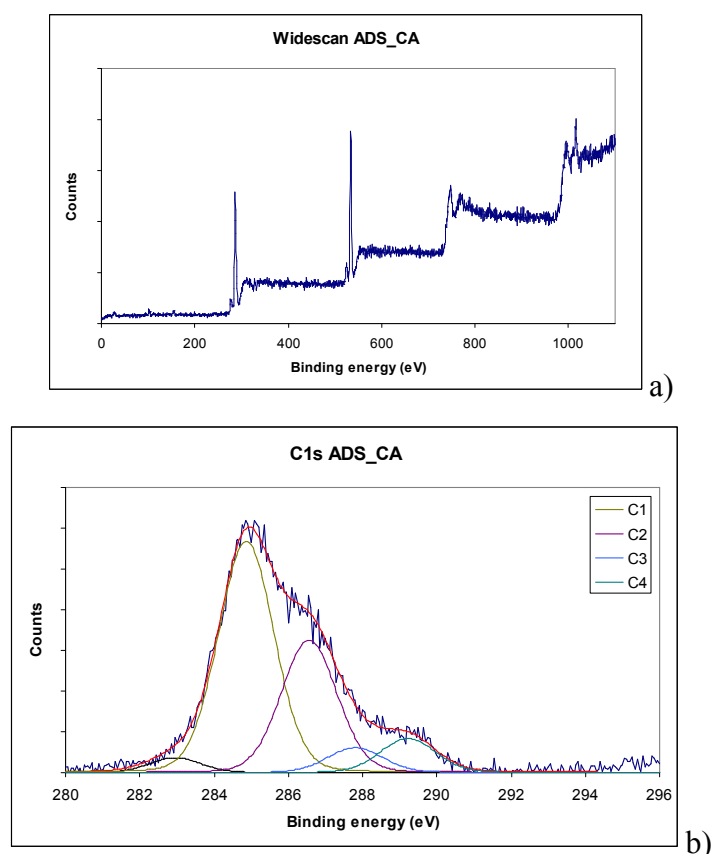


Figure 3.4.21. Non oxidated mat treated with cysteamine and sodium cyanoborohydride: widescan (a), C1s envelope and its components (b).

The last step of the functionalization procedure was the “click” reaction assisted by UV radiation of oligo(γ -Et-L-Glu-co-L-Leu) onto the thiol group of the aminated electrospun p(SL) mat (Figure 3.4.22). After reaction, the fiber mats were subjected to XPS analysis. The XPS widescan surface analysis (not reported) shows the presence of sulfur, carbon, nitrogen and oxygen. The experimental atomic ratios obtained from the widescan are collected in Table 3.4.7.

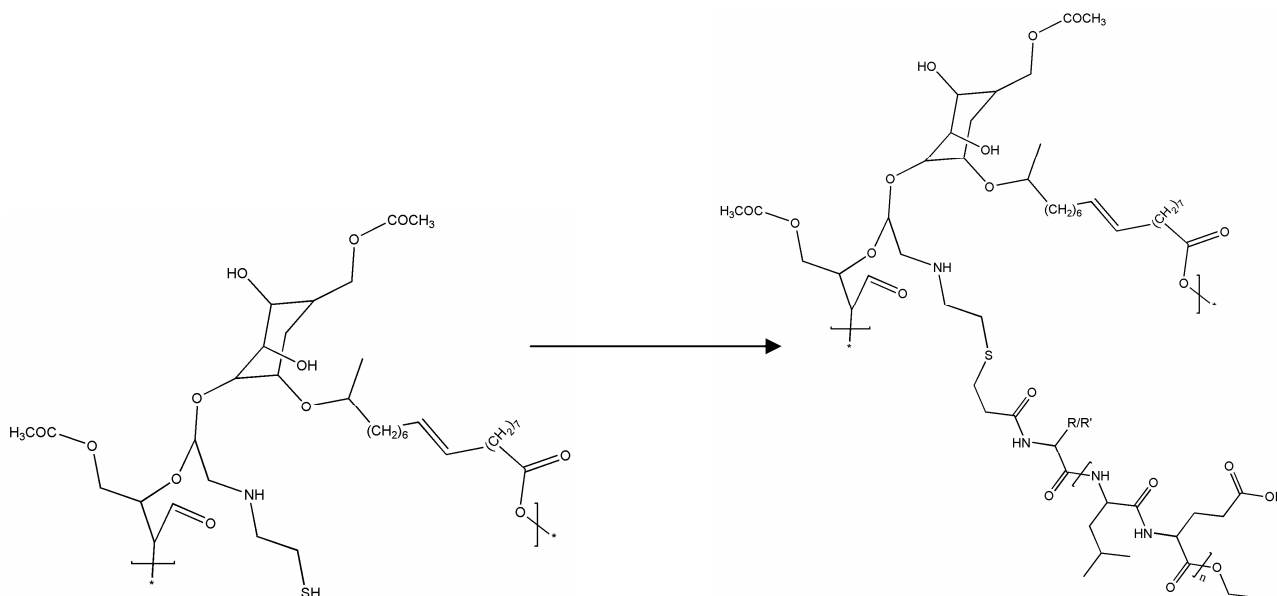


Figure 3.4.22 UV “click” reaction of thiol and double bond.

Table 3.4.7 Experimental atomic ratios (by XPS) of p(SL)fibers functionalized with oligo(γ -Et-L-Glu-co-L-Leu).

t.o.a	O/C	N/C	S/C	N/O	N/S	S/O
45°	0,3436	0,1047	0,0141	0,3049	7,4100	0,0411
80°	0,3170	0,1034	0,0138	0,3262	7,4758	0,0436

The atomic ratios at the surface of the functionalized fibers can be calculated on the hypothesis that all thiol groups, that is one group per residue on the average, have reacted. This means that one oligo(γ -Et-L-Glu-co-L-Leu) is expected in each repeating unit. Table 3.4.8 collects the values of the atomic ratios calculated considering the two terminal group options (see Figure 3.4.12).

Table 3.4.8 Calculated atomic ratios, assuming that all thiol groups (1 per residue) have reacted in the click functionalization reaction

For terminal group = LEU (co- [Leu]₃₀/[Glu]₇₀), C₁₂₄O₅₀N₁₆S

O/C N/C S/C N/O N/S S/O

0.403 0.130 0.00805 0.323 16.2 0.0200

For terminal group = GLU (co- [Leu]₃₀/[Glu]₇₀), C₁₂₃O₅₂N₁₆S

O/C N/C S/C N/O N/S S/O

0.423 0.131 0.00811 0.311 16.2 0.192

Owing to the many factors that determine composition of the sample surface (number of SH groups actually present, number of groups that give rise to the click reaction etc), analysis of the atomic ratios is rather complex. To get an idea, however, of the degree of surface functionalization with oligopeptidic chains one can look at the N/S ratio that must change when the oligopeptide chain is grafted on the p(SL) chain via click reaction with the thiol group. Indeed in the case of reaction of all SH groups, this ratio should be equal to 16 (see Table 3.4.8), whereas if the click reaction does not take place this ratio must remain equal to 1. The experimental N/S ratio is equal to 7.4 in Table 3.4.7 suggesting that nearly 1 out of 2 SH groups gives rise to the click reaction. Given that, as discussed above, the p(SL) chains at the fiber surface carry one oligopeptide chain every two residues.

Confirmation of the presence of the oligopeptide units at the fibers surface comes from the C1s envelope profile shown in Figure 3.4.23. The signal (pale blue) characteristic of aliphatic amide introduced by the oligopeptide, that is centered at 288 eV, clearly contributes to the component that generates the very evident shoulder in the C1s envelope.

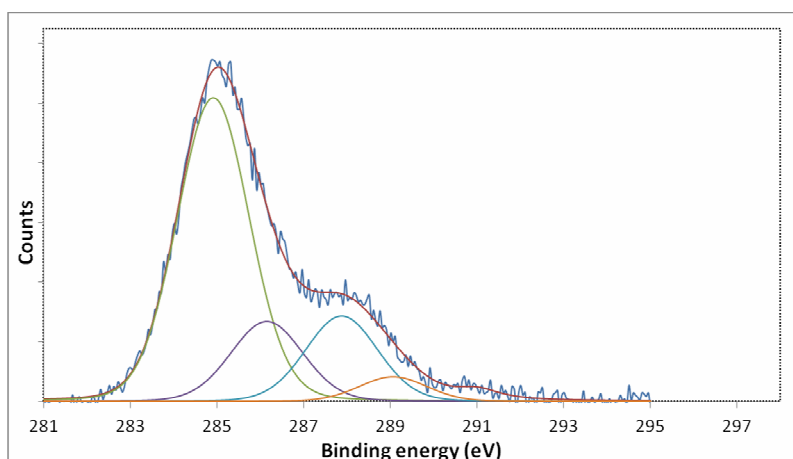


Figure 3.4.23 XPS C1s envelope deconvolution of p(SL) mats after the click reaction.

In order to exclude that the observed XPS spectral changes are caused by absorption and not grafting of oligo(γ -Et-L-Glu-co-L-Leu), the reaction was repeated on aminated es-p(SL) mats, in identical experimental conditions but excluding UV irradiation and the resulting mats were analyzed by XPS. The obtained C1s envelope deconvolution is shown in Figure 3.4.24 and the atomic ratios derived from the widescan spectrum are reported in Table 3.4.9.

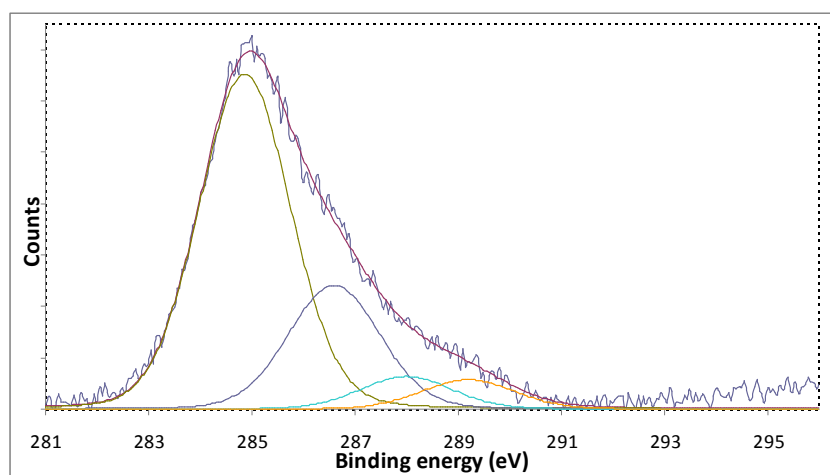


Figure 3.4.24 C1s envelope deconvolution of a mat subjected to the click reaction in the absence of UV radiation.

Table 3.4.9 Experimental atomic ratios by XPS of p(SL) fibers subjected to the click reaction in the absence of UV radiation.

t.o.a	O/C	N/C	S/C	N/O	N/S	S/O
45°	0.323	0.0726	0.0294	0.198	2.47	0.0800
80°	0.337	0.0695	0.0285	0.187	2.44	0.0768

From the measured atomic ratios after the adsorption test, it is clear that some oligopeptide is adsorbed ($N/S > 1$) at the fiber surface. The N/S value around 2.4 suggests that about 1/3 of the oligo(γ -Et-L-Glu-co-L-Leu) groups revealed by XPS in the spectra of functionalized mats ($N/S = 7.4$ in Table 3.4.7) are due to physically adsorbed – instead of chemically bound - oligomers. Thus it can be suggested from the XPS results that one oligopeptide group every 3 repeating units is effectively grafted onto the p(SL) chain.

3.4.5 Conclusion

This work deals with the characterization of a polysphorolipid in terms of thermal, structural and mechanical properties and with the fabrication of micrometric fiber mats via electrospinning. Furthermore, a new reaction pathway for the functionalization of electrospun p(SL) fibres with biomolecules was implemented. A oligo(γ -Et-L-Glu-co-L-Leu) peptide was used as the biomolecule in this ‘proof-of-concept’ study. The reaction, involving oxidation followed by reductive amination and final click reaction was efficiently developed, reaching a degree of functionalization of one oligopeptide every three sophorolipid repeating units.

4 Conclusions

In the present PhD thesis polymeric fiber mats were developed, by means of electrospinning, for potential application in the field of tissue engineering. Scaffolds made of nano- or microfiber resemble the structure of extracellular matrix and this is the main reason for the use of electrospun scaffolds as biomaterials. In addition to morphological biomimetism, biomimetic properties can be enhanced by acting on the chemical characteristics of the materials used for scaffold fabrication, mainly in terms of improved cell response (i.e. proliferation, viability and differentiation).

In the present Thesis enhanced biomimetism was achieved by modifying the chemical properties of electrospun scaffolds by following two approaches:

(1) the use of natural biomacromolecules (gelatin and collagen) instead of synthetic polymers as scaffold materials, and (2) modification of the surface chemistry of the polymeric fibers (plasma treatment or surface grafting of biomolecules).

Concerning the first approach, the physical properties of gelatin scaffolds were optimized by co-electrospinning with suitable amount of the biocompatible PLLA polyester. Gelatin greatly enhanced cell response, while PLLA improved the mechanical properties of the scaffold that could be tailored to specific applications such as cartilage-bone interfaces, by playing on gelatin/PLLA content ratio.

Collagen, the most abundant protein in extracellular matrix, was electrospun to provide a natural environment to cells and it was crosslinked by using, for the first time, a cheap and very efficient crosslinking agent. Fibre morphology and biocompatibility of the scaffold were preserved and cells cultured on electrospun collagen scaffolds showed encouraging results in terms of cell adhesion and morphology.

The second approach to biomimetism was modification of the surface chemistry, via physical or chemical methods.

When plasma was applied to PLLA electrospun scaffolds the surface was chemically modified by introducing carboxylic functional groups, thus increasing hydrophilicity and wettability of scaffolds, without damaging the fibers morphology. This chemical modifications resulted in a scaffold more compatible for fibroblast cells, which were more spread and showed higher vitality with respect to untreated PLLA.

The functionalization of a polysphorolipid, a very attractive polymer for its amphiphilic and biological properties, was a “proof-of-concept” study, where a sequence of chemical reactions were successfully developed in order to graft, through a “click” reaction, an oligopeptide on the surface

of polysphorolipid electrospun fiber mats. The functionalization procedure leads to one oligopeptide grafted every three polymer repeating unit. This demonstrated the feasibility of such approach, that opens the way to the introduction of new and interesting biomolecules with specific functionalities.

The results obtained and reported herein confirm that the strategy of act on chemical properties of electrospun scaffolds was effectively a suitable way to develop newly and highly efficient materials to be used in tissue engineering applications.

5 References

- [1] R. Langer, J. P. Vacanti “Tissue engineering” *Science* 260, 920-6, 1993
- [2] R. Skalak, C. F. Fox Tissue engineering. *Tissue Engineering, Proceedings for a Workshop held at Granlibakken, Lake Tahoe, California, February 26-29, 1988*
- [3] T. Dvir, B. P. Timko, D. S. Kohane, R. Langer “Nanotechnological strategies for engineering complex tissues” *Nature Nanotechnology* 6, 13-22, 2011
- [4] A. J. Russell, T. Bertram Chapter 3 Moving into the Clinic in R. P. Lanza, R. Langer, J. P. Vacanti (Eds.), *Principles of Tissue Engineering* (third ed.), Elsevier Academic Press, San Diego, 2007, pp. 15-31
- [5] R. M. Nerem Chapter 2 The Challenge of Imitating Nature in R. P. Lanza, R. Langer, J. P. Vacanti (Eds.), *Principles of Tissue Engineering* (third ed.), Elsevier Academic Press, San Diego, 2007, pp. 7-14
- [6] C. Ricordi “Islet transplantation: a brave new world” *Diabetes* 52, 1595-1603, 2003
- [7] <http://www.fda.gov/>
- [8] <http://www.ema.europa.eu/ema/>
- [9] <http://www.agenziafarmaco.gov.it/>
- [10] J.P. Fisher, A.G. Mikos, J.D. Bronzino *Tissue Engineering*. New York: CRC Press, 2007
- [11] R.O. Hynes “The Extracellular Matrix: Not Just Pretty Fibrils” *Science* 326, 1216-19, 2009
- [12] F. M. Watt, W. T. S. Huck “Role of the extracellular matrix in regulating stem cell fate” *Nature Reviews Molecular Cell Biology* 14, 467-73, 2013
- [13] a) C. Nathan, M. Sporn “Cytokines in context” *J. Cell Biol.* 113, 981-86, 1991 b) T. Miralem, R. Steinberg, D. Price, H. Avraham “VEGF(165) requires extracellular matrix components to induce mitogenic effects and migratory response in breast cancer cells” *Oncogene* 20, 5511-5524, 2001 c) S. Sakakura, S. Saito, H. Morikawa “Stimulation of DNA synthesis in trophoblasts and human umbilical vein endothelial cells by hepatocyte growth factor bound to extracellular matrix” *Placenta* 20, 683-693, 1999
- [14] a) V. Ottani, D. Martini, M. Franchi, A. Ruggeri, M. Raspanti “Hierarchical structures in fibrillar collagens” *Micron* 33, 587-96, 2002 b) K. Gelse, E. Poschl, T. Aigner “Collagens structure, function, and biosynthesis” *Adv. Drug Deliv. Rev.* 55, 1531-46, 2003
- [15] a) U. Hersel, C. Dahmen, H. Kessler “RGD modified polymers: biomaterials for stimulated cell adhesion and beyond” *Biomaterials* 24, 4385-415, 2003 b) H. Shin, K. Zygourakis, M.C. Farach-Carson, M.J. Yaszemski, A.G. Mikos “Attachment, proliferation, and migration of marrow

- stromal osteoblasts cultured in biomimetic hydrogels modified with an osteopontin-derived peptide” *Biomaterials* 25, 895-906, 2004
- [16] B. Grimpe, J. Silver “The extracellular matrix in axon regeneration” *Prog. Brain Res.* 137, 333-49, 2002
- [17] J.D. Esko, S.B. Selleck “Order out of chaos: assembly of ligand binding sites in heparin sulphate” *Annu. Rev. Biochem.* 71, 435-71, 2002
- [18] J.M. Trowbridge, R.L. Gallo "Dermatan sulfate: new functions from an old glycosaminoglycan" *Glycobiology* 12, 117R-125R, 2002
- [19] K. E. Rhodes, J. W. Fawcett "Chondroitin sulphate proteoglycans: Preventing plasticity or protecting the CNS?" *Journal of Anatomy* 204, 33-48, 2004
- [20] E.H. Sage, W.R. Gray "Evolution of elastin structure". *Adv. Exp. Med. Biol.* 79, 291-312, 1977
- [21] P.D. Yurchenco, S. Smirnov, T. Mathus “Analysis of basement membrane self-assembly and cellular interactions with native and recombinant glycoproteins” *Meth. Cell Biol.* 69, 111-44, 2002
- [22] D.J. Hulmes “Building collagen molecules, fibrils, and suprafibrillar structures” *J. Struct. Biol.* 137, 2–10, 2002
- [23] R. I. Freshney, B. Obradovic, W. Grayson, C. Cannizzaro, G. Vunjake-Novakovic Chapter 12 Principles of tissue culture and bioreactor design in: R. P. Lanza, R. Langer, J. P. Vacanti (Eds.), *Principles of Tissue Engineering* (third ed.), Elsevier Academic Press, San Diego, 2007, pp. 155-83.
- [24] L. E. Freed, G. Vunjaknovakovic, R. J. Biron, D. B. Eagles, D. C. Lesnoy, S. K. Barlow, R. Langer “Biodegradable polymer scaffolds for tissue engineering” *Biotechnology* 12, 689-93, 1994
- [25] S. Yang, K. Leong, Z. Du, C. Chua “The design of scaffolds for use in tissue engineering. Part I. Traditional factors” *Tissue Eng* 7, 679-89, 2001
- [26] a) J. K. Sherwood, S. L. Riley, R. Palazzolo, S. C. Brown, D. C. Monkhouse, M. Coates, L. G. Griffith, L. K. Landeen, A. Ratcliffe “A three-dimensional osteochondral composite scaffold for articulate cartilage repair” *Biomaterials* 23, 4739-51, 2002 b) X. X. Shao, D. W. Hutmacher, S. T. Ho, J. Goh, E. H. Lee “Evaluation of a hybrid scaffold/cell construct in repair of high-load-bearing osteochondral defects in rabbits” *Biomaterials* 27, 1071-80, 2006
- [27] T. S. Karande, J. L. Ong, C. M. Agrawal “Diffusion in musculoskeletal tissue engineering scaffolds: design issues related to porosity, permeability, architecture, and nutrient mixing” *Ann. Biomed. Eng.* 32, 1728-43, 2004
- [28] H. Elema, J. H. de Groot, A. J. Hijenhuis, A. J. Pennings, R. P. H. Veth, J. Klompmaker, H. W. B. Jansen “Use of porous biodegradable polymer implants in meniscus reconstruction. 2) Biological evaluation of porous biodegradable implants in menisci” *Colloids Polym. Sci.* 268, 1082-8, 1990

- [29] S. Forman, J. Kas, F. Fini, M. Steinberg, T. Ruml “The effect of different solvents on the ATP/ADP content and growth properties of HeLa Cells” *J. Biochem. Mol. Toxicol.* 13, 11-5, 1999
- [30] J. C. Middleton, A. J. Tipton “Synthetic biodegradable polymers as orthopedic devices” *Biomater.* 21, 2335-46, 2000
- [31] D.W. Hutmacher, in: Muellhaupt, et al. (Eds.), *Polymers for medical applications*, in *Encyclopedia of Materials: Science and Technology*, Elsevier Science, 2001.
- [32] B. D. Boyan, T. W. Hummert, D. D. Dean, Z. Schwartz “Role of material surfaces in regulating bone and cartilage cell response” *Biomater.* 17, 137-46, 1996
- [33] a) Z. Ma, Z. Mao, C. Gao “Surface modification and property analysis of biomedical polymers used for tissue engineering” *Colloids and Surfaces B: Biointerfaces* 60, 137-57, 2007 b) J. M. Goddard, J. H. Hotchkiss “Polymer surface modification for the attachment of bioactive compounds” *Progress in Polymer Science* 32, 698-725, 2007 c) W. M. Saltzman, T. R. Kyriakides, Chapter 20 Cell interactions with polymers, in: R. P. Lanza, R. Langer, J. P. Vacanti (Eds.), *Principles of Tissue Engineering* (third ed.), Elsevier Academic Press, San Diego, 2007, pp. 279-96.
- [34] a) D. E. Discher, P. Janmey, Yu-li Wang “Tissue Cells Feel and Respond to the Stiffness of Their Substrate” *Science* 310, 1139-43, 2005 b) G. C. Reilly, A. J. Engler “Intrinsic extracellular matrix properties regulate stem cell differentiation” *Journal of Biomechanics* 43, 55-62, 2010
- [35] R. M. Nerem Chapter 2 The Challenge of Imitating Nature in R. P. Lanza, R. Langer, J. P. Vacanti (Eds.), *Principles of Tissue Engineering*, (third ed.), Elsevier Academic Press, San Diego, 2007, pp. 7-14
- [36] a) A. Kramschuster, L. S. Turng Chapter 17 Fabrication of Tissue Engineering Scaffolds in S. Ebnesajjad (Eds.), *Handbook of Biopolymers and Biodegradable Plastics*, Elsevier Science Ltd, 2013, pp. 427-46 b) M. B. Murphy, A. G. Mikos Chapter 22 Polymer Scaffold Fabrication in R. P. Lanza, R. Langer, J. P. Vacanti (Eds.), *Principles of Tissue Engineering*, (third ed.), Elsevier Academic Press, San Diego, 2007, pp. 309-21
- [37] J. H. Jang, T. L. Houchin, L. D. Shea “Gene delivery from polymer scaffolds for tissue engineering” *Exp. Rev. Med. Dev.* 1, 127-38, 2004
- [38] A. G. Mikos, A. J. Thorsen, L. A. Czerwonka, Y. Bao, R. Langer “Preparation and characterization of poly(L-lactic acid) foams” *Polymer* 35, 1068-77, 1994
- [39] M. C. Wake, P. K. Gupta, A. G. Mikos “Fabrication of pliable biodegradable polymer foams to engineer soft tissues” *Cell Transplant.* 5, 465-73, 1996
- [40] C. E. Holy, S. M. Dang, J. E. Davies, M. S. Shoichet “In vitro degradation of a novel poly(lactide-co-glycolide) 75/25 foam” *Biomaterials* 20, 1177-85, 1999

- [41] M. Hacker, J. Tessmar, M. Neubauer, A. Blaimer, T. Blunk, A. Gopferich, M. B. Schulz "Towards biomimetic scaffolds: anhydrous scaffold fabrication from biodegradable amine-reactive diblock copolymers" *Biomaterials* 24, 4459-73, 2003
- [42] D. J. Mooney, P. M. Kaufmann, K. Sano, K. M. McNamara, J. P. Vacanti, R. Langer "Transplantation of hepatocytes using porous, biodegradable sponges" *Transplant. Proc.* 26, 3425-6, 1994
- [43] D. J. Mooney, D. F. Baldwin, N. P. Suh, J. P. Vacanti, R. Langer "Novel approach to fabricate porous sponges of poly(D,L-lactic-co-glycolic acid) without the use of organic solvents" *Biomaterials* 17, 1417-22, 1996
- [44] L. D. Harris, B. S. Kim, D. J. Mooney "Open-pore biodegradable matrices formed with gas foaming" *J. Biomed. Mater. Res.* 42, 396-402, 1998
- [45] K. Whang, C. H. Thomas, K. E. Healy, G. Nuber "A novel method to fabricate bioabsorbable scaffolds" *Polymer* 36, 837-42, 1995
- [46] Y. Y. Hsu, J. D. Gresser, D. J. Trantolo, C. M. Lyons, P. R. Gangadharam, D. L. Wise "Effect of polymer foam morphology and density on kinetics of in vitro controlled release of isoniazid from compressed foam matrices" *J. Biomed. Mater. Res.* 35, 107-16, 1997
- [47] a) I. V. Yannas, J. F. Burke, P. L. Gordon, C. Huang, R. H. Rubenstein "Design of an artificial skin. Part II. Control of chemical composition" *Biomaterials* 14, 107-31, 1980 b) A. Tampieri, M. Sandri, E. Landi, D. Pressato, S. Francioli, R. Quarto, I. Martin "Design of graded biomimetic osteochondral composite scaffolds" *Biomaterials* 29, 3539-46, 2008
- [48] R. A. Giordano, B. M. Wu, S. W. Borland, L. G. Cima, E. M. Sachs, M. J. Cima "Mechanical properties of dense polylactic acid structures fabricated by three-dimensional printing" *J. Biomater. Sci. Polym. Ed.* 8, 63-75, 1996
- [49] K. H. Tan, C. K. Chua, K. F. Leong, C. M. Cheah, W. S. Gui, W. S. Tan, F. E. Wiria "Selective laser sintering of biocompatible polymers for applications in tissue engineering" *Biomed. Mater. Eng.* 15, 113-24, 2005
- [50] B. Dhariwala, E. Hunt, T. Boland "Rapid prototyping of tissue-engineering constructs, using photopolymerizable hydrogels and stereolithography" *Tissue Eng.* 10, 1316-22, 2004
- [51] K. F. Leong, C. M. Cheah, C. K. Chua "Solid free-form fabrication of three-dimensional scaffolds for engineering replacement tissues and organs" *Biomaterials* 24, 2363-78, 2003
- [52] T. A. Osswald, G. Menges Chapter 6 Introduction to processing in T.A. Osswald, G. Menges (Eds.), *Materials Science of Polymers for Engineers*, (second ed.), Carl Hanser Verlag, Munich, 2003, pp. 185-281

- [53] M. S. Widmer, P. K. Gupta, L. Lu, R. K. Meszlenyi, G. R. Evans, K. Brandt, T. Savel, A. Gurlek, C. W. Jr. Patrick, A. G. Mikos "Manufacture of porous biodegradable polymer conduits by an extrusion process for guided tissue regeneration" *Biomaterials* 19, 1945-55, 1998
- [54] N.R. Washburn, C.G. Simon Jr., A. Tona, H.M. Elgandy, A. Karim, E.J. Amis "Co-extrusion of biocompatible polymers for scaffolds with co-continuous morphology" *J. Biomed. Mater. Res.* 60, 20-9, 2002
- [55] T. A. Osswald, L. S. Turng, P. Gramann *Injection Molding Handbook*, (second ed.), Hanser Publishers, 2008
- [56] a) N.M. Neves, A. Kouyumdzhiev, R.L. Reis "The morphology, mechanical properties and ageing behavior of porous injection molded starchbased blends for tissue engineering scaffolding" *Mater. Sci. Eng. C* 25, 195-200, 2005 b) S. Leicher, J. Will, H. Haugen, E. Wintermantel "MuCell technology for injection molding: a processing method for polyethereurethane scaffolds" *J. Mater. Sci.* 40, 4613-8, 2005
- [57] R. C. Thomson, M. J. Yaszemski, J. M. Powers, A. G. Mikos "Poly(alpha-hydroxy ester)/short-fiber hydroxyapatite composite foams for orthopedic applications" *Polym. Med. Pharm.* 394, 25-30, 1995
- [58] F. J. Hua, G. E. Kim, J. D. Lee, Y. K. Son, D. S. Lee "Macroporous poly(l-lactide) scaffold 1. Preparation of a macroporous scaffold by liquid-liquid phase separation of a PLLA-dioxane-water system" *J. Biomed. Mater. Res.* 63, 161-7, 2002
- [59] A. G. Mikos, Y. Bao, L. G. Cima, D. E. Ingber, J. P. Vacanti, R. Langer "Preparation of poly(glycolic acid) bonded fiber structures for cell attachment and transplantation" *J. Biomed. Mater. Res.* 27, 183-9, 1993
- [60] A. C. Mendes, E. T. Baran, R. L. Reis, H. S. Azevedo "Self-assembly in nature: using the principles of nature to create complex nanobiomaterials" *WIREs Nanomed. Nanobiotechnol.* 5, 582-612, 2013
- [61] M. J. Yaszemski, R. G. Payne, W. C. Hayes, R. Langer, A. G. Mikos "In vitro degradation of a poly(propylene fumarate)-based composite material" *Biomaterials* 17, 2127-30, 1996
- [62] A. Formhals, US Patent 1,975,504, 1934
- [63] J. Doshi, D. H. Reneker "Electrospinning process and applications of electrospun fibers" *Journal of Electrostatics* 35, 151-160, 1995
- [64] D. Li, Y. Xia "Electrospinning of Nanofibers: Reinventing the Wheel?" *Advanced Materials* 16, 1151-70, 2004
- [65] A. Greiner, J.H. Wendorff "Electrospinning: A Fascinating Method for the Preparation of Ultrathin Fibers" *Angew. Chem. Int. Ed.* 46, 5670-5703, 2007

- [66] S. Agarwal, J. H. Wendorff, A. Greiner "Use of electrospinning technique for biomedical applications" *Polymer* 49, 5603-21, 2008
- [67] H. S. Yoo, T. G. Kim, T. G. Park "Surface-functionalized electrospun nanofibers for tissue engineering and drug delivery" *Advanced Drug Delivery Reviews* 61, 1033-42, 2009
- [68] R. C. Thomson, M. C. Wake, M. J. Yaszemski, A. G. Mikos Biodegradable polymer scaffolds to regenerate organs in N. A. Peppas, R. S. Langer (Eds.), *Biopolymers II, Advances in Polymer Science*, Springer Berlin Heidelberg, 1995, pp 245-274
- [69] R. E. Drumright, P. R. Gruber, D. E. Henton "Polylactic Acid Technology" *Adv. Mater.* 12, 1841-6, 2000
- [70] M. A. Woodruff, D. W. Hutmacher "The return of a forgotten polymer - Polycaprolactone in the 21st century" *Progress in Polymer Science* 35, 1217-56, 2010
- [71] K. Gelse, E. Pöschl, T. Aigner "Collagens-structure, function, and biosynthesis" *Advanced Drug Delivery Reviews* 55, 1531-46, 2003
- [72] A. M. Ferreira, P. Gentile, V. Chiono, G. Ciardelli "Collagen for bone tissue regeneration" *Acta Biomaterialia* 8, 3191-3200, 2012
- [73] K. E. Kadler, D. F. Holmes, J. A. Trotter, J. A. Chapman "Collagen fibril formation" *Biochem. J.* 316, 1-11, 1996
- [74] A. Bigi, G. Cojazzi, S. Panzavolta, K. Rubini, N. Roveri "Mechanical and thermal properties of gelatin films at different degrees of glutaraldehyde crosslinking" *Biomaterials* 22, 763-8, 2001
- [75] A. J. Kuijpers, G. H. Engbers, J. Krijgsveld, S. A. Zaat, J. Dankert, J. Feijen "Cross-linking and characterisation of gelatin matrices for biomedical applications" *J Biomater Sci Polym Ed.* 11, 225-43, 2000
- [76] S. Panzavolta, M. Gioffrè, M. L. Focarete, C. Gualandi, L. Foroni, A. Bigi "Electrospun gelatin nanofibers: Optimization of genipin cross-linking to preserve fiber morphology after exposure to water" *Acta Biomaterialia* 7, 1702-9, 2011
- [77] A. Bigi, S. Panzavolta, K. Rubini "Relationship between triple-helix content and mechanical properties of gelatin films" *Biomaterials* 25, 5675-80, 2004
- [78] W. Gao, R. Hagver, V. Shah, W. Xie, R. A. Gross, M. F. Ilker, Chrissy Bell, K. A. Burke, E. B. Coughlin "Glycolipid Polymer Synthesized from Natural Lactonic Sophorolipids by Ring-Opening Metathesis Polymerization" *Macromolecules* 40, 145-7, 2007
- [79] P. A. Felse, V. Shah, J. Chan, K. J. Rao, R. A. Gross "Sophorolipid biosynthesis by *Candida bombicola* from industrial fatty acid residues" *Enzyme and Microbial Technology* 40, 316-23, 2007
- [80] Luisa Stella Dolci, Santiago David Quiroga, Matteo Gherardi, Romolo Laurita, Anna Liguori, Paolo Sanibondi, Andrea Fiorani, Laura Calzà, Vittorio Colombo, Maria Letizia Focarete

“Carboxyl Surface Functionalization of Poly(L-lactic acid) Electrospun Nanofibers through Atmospheric Non-Thermal Plasma Affects Fibroblast Morphology” *Plasma Processes and Polymers* 2013, DOI:10.1002/ppap.201300104

[81] G. Janairo, M.L. Sy, L. Yap, N. Llanos-Lazaro, J. Robles, Determination of the sensitivity range of Biuret test for undergraduate biochemistry experiments, *e-JST*, 62011, 81–87.

[82] S. Samavedi, C. Olsen Horton, S. A. Guelcher, A. S. Goldstein, A. R. Whittington “Fabrication of a model continuously graded co-electrospun mesh for regeneration of the ligament–bone interface” *Acta Biomater.* 7, 4131-38, 2006

[83] H. H. Lu, J. Jiang “Interface tissue engineering and the formulation of multiple-tissue systems” in: K. Lee, D.L. Kaplan (Eds.), *Advances in Biochemical Engineering and Biotechnology*, vol. 102, Springer Verlag, New York, 2006, p. 91.

[84] M. R. Ladd, S. J. Lee, J. D. Stitzel, A. Atala, J. J. Yoo “Co-electrospun dual scaffolding system with potential for muscle–tendon junction tissue engineering” *Biomaterials* 32, 1549-59, 2011

[85] A. Sionkowska “Current research on the blends of natural and synthetic polymers as new biomaterials: review” *Prog. Polym. Sci.* 36, 1254-76, 2011

[86] S. Agarwal, J. H. Wendorff, A. Greiner “Use of electrospinning technique for biomedical applications” *Polymer* 49, 5603-21, 2008

[87] T. J. Sill, H. A. von Recum, “Electrospinning: applications in drug delivery and tissue engineering” *Biomaterials* 29, 1989-2006, 2008

[88] Q. P. Pham, U. Sharma, A. G. Mikos “Electrospinning of polymeric nanofibers for tissue engineering applications: a review” *Tissue Eng.* 12, 1197-1211, 2006

[89] J. Han, P. Lazarovici, C. Pomerantz, X. Chen, Y. Wei, P. I. Leikes “Co-electrospun blends of PLGA, gelatin, and elastin as potential nonthrombogenic scaffolds for vascular tissue engineering” *Biomacromolecules* 12, 399-408, 2010

[90] K. Kwon II, T. Matsuda “Co-electrospun nanofiber fabrics of poly(L-lactide-co- ϵ -caprolactone) with type I collagen or heparin” *Biomacromolecules* 6, 2096-2105, 2005

[91] J. Lin, C. Li, Y. Zhao, J. Hu, L. M. Zhang “Co-electrospun nanofibrous membranes of collagen and zein for wound healing” *ACS Appl. Mater. Interfaces* 4, 1050-57, 2012

[92] S. Y. Gu, Z. M. Wang, J. Ren, C. Y. Zhang “Electrospinning of gelatin and gelatin/poly(L-lactide) blend and its characteristics for wound dressing” *Mater. Sci. Eng. C* 29, 1822-28, 2009

[93] S. E. Kim, D. N. Heo, J. B. Lee, J. R. Kim, S. H. Park, S. Jeon, K. Kwon II, “Electrospun gelatin/polyurethane blended nanofibers for wound healing” *Biomed. Mater.* 4, 044106, 2009

- [94] M. Deng, S. G. Kumbar, L. S. Nair, A. L. Weikel, H. R. Allcock “Biomimetic structures: biological implications of dipeptide-substituted polyphosphazene–polyester blend nanofiber matrices for load-bearing bone regeneration” *Adv. Funct. Mater.* 21, 2641-51, 2011
- [95] M. P. Prabhakaran, J. Venugopal, S. Ramakrishna “Electrospun nanostructured scaffolds for bone tissue engineering” *Acta Biomater.* 5, 2884-93, 2009
- [96] J. H. Jang, O. Castano, H. W. Kim “Electrospun materials as potential platforms for bone tissue engineering” *Adv. Drug Deliv. Rev.* 61, 1065-83, 2009
- [97] J. P. Chen, C. H. Su “Surface modification of electrospun PLLA nanofibers by plasma treatment and cationized gelatin immobilization for cartilage tissue engineering” *Acta Biomater.* 7, 234-43, 2011
- [98] R. Ravichandran, J.R. Venugopal, S. Sundarajan, S. Mukherjee, S. Ramakrishna, “Precipitation of nanohydroxyapatite on PLLA/PBLG/Collagen nanofibrous structures for the differentiation of adipose derived stem cells to osteogenic lineage” *Biomaterials* 33, 846-6, 2012
- [99] M. S. Kim, I. Jun, Y. M. Shin, W. Jang, S. I. Kim, H. Shin “The development of genipin-crosslinked poly(caprolactone) (PCL)/gelatin nanofibers for tissue engineering applications” *Macromol. Biosci.* 10, 91-100, 2010
- [100] Z. X. Meng, X. X. Xu, W. Zheng, H. M. Zhou, L. Li, Y. F. Zheng, X. Lou “Preparation and characterization of electrospun PLGA/gelatin nanofibers as a potential drug delivery system” *Colloids Surf. B* 84, 97-102, 2011
- [101] Y. J. Lin, Q. Cai, L. Li, Q. F. Li, X. P. Yang, R. J. Jin “Co-electrospun composite nanofibers of blends of poly[(amino acid ester)phosphazene] and gelatin” *Polym. Int.* 59, 610-16, 2010
- [102] H. W. Kim, H. S. Yu, H. H. Lee “Nanofibrous matrices of poly(lactic acid) and gelatin polymeric blends for the improvement of cellular responses” *J. Biomed. Mater. Res. A* 87, 25–32, 2007
- [103] B. M. Baker, A. O. Gee, R. B. Metter, A. S. Nathan, R. A. Marklein, J. A. Burdick, R. L. Mauck “The potential to improve cell infiltration in composite fiber-aligned electrospun scaffolds by the selective removal of sacrificial fibers” *Biomaterials* 29, 2348-58, 2008
- [104] Z. Chen, L. Cao, L. Wang, H. Zhu, H. Jiang “Effect of fiber structure on the properties of the electrospun hybrid membranes composed of poly(ϵ -caprolactone) and gelatin” *J. Appl. Polym. Sci.* 127, 4225-32, 2013
- [105] N. Detta, C. Errico, D. Dinucci, D. Puppi, D. Clarke, G. Reilly, F. Chiellini “Novel electrospun polyurethane/gelatin composite meshes for vascular grafts” *J. Mater. Sci. Mater. Med.* 21, 1761-69, 2010

- [106] B. Ding, E. Kimura, T. Sato, S. Fujita, S. Shiratori “Fabrication of blend biodegradable nanofibrous nonwoven mats via multi-jet electrospinning” *Polymer* 45, 1895-1902, 2004
- [107] B. Duan, L. Wu, X. Yuan, Z. Hu, X. Li, Y. Zhang, K. Yao, M. Wang “Hybrid nanofibrous membranes of PLGA/chitosan fabricated via an electrospinning array” *J. Biomed. Mater. Res. A* 83, 868-78, 2007
- [108] S. Kidoaki, I. K. Kwon, T. Matsuda “Mesoscopic spatial designs of nano- and microfiber meshes for tissue-engineering matrix and scaffold based on newly devised multilayering and mixing electrospinning techniques” *Biomaterials* 26, 37–46, 2005
- [109] C. H. Kim, M. S. Khil, H. Y. Kim, H. U. Lee, K. Y. Jahng “An improved hydrophilicity via electrospinning for enhanced cell attachment and proliferation” *J. Biomed. Mater. Res. B* 78, 283-90, 2006
- [110] S. Madhugiri, A. Dalton, J. Gutierrez, J. P. Ferraris, K. J. Balkus, “Electrospun MEH-PPV/SBA-15 composite nanofibers using a dual syringe method” *J. Am. Chem. Soc.* 125, 14531-38, 2003
- [111] S. Soliman, S. Pagliari, A. Rinaldi, G. Forte, R. Fiaccavento, F. Pagliari, O. Franzese, M. Minieri, P. Di Nardo, S. Licocchia, E. Traversa “Multiscale three-dimensional scaffolds for soft tissue engineering via multimodal electrospinning” *Acta Biomater.* 6, 1227-37, 2010
- [112] Paola Torricelli, Michela Gioffrè, Andrea Fiorani, Silvia Panzavolta, Chiara Gualandi, Milena Fini, Maria Letizia Focarete, Adriana Bigi “Co-electrospun gelatin-poly(L-lactic acid) scaffolds: Modulation of mechanical properties and chondrocyte response as a function of composition” *Materials Science and Engineering: C* 36, 130-8, 2014
- [113] P. Bergo, P. J. A. Sobral “Effects of plasticizer on physical properties of pigskin gelatin films” *Food Hydrocoll.* 21, 1285-89, 2012
- [114] D. M. Hashim, Y. B. Che Man, R. Norakasha, M. Shuhaimi, Y. Salmah, Z. A. Syahariza “Potential use of Fourier transform infrared spectroscopy for differentiation of bovine and porcine gelatins” *Food Chem.* 118, 856-60, 2010
- [115] S. Panzavolta, M. Gioffrè, M.L. Focarete, C. Gualandi, L. Foroni, A. Bigi, “Electrospun gelatin nanofibers: optimization of genipin cross-linking to preserve fiber morphology after exposure to water” *Acta Biomater.* 7, 1702-09, 2011
- [116] R. Touyama, Y. Takeda, K. Inoue, I. Kawamura, M. Yatsuzuka, T. Ikumoto, T. Shingu, T. Yokoi, H. Inouye "Studies on the blue pigments produced from genipin and methylamine. I. Structures of the brownish-red pigments, intermediates leading to the blue pigments” *Chem. Pharm. Bull.* 42, 668-73, 1994

- [117] J. W. Lu, Z. P. Zhang, X. Z. Ren, Y. Z. Chen, J. Yu, Z. X. Guo “High-elongation fiber mats by electrospinning of polyoxymethylene” *Macromolecules* 41, 3762-64, 2008
- [118] A. Baici, A. Lang, R. Horler, M. Knopfel “Cathepsin B as a marker of the dedifferentiated chondrocyte phenotype” *Ann. Rheum. Dis.* 47, 684-91, 1988
- [119] T. Andric, L. D. Wright, J. W. Freeman “Rapid mineralization of electrospun scaffolds for bone tissue engineering” *J. Biomater. Sci. Polym. Ed.* 22, 1535-50, 2011
- [120] Q. Cai, Q. Xu, Q. Feng, X. Cao, X. Yang, X. Deng “Biom mineralization of electrospun poly(L-lactic acid)/gelatin composite fibrous scaffold by using a supersaturated simulated body fluid with continuous CO₂ bubbling” *Appl. Surf. Sci.* 257, 10109-118, 2011
- [121] X. Yang, Q. Xu, N. Yan, G. Sui, Q. Cai, X. Deng “Structure and wettability relationship of coelectrospun poly (L-lactic acid)/gelatin composite fibrous mats” *Polym. Adv. Technol.* 22, 2222-30, 2011
- [122] A. Bigi, E. Boanini, B. Bracci, A. Facchini, S. Panzavolta, F. Segatti, L. Sturba “Nanocrystalline hydroxyapatite coatings on titanium: a new fast biomimetic method” *Biomaterials* 26, 4085-89, 2005
- [123] J. Riesle, A. P. Hollander, R. Langer, L. E. Freed, G. Vunjak-Novakovic “Collagen in tissue-engineered cartilage: Types, structure, and crosslinks” *J Cell Biochem* 71, 313-27, 1998
- [124] S. J. Kew, J. H. Gwynne, D. Enea, M. Abu-Rub, A. Pandit, D. Zeugolis, R. A. Brooks, N. Rushton, S. M. Best, R. E. Cameron “Regeneration and repair of tendon and ligament tissue using collagen fibre biomaterials” *Acta Biomater* 7, 3237-47, 2011
- [125] A. M. Ferreira, P. Gentile, V. Chiono, G. Ciardelli “Collagen for bone tissue regeneration” *Acta Biomater* 8, 3191-200, 2012
- [126] E. A. Abou Neel, L. Bozec, J. C. Knowles, O. Syed, V. Mudera, R. Day, J. K. Hyun “Collagen-Emerging collagen based therapies hit the patient” *Adv Drug Delivery Rev* 65, 429-56, 2013
- [127] W. Friess “Collagen - biomaterial for drug delivery” *Eur J Pharm Biopharm* 45, 113-36, 1998
- [128] J. D. Shiffman, C. L. Schauer “A review: electrospinning of biopolymer nanofibers and their applications” *Polym Rev* 48, 317-52, 2008
- [129] S. Agarwal, J. H. Wendorff, A. Greiner “Use of electrospinning technique for biomedical applications” *Polymer* 49, 5603-21, 2008
- [130] L. Huang, K. Nagapudi, R. P. Apkarian, E. L. Chaikof “Engineered collagen-PEO nanofibers and fabrics” *J Biomater Sci, Polym Ed* 12, 979-93, 2001
- [131] J. A. Matthews, G. E. Wnek, D. G. Simpson, G. L. Bowlin “Electrospinning of collagen nanofibers” *Biomacromolecules* 3, 232-8, 2002

- [132] D. B. Khadka, D. T. Haynie “Protein and peptide-based electrospun nanofibers in medical biomaterials” *Nanomedicine* 8, 1242-62, 2012
- [133] D. I. Zeogolis, S. T. Khew, E. S. Y. Yew, A. K. Ekaputra, Y. W. Tong, L. Y. L. Yung, D. W. Hutmacher, C. Sheppard, M. Raghunath “Electro-spinning of pure collagen nano-fibres - Just an expensiveway to make gelatin?” *Biomaterials* 29, 2293-305, 2008
- [134] L. Yang, C. F. C. Fitie, K. O. van der Werf, M. L. Bennink, P. J. Dijkstra, J. Feijen “Mechanical properties of single electrospun collagen type I fibers” *Biomaterials* 29, 955-62, 2008
- [135] B. Dong, O. Arnoult, M. E. Smith, G. E. Wnek “Electrospinning of collagen nanofiber scaffolds from benign solvents” *Macromol Rapid Commun* 30, 539-42, 2009
- [136] T. Liu, W. K. Teng, B. P. Chan, S. Y. Chew “Photochemical crosslinked electrospun collagen nanofibers: Synthesis, characterization and neural stem cell interactions” *J Biomed Mater Res, Part A* 95A, 276-82, 2010
- [137] K. Hofman, N. Tucker, J. Stanger, M. Staiger, S. Marshall, B. Hall “Effects of the molecular format of collagen on characteristics of electrospun fibres” *J Mater Sci* 47, 1148-55, 2012
- [138] Q. Jiang, N. Reddy, S. Zhang, N. Roscioli, Y. Yang “Water-stable electrospun collagen fibers from a nontoxic solvent and crosslinking system” *J Biomed Mater Res, Part A* 101A, 1237-47, 2013
- [139] J. Burck, S. Heissler, U. Geckle, M. Fotouhi Ardakani, R. Schneider, A. S. Ulrich, M. Kazanci “Resemblance of electrospun collagen nanofibers to their native structure” *Langmuir* 29, 1562-72, 2013
- [140] P. Luo, R. L. Baldwin “Mechanism of helix induction by trifluoroethanol: a framework for extrapolating the helix-forming properties of peptides from trifluoroethanol/water mixtures back to water” *Biochemistry* 36, 8413-21, 1997
- [141] T. A. Telemeco, C. Ayres, G. L. Bowlin, G. E. Wnek, E. D. Boland, N. Cohen, C. M. Baumgarten, J. Mathews, D. G. Simpson “Regulation of cellular infiltration into tissue engineering scaffolds composed of submicron diameter fibrils produced by electrospinning” *Acta Biomater* 1, 377-85, 2005
- [142] B. S. Jha, C. E. Ayres, J. R. Bowman, T. A. Telemeco, S. A. Sell, G. L. Bowlin, Simpson D. G. “Electrospun collagen: a tissue engineering scaffold with unique functional properties in a wide variety of applications” *J Nanomater* 348268, 2011
- [143] C. L. Casper, W. Yang, M. C. Farach-Carson, J. F. Rabolt “Coating electrospun collagen and gelatin fibers with perlecan domain I for increased growth factor binding” *Biomacromolecules* 8, 1116-23, 2007

- [144] D. Newton, R. Mahajan, C. Ayres, J. R. Bowman, G. L. Bowlin, D. G. Simpson “Regulation of material properties in electrospun scaffolds: Role of cross-linking and fiber tertiary structure” *Acta Biomater* 5, 518-29, 2009
- [145] H. W. Kim, J. H. Song, H. E. Kim “Nanofiber generation of gelatin-hydroxyapatite biomimetics for guided tissue regeneration” *Adv Funct Mater* 15, 1988-94, 2005
- [146] L. Buttafoco, N. G. Kolkman, P. Engbers-Buijtenhuijs, A. A. Poot, J. Dijkstra, I. Vermes, J. Feijen “Electrospinning of collagen and elastin for tissue engineering applications” *Biomaterials* 27, 724-34, 2006
- [147] L. Meng, O. Arnoult, M. Smith, G. E. Wnek “Electrospinning of in situ crosslinked collagen nanofibers” *J Mater Chem* 22, 19412-17, 2012
- [148] S. Torres-Giner, J. V. Gimeno-Alcaniz, O. Okuyama, J. M. Laragon “Comparative performance of electrospun collagen nanofibers cross-linked by means of different methods” *ACS Appl Mater Interfaces* 1, 218-23, 2009
- [149] C. Nishi, N. Nakajima, Y. Ikada “In vitro evaluation of cytotoxicity of diepoxy compounds used for biomaterial modification” *J Biomed Mater Res* 29, 829-34, 1995
- [150] L. Zhang, A. Aksan “Fourier transform infrared analysis of the thermal modification of human cornea tissue during conductive keratoplasty” *Appl Spectrosc* 64, 23-9, 2010
- [151] J. H. Muyonga, C. G. B. Cole, K. G. Duodu “Fourier transform infrared (FTIR) spectroscopic study of acid soluble collagen and gelatin from skins and bones of young and adult Nile perch (*Lates niloticus*)” *Food Chem* 86, 325-32, 2004
- [152] M. S. Ackerman, M. Bhate, N. Shenoy, K. Beck, J. A. Ramshaw, B. Brodsky “Sequence dependence of the folding of collagen-like peptides single amino acids affect the rate of triple-helix nucleation”. *J Biol Chem* 274, 7668-73, 1999
- [153] O. Okuyama “Revisiting the molecular structure of collagen” *Connect Tissue Res* 49, 299-310, 2008
- [154] Khor E. Methods for the treatment of collagenous tissues for bioprostheses. *Biomaterials*. 1997;18:95-105
- [155] Olde Damink LHH, Dijkstra PJ, van Luyn MJA, van Wachem PB, Nieuwenhuis P, Feijen J. Crosslinking of dermal sheep collagen using a water-soluble carbodiimide. *Biomaterials* 1996;17:765-73
- [156] S. Zhong, W. E. Teo, X. Zhu, R. W. Beuerman, S. Ramakrishna, L. Y. L. Yung LYL “An aligned nanofibrous collagen scaffold by electrospinning and its effects on in vitro fibroblast culture” *J Biomed Mater Res* 79A, 456-63, 2006

- [157] C. P. Barnes, C. W. Pemple, D. D. Brand, D. G. Simpson, G. L. Bowlin “Cross-linking electrospun type II collagen tissue engineering scaffolds with carbodiimide in ethanol” *Tissue Eng* 13, 1593-605, 2007
- [158] R. Zeeman, P. J. Dijkstra, P. B. van Wachem, M. J. A. van Luyn, M. Hendriks, P. T. Cahalan, J. Feijen “The kinetics of 1,4-butanediol diglycidyl ether crosslinking of dermal sheep collagen” *J Biomed Mater Res* 51, 541-8, 2000
- [159] A. Nicoletti, M. Fiorini, J. Paolillo, L. Dolcini, M. Sandri, D. Pressato “Effects of different crosslinking conditions on the chemical-physical properties of a novel bio-inspired composite scaffold stabilised with 1,4-butanediol diglycidyl ether (BDDGE)” *J Mater Sci: Mater Med* 24, 17-35, 2013
- [160] G. Argento, M. Simonet, C. W. J. Oomens, F. P.T. Baaijens. “On the importance of fiber curvature to the elastic moduli of electrospun nonwoven fiber meshes” *Journal of Biomechanics* 45, 2893-8, 2012
- [161] C. L. Pai, M. C. Boyce, G. C. Rutledge “On the importance of fiber curvature to the elastic moduli of electrospun nonwoven fiber meshes” *Polymer*.52, 6126-33, 2011
- [162] T. V. Kumari, U. Vasudev, A. Kumar , B. Menon “Cell surface interactions in the study of biocompatibility” *Trends Biomater Artif Org.*15,37-41, 2002
- [163] K. Anselme “Osteoblast adhesion on biomaterials” *Biomaterials* 21,667-81, 2002
- [164] E. S. Place, N. D. Evans, M. M. Stevens *Nat. Mater.* 8, 457, 2009
- [165] J. M. Goddard, J. H. Hotchkiss *Prog. Polym. Sci.* 32, 698, 2007
- [166] G. Delaittre, A. M. Greiner, T. Pauloehrl, M. Bastmeyer, C. Barner-Kowollik *Soft Matter* 8,7323, 2012
- [167] P. K. Chu, J. Y. Chen, L. P. Wang, N. Huang *Mater. Sci. Eng. R Rep.* 36, 143, 2002
- [168] T. Desmet, R. Morent, N. De Geyter, C. Leys, E. Schacht, P. Dubruel *Biomacromolecules* 10, 2351, 2009
- [169] R. Morent, N. De Geyter, T. Desmet, P. Dubruel, C. Leys, *Plasma Process. Polym.* 8, 171, 2011
- [170] V. N. Vasilets, A. V. Kuznetsov, V. I. Sevast'yanov *High Energy Chem.* 40, 79, 2006
- [171] T. Lu, Y. Qiao, X. Liu *Interface Focus* 2, 325, 2012
- [172] F. Intranuovo, A. Gloria, R. Gristina, L. Ambrosio, P. Favia, P. Bartolo, *Acta Biomater* 9, 5997, 2013
- [173] Z. Fang, Y. Qiu, Y. Luo *J. Phys. D: Appl. Phys.* 36, 2980, 2003
- [174] G. Fridman, G. Friedman, A. Gutsol, A. B. Shekhter, V. N. Vasilets, A. Fridman *Plasma Process. Polym.* 5, 503. 2008

- [175] P. Bruggeman, C. Leys *J. Phys. D: Appl. Phys.* 42, 053001, 2009
- [176] J. Ehlbeck, U. Schnabel, M. Polak, J. Winter, Th. von Woedtke, R. Brandenburg, T. von dem Hagen, K. D. Weltmann *J. Phys. D: Appl. Phys.*, 44, 013002, 2011
- [177] P. L. Girard-Lauriault, F. Mwale, M. Iordanova, C. Demers, P. Desjardins, M. R. Wertheimer *Plasma Process. Polym.* 2, 263, 2005
- [178] C. Sarra-Bournet, S. Turgeon, D. Mantovani, G. Laroche *J. Phys. D: Appl. Phys.* 39, 3461, 2006
- [179] X. L. Wang, M. G. McCord *J. Appl. Polym. Sci.* 104, 3614, 2007
- [180] L. Hyun-Uk, J. Ye-Sul, J. Se-Young, P. So-Young, B. Jong-Seong, K. Hyun-Gyu, C. Chae-Ryong *Appl. Surf. Sci.* 254, 5700, 2008
- [181] J. K. Wang, X. Y. Liu, H. S. Choi *J. Polym. Sci. Pol. Phys.* 46, 1594, 2008
- [182] H.-U. Lee, S.-Y. Park, Y.-H. Kang, S.-Y. Jeong, S.-H. Choi, K.-Y. Jahng, C.-R. Cho *Acta Biomater* 6, 519, 2010
- [183] M. Gu, J. E. Kilduff, G. Belfort *Biomaterials* 33, 1261, 2012
- [184] P. P. Tsai, J. R. Roth, C. Weiwei, *Text. Res. J.* 75, 819, 2005
- [185] F. Sun, X.-S. Li, J.-K. Xu, P.-T. Cao *Chin. J. Polym. Sci.* 28, 705, 2010
- [186] Y. H. Kang, K. Ahn, S. Y. Jeong, J. S. Bae, J. S. Jin, H. G. Kim, S. W. Hong, C. R. Cho *Thin Solid Films* 519, 7090, 2011
- [187] L. Hyun-Uk, K. Yoon-Hee, J. Se-Young, K. Kwangnak, K. JongPil, B. Jong-Seong, C. Chae-Ryong *Polym. Degrad. Stabil.* 96, 1204, 2011
- [188] G.-Y. Heo, S.-J. Park *Carbohydr. Polym.* 88, 562, 2012
- [189] K. Park, Y. M. Ju, J. S. Son, K. D. Ahn, D. K. Han *J. Biomater. Sci.-Polym. E* 18, 369, 2007
- [190] H. Park, K. Y. Lee, S. J. Lee, K. E. Park, W. H. Park *Macromol. Res.* 15, 238, 2007
- [191] A. Martins, E. D. Pinho, S. Faria, I. Pashkuleva, A. P. Marques, R. L. Reis, N. M. Neves *Small* 5, 1195, 2009
- [192] H. S. Yoo, T. G. Kim, T. G. Park *Adv. Drug Deliv. Rev.* 61, 1033, 2009
- [193] A. Polini, S. Pagliara, R. Stabile, G. Stefano Netti, L. Roca, C. Prattichizzo, L. Gesualdo, R. Cingolania, D. Pisignano *Soft Matter* 6, 1668, 2010
- [194] H. Park, J. W. Lee, K. E. Park, W. H. Park, K. Y. Lee *Colloid Surf. B* 77, 90, 2010
- [195] R. Wyrwa, B. Finke, H. Rebl, N. Mischner, M. Quaas, J. Schaefer, C. Bergemann, J. B. Nebe, K. Schroeder, K.-D. Weltmann, M. Schnabelrauch *Adv. Eng. Mater.* 13, B165, 2011
- [196] J. P. Chen, C. H. Su *Acta Biomater* 7, 234, 2011
- [197] C. Zandén, M. Voinova, J. Gold, D. Mörsdorf, I. Bernhardt, J. Liu, *Eur. Polym. J.* 48, 472, 2012

- [198] Q. Cheng, B. L. Lee, K. Komvopoulos, Z. Yan, S. Li, *Tissue Eng. A* 2013, 19, 1188.
- [199] F. Taraballi, S. Zanini, C. Lupo, S. Panseri, C. Cunha, C. Riccardi, M. Marcacci, M. Campione, L. Cipolla *J. Colloid Interface Sci.* 394, 590, 2013
- [200] Q. P. Pham, U. Sharma, A. G. Mikos, *Tissue Eng.* 12, 1197, 2006
- [201] S. P. Zhong, Y. Z. Zhang, C. T. Lim, *WIREs Nanomed. Nanobiotechnol.* 2, 510, 2010
- [202] F. Yang, R. Murugan, S. Wang, S. Ramakrishna *Biomaterials*, 26, 2603, 2005
- [203] S. Mukherjee, C. Gualandi, M. L. Focarete, R. Ravichandran, J. R. Venugopal, M. Raghunath, S. Ramakrishna *J. Mater. Sci.: Mater. Med.* 22, 1689, 2011
- [204] D. W. Hutmacher *Biomaterials* 21, 2529, 2000
- [205] T. Callebaut, I. Kochetov, Y. Akishev, A. Napartovich, C. Leys, *Plasma Sources Sci. Technol.* 13, 245, 2004
- [206] X. Zhong, K. Kim, D. Fang, S. Ran, B. S. Hsiao, B. Chu, *Polymer* 43, 4403, 2002
- [207] C. Gualandi, M. Govoni, L. Foroni, S. Valente, M. Bianchi, E. Giordano, G. Pasquinelli, F. Biscarini, M. L. Focarete *Eur. Polym. J.* 48, 2008, 2012
- [208] C. M. Chan, T. M. Ko, H. Hiraoka, *Surface Sci. Rep.* 24,1, 1996
- [209] K. S. Siow, L. Britcher, S. Kumar, H. J. Griesser, *Plasma Process. Polym.* 3, 392, 2006
- [210] G. T. Hermanson, *Bioconjugate Techniques*, 2nd ed., Academic Press, New York 2008.
- [211] E. Zamir, B. Geiger, *J. Cell Sci.* 20, 3583, 2001
- [212] B. Greig, J. P. Spatz, A. D. Bershadsky *Nat. Rev. Mol. Cell Biol.* 10, 21, 2009
- [213] P. Amornsudthiwat, R. Mongkolnavin, S. Kanokpanont, J. Panpranot, C. S. Wong, S. Damrongsakkul, *Colloids Surf. Biointerfaces* 111, 579, 2013
- [214] A. M. Davila, R. Marchal, N. Monin and J. P. Vandecasteele "Identification and determination of individual sophorolipids in fermentation products by gradient elution high-performance liquid chromatography with evaporative light-scattering detection" *J. Chromatog.* 648, 139-49, 1993.
- [215] P. A. J. Gorin, J. F. T. Spencer and A. P. Tulloch "Hydroxy fatty acid glycosides of sophorose from *torulopsis magnoliae*" *Can. J. Chem.* 39, 846-95, 1961.
- [216] I. N. Van Bogaert, J. Zhang and W. Soetaert "Microbial synthesis of sophorolipids" *Process Biochemistry* 46, 821-33, 2011.
- [217] E. Zini, M. Gazzano, M. Scandola, S. R. Wallner and R. A. Gross "Glycolipid Biomaterials: Solid-State Properties of a Poly(sophorolipid)," *Macromolecules* 41, 7463-68, 2008.

- [218] Y. Peng, J. Decatur, M. A. R. Meier and R. A. Gross "Ring-Opening Metathesis Polymerization of a Naturally Derived Macrocyclic Glycolipid" *Macromolecules* 46, 3293-300, 2013.
- [219] M. Bertoldo, G. Zampano, F. La Terra, V. Villari, V. Castelvetro "Amphiphilic Amylose-g-poly(meth)acrylate Copolymers through "Click" onto Grafting Method" *Biomacromolecules* 12, 388-98, 2011
- [220] G. G. d'Ayala, M. Malinconico, P. Laurienzo "Marine Derived Polysaccharides for Biomedical Applications: Chemical Modification Approaches" *Molecules* 13, 2069-106, 2008
- [221] R. P. Tripathi, S. S. Verma, J. Pandey, V. K. Tiwari "Recent Development on Catalytic Reductive Amination and Applications" *Current Organic Chemistry* 12, 1093-1115, 2008
- [222] C. E. Hoyle, C. N. Bowman "Thiol-Ene Click Chemistry" *Angew. Chem. Int. Ed.* 49, 1540-73, 2010
- [223] E. Zini, M. Scandola, P. Gatenholm, *Biomacromolecules* 4, 821-7, 2003
- [224] D. Klemm, B. Philipp, T. Heinze, U. Heinze, W. Wagenknecht, In *Comprehensive Cellulose Chemistry*; Wiley-VCH: Weinheim, Germany, 1998; Vol.1.
- [225] *High Polymers. Part I: Crystalline Olefin Polymers*; Raff, R. A., Doak, K. W., Eds.; John Wiley & Sons: New York, 1965; Vol.XX
- [226] F. Kaneko, K. Yamazaki, K. Kitagawa, T. Kikyo, M. Kobayashi, Y. Kitagawa, Y. Matsuura, K. Sato and M. Suzuki "Structure and Crystallization Behaviour of the β Phase of oleic acid" *J. Phys. Chem. B* 101, 1803-09, 1997 .
- [227] P. Tandon, G. Forster, R. Neubert and S. Wartewig "Phase transitions in oleic acid as studied by X-ray diffraction and FT-Raman spectroscopy" *J. Mol. Struct* 524, 201-15, 2000.

List of Publications

Paola Torricelli, Michela Gioffrè, Andrea Fiorani, Silvia Panzavolta, Chiara Gualandi, Milena Fini, Maria Letizia Focarete, Adriana Bigi “Co-electrospun gelatin-poly(L-lactic acid) scaffolds: Modulation of mechanical properties and chondrocyte response as a function of composition” *Materials Science and Engineering C* 36 (2014) 130–138

Luisa Stella Dolci, Santiago David Quiroga, Matteo Gherardi, Romolo Laurita, Anna Liguori, Paolo Sanibondi, Andrea Fiorani, Laura Calzà, Vittorio Colombo, Maria Letizia Focarete “Carboxyl Surface Functionalization of Poly(L-lactic acid) Electrospun Nanofibers through Atmospheric Non-Thermal Plasma Affects Fibroblast Morphology” *Plasma Process. Polym.* 2013, DOI: 10.1002/ppap.201300104

Andrea Fiorani, Chiara Gualandi, Silvia Panseri, Monica Montesi, Maurilio Marcacci, Maria Letizia Focarete, Adriana Bigi “Comparative performance of collagen nanofibers electrospun from different solvents and stabilized by different crosslinkers” *Journal of Materials Science, Materials in Medicine*, accepted for publication.

Scientific congress and schools

XVII National School of Material Science

Harnessing Complexity of Materials: Hybrid-Functional and Biomimetic Systems

Bressanone (BZ), September 26-30, 2011

Poster “Biomimetic Gelatin/Poly(L-lactic acid) composite scaffolds by co-electrospinning”

National Congress on Biomaterials (SIB)

University of Salento, Lecce, 18-20 June 2012,

Oral presentation, “Scaffold compositi biomimetici di gelatina e acido poli(L)lattico”

MIME -Materials in Medicine , International Conference

Fiorani Andrea, Panseri Silvia, Gualandi Chiara, Marcacci Maurillo, Focarete Maria Letizia

Biomimetic electrospun collagen scaffolds for cartilage repair applications

Oral presentation, Faenza 8-11 October 2013

Acknowledgments

Prof. Adriana Bigi, Dr. Silvia Panzavolta, Dr. Michela Gioffrè

Department of Chemistry “G. Ciamician” and National Consortium of Materials Science and Technology (INSTM, Bologna RU), University of Bologna, Italy

Prof. Paola Torricelli, Dr. Milena Fini

Preclinical and Surgical Studies Laboratory, Codivilla Putti Research Institute, Rizzoli Orthopaedic Institute and Laboratory of Biocompatibility, Innovative Technologies and Advanced Therapies-Department Rizzoli Research, Innovation, Technology, via di Barbiano, 1/10, 40136 Bologna, Italy

Prof. Laura Calzà

Health Sciences and Technologies, Center for Industrial Research (HST-ICIR), University of Bologna, Via Tolara di Sopra 50, 40064 Ozzano dell’Emilia, Bologna, Italy and IRET Foundation, Via Tolara di Sopra 41/E, 40064 Ozzano dell’Emilia, Bologna, Italy

Dr. Luisa Stella Dolci

Health Sciences and Technologies, Center for Industrial Research (HST-ICIR), University of Bologna, Via Tolara di Sopra 50, 40064 Ozzano dell’Emilia, Bologna, Italy

Prof. Vittorio Colombo

Advanced Mechanics and Materials, Interdepartmental Center for Industrial Research (AMM-ICIR), University of Bologna, Via Saragozza 8, 40123 Bologna, Italy and Department of Industrial Engineering (DIN), University of Bologna, Via Saragozza 8, 40123 Bologna, Italy

Dr. Matteo Gherardi, Dr. Paolo Sanibondi, Romolo Laurita, Anna Liguori

Department of Industrial Engineering (DIN), University of Bologna, Via Saragozza 8, 40123 Bologna, Italy

Prof. Maurilio Marcacci

Laboratory of Biomechanics and Technology Innovation, Rizzoli Orthopaedic Institute, Bologna, Italy

Dr. Silvia Panseri

Laboratory of Biomechanics and Technology Innovation, Rizzoli Orthopaedic Institute, Bologna, Italy and Institute of Science and Technology for Ceramics, National Research Council of Italy ISTECCNR, Faenza, Italy

Dr. Monica Montesi

Institute of Science and Technology for Ceramics, National Research Council of Italy ISTECCNR, Faenza, Italy

Prof. Richard A. Gross, Yifeng Peng

Department of Chemistry and Chemical Biology, Rensselaer Polytechnic Institute, Troy, NY, USA